

# UC Berkeley

## UC Berkeley Electronic Theses and Dissertations

### Title

The role of ion channels in developmental patterning and growth

### Permalink

<https://escholarship.org/uc/item/7z46j4b7>

### Author

Emmons-Bell, Maya

### Publication Date

2021

Peer reviewed|Thesis/dissertation

The role of ion channels in developmental patterning and growth

by

Maya K Emmons-Bell

A dissertation submitted in partial satisfaction of the

requirements for the degree of

Doctor of Philosophy

in

Molecular and Cell Biology

in the

Graduate Division

of the

University of California, Berkeley

Committee in charge:

Professor Iswar Hariharan, Chair

Professor David Bilder

Professor Ehud Isacoff

Professor Caroline Williams

Spring 2021

# **The role of ion channels in developmental patterning and growth**

Copyright 2021  
by  
Maya K Emmons-Bell

## Abstract

The role of ion channels in developmental patterning and growth

by

Maya K Emmons-Bell

Doctor of Philosophy in Molecular and Cell Biology

University of California, Berkeley

Professor Iswar Hariharan, Chair

Life as a multicellular organism begins simply, as a single fertilized egg. However, simplicity begets complexity as cells divide, differentiate, and organize themselves into the tissues and organs that comprise complex lifeforms. The process by which this complexity is generated and constrained during development has held the fascination of scientists for centuries.

Seminal genetic screens carried out in the vinegar fly *Drosophila melanogaster* identified genes required for proper developmental growth and patterning. These genes were found to encode molecules with similar properties; many were secreted in specific locations in the animal, and influenced the gene expression of surrounding cells. It was proposed that these molecules, termed “morphogens”, directed development by imparting patterning information across a tissue.

Although a century of developmental genetics has identified many evolutionarily conserved factors with morphogen-like properties, we are still without a full understanding of the processes that shape development. Recently, non-morphogen-encoded signals, including physical forces and electrical signaling, have been shown to be instructive in development, suggesting that the process of development is an emergent property of many signaling modalities and cell interactions.

In Chapter 1, I present an overview of our current understanding of developmental morphogenesis, and describe the biology of the *Drosophila* wing imaginal disc, a model epithelial structure which undergoes a stereotyped program of growth and patterning. I highlight signaling modalities that have been shown to be important for development, including electrochemical signaling, the focus of my dissertation research.

Ion channels, proteins that mediate ionic flux across cell membranes, are increasingly understood to be critical regulators of cell behavior, but their role in development has only begun to be explored. I found that expression of ion channels is patterned in the *Drosophila* wing imaginal disc, giving rise to localized depolarization in the tissue. This physiological pattern promotes signaling through the conserved Hedgehog (Hh) pathway. This work, described in Chapter 2, adds to our understanding of critical signaling modalities in the development of the wing disc, and suggests that the Hh pathway is regulated in part by cell physiology.

During development, patterning occurs concomitantly with growth. The regulation of growth, which occurs both cell-intrinsically and -extrinsically, is an area of immense research interest with profound implications for cancer biology. I found that the mechanosensitive ion channel Piezo is involved in the growth regulation of the wing disc. Piezo is expressed in a sparse population of cells scattered throughout the disc, and impacts organ size by modulating cell size. Chapter 3 describes this work, which implicates mechanosensitive ion channels in growth regulation.

In the course of exploring effects of modulating membrane potential, I made the surprising discovery that cells of altered membrane potential are recovered preferentially between the anterior and posterior regions of the wing disc. This process is mediated by a mechanism reminiscent of a cell-cell interaction termed “cell competition”. This work, described in Chapter 4, is the first report of compartment-specific cell competition in *Drosophila*, and suggests that membrane potential is a component of cell fitness.

A previous graduate student in the laboratory, Jo Bairzin, discovered that clones of cells which express a constitutively active allele of the Hippo pathway co-effector Yorkie overgrow, and misexpress developmental selector genes. I contributed to this work by defining the requirement of Scalloped in Yki-mediated misexpression of Ci, and validating other results. This work, presented in Chapter 5, highlights transcriptional plasticity in tumor models, as well as identifies the tumor boundary as an important signaling center.

Taken together, my work characterizes the role of ion channels in developmental growth and patterning, and presents new applications of tools used to study cell physiology in development.

## Contents

<b>Contents</b> .....	i
<b>List of Figures</b> .....	iii
<b>1. Introduction</b> .....	1
<i>Morphogenesis is a function of cellular growth, proliferation, and signaling</i> .....	2
<i>Drosophila imaginal discs as a model for studying organ growth and morphogenesis</i> ..	4
<i>Ion channels in developmental morphogenesis</i> .....	11
<i>Summary of dissertation work</i> .....	13
<b>2. Membrane potential modulates Hedgehog signaling in the wing imaginal disc</b> .....	15
<i>Abstract</i> .....	16
<i>Introduction</i> .....	16
<i>Materials and Methods</i> .....	17
<i>Results</i> .....	19
<i>Discussion</i> .....	25
<i>Figures</i> .....	28
<b>3. Piezo-expressing cells regulate organ size in the wing imaginal disc</b> .....	47
<i>Abstract</i> .....	48
<i>Introduction</i> .....	48
<i>Materials and Methods</i> .....	49
<i>Results</i> .....	51
<i>Discussion</i> .....	53
<i>Figures</i> .....	55
<b>4. Membrane potential mediates compartment-specific cell competition in the wing imaginal disc</b> .....	61
<i>Abstract</i> .....	62
<i>Introduction</i> .....	62
<i>Materials and Methods</i> .....	63
<i>Results</i> .....	64
<i>Discussion</i> .....	65
<i>Figures</i> .....	67
<b>5. The Hippo pathway coactivator Yorkie can reprogram cell fates and create compartment-boundary-like interactions at clone margins</b> .....	71
<i>Abstract</i> .....	72
<i>Introduction</i> .....	72
<i>Materials and Methods</i> .....	73
<i>Results</i> .....	75
<i>Discussion</i> .....	80
<i>Figures</i> .....	82

**References** ..... 95

## List of Figures

1.1 <i>Drosophila</i> development and wing anatomy .....	6
1.2 Hedgehog signaling in the wing imaginal disc .....	9
2.1 Membrane potential is patterned in the third-instar wing imaginal disc .....	28
2.2 Expression of endogenous channels is patterned and contributes to depolarization anterior to the compartment boundary .....	30
2.3 Patterned Rpk and ATP $\alpha$ expression and membrane depolarization require Hh signaling .....	32
2.4 The ENaC channel Rpk is required for Hh signal transduction.....	34
2.5 Membrane potential modulates Smo membrane abundance and downstream Hh signal transduction in larval salivary glands .....	35
2.6 $V_{mem}$ regulates Smo membrane localization independently of Ptc in the wing imaginal disc .....	37
2.7 Membrane potential modulates Hh signalling at the anteroposterior compartment boundary .....	39
2.8 <i>rpk</i> knockdown decreases DiBAC staining and Rpk expression at the A-P compartment boundary .....	40
2.9 Patterned Rpk and ATP $\alpha$ expression and membrane depolarization require Hh signaling .....	41
2.10 Hh pathway activation results in depolarization .....	42
2.11 Manipulating levels of the ion channel Rpk impacts both Hh and Wg signal transduction .....	44
2.12 Optogenetic manipulation of $V_{mem}$ in <i>Drosophila</i> salivary glands .....	46
3.1 A sparse population of Piezo-expressing cells in the wing imaginal disc .....	55
3.2 Expression patterns of other mechanosensitive ion channels in the disc .....	56
3.3 Loss of Piezo results in larger adult organs and imaginal wing discs .....	57
3.4 Loss of Piezo results in larger adult organs.....	58
3.5 Piezo modulates cell size .....	59
3.6 Signaling downstream of Piezo .....	60
4.1 Altered membrane potential induces compartment-specific cell elimination .....	67
4.2 Patterns of apoptotic death in NaChBac-expressing clones .....	68
4.3 Blockade of apoptosis in NaChBac-expressing clones .....	69
5.1 Constitutively active Yorkie (Yki <sup>CA</sup> ) disrupts stable selector gene expression .....	82
5.2 <i>yki</i> <sup>CA</sup> clones require <i>sd</i> , <i>ban</i> , and <i>tara</i> to disrupt patterning gene expression .....	84
5.3 <i>ban</i> and <i>tara</i> in combination induce ectopic patterning gene expression .....	86
5.4 <i>yki</i> <sup>CA</sup> clones activate a developmental signaling cascade .....	87
5.5 Ectopic Ci activation requires high Yki activity .....	89
5.6 <i>yki</i> <sup>CA</sup> clones disrupt patterning gene expression late in clone development .....	90
5.7 Manipulating <i>ban</i> or <i>tara</i> alone in wild-type cells does not alter Ci levels .....	91
5.8 <i>yki</i> <sup>CA</sup> clones do not show alterations in all chromatin markers. ....	92
5.9 Overgrowth and ectopic Ci expression in <i>yki</i> <sup>CA</sup> clones is not dependent on Hh signaling or the JNK pathway .....	93

## Acknowledgements

By far the most important section of my dissertation is this one, and yet I cannot possibly produce language that captures the immense gratitude and fondness I feel for the small army of people who helped me complete this work. Read the following, multiply it by ten, and that may come close to half of what they deserve.

First, I must thank my advisor, Iswar Hariharan, for giving me an intellectual home for the last five years. Iswar's scientific mentorship has taught me to think from first principles, to approach complex problems with creativity and an open mind, and to be exacting and rigorous in my experimentation. Iswar is also an immensely understanding, empathetic, and supportive group leader, who cares deeply about the well-being of his students. Without a doubt, I am a better person and scientist for having worked with him, and I will rely on the lessons I've learned during my time in the Hariharan lab for the rest of my career.

I am also indebted to the incredible colleagues with whom I've worked. Linda Setiawan, Taryn Sumabat, Jo Bairzin, Rob Harris, and Melanie Worley made my rotation so invigorating and fun that I couldn't help but join the lab, and imparted vital wisdom spanning from experiment design to personal finance to workout routines. Jamie Lahvic, Nick Everetts, Sophia Friesen, Danielle Spitzer, Riku Yasutomi, Melanie Worley and Joyner Cruz have been constant sources of support, laughter, and brilliant ideas over the last few years. Together, we weathered a laboratory move, devastating wildfires, a global pandemic, and a disastrous presidential administration. I am immensely grateful to have had them by my side through it all. I am also grateful to have had David Bilder's lab as next-door neighbors, a group of hugely talented and generous scientists who shared reagents and ideas with me. My rotation-buddy and co-GSI Mark Khoury, who is one of the most talented scientists I've ever met, was a never-ending source of critical feedback, cheerleading, and commiseration. The members of my thesis committee, David Bilder, Caroline Williams, and Ehud Isacoff, were instrumental in shaping the direction of this work. A special thank you to Riku Yasutomi, who was my first formal mentee, and by virtue of his immense raw talent, made the experience effortless.

Outside of lab, there are even more people to thank. The inhabitants of Blue House -- Tess Linden, Paige Diamond, Justin Roncioli, and Josh Cofsky (and honorary housemates Ellie Bondra, Perri Callaway, and William Worm) provided me with a home full of laughter and love. Annaick Miller, Elizabeth Berrang, Colby Sameshima, Rachel Frankel, Simone Riley, Alison Sikowitz, Reavey Fike, Camille Baptista, and Kate Carlin know me better than most people in the world, and have been my most enthusiastic cheerleaders and support system for more than ten years. I feel so grateful to have been a part of the MCB graduate student community (there are too many wonderful people to list). They are great friends and inspiring colleagues, and I am proud of the hard work we've done to cultivate a community that fosters intellectual engagement and joy. The future of science is bright with them in the lead.

But most importantly, I must thank my family. My parents, Chalon Emmons and Greg Bell, have been unrelentingly supportive of my interest in science, letting all manner of pets and experiments into our home, asking thoughtful questions about my research interests, and indulging me in countless visits to science museums and libraries. Their understanding and love helped me weather the harder parts of graduate school, and relish the bright moments. I feel immensely lucky to have been able to complete my Ph.D. so close to home. My sister, Sophia Emmons-Bell, was a source of wisdom well beyond her years, and is my hero in every way. And to my grandparents, who are master classes in curiosity-driven living, and who great challenge with endurance, bravery, and grace - thank you for leading by example.

## **Chapter 1**

### **Introduction**

## 1.1 Morphogenesis is a function of cellular growth, proliferation, and signaling

Multicellularity, an astounding feat of evolution, requires the generation and maintenance of cellular diversity, as well as tight coordination of the abundances of different cell types. Together, these parameters define the cellular makeup of an organism. Although a seemingly simple equation, understanding how a multicellular animal constructs diverse tissue types of reproducible size and shape has engaged biologists for more than a century.

The development of tissues and organs, or morphogenesis, is an emergent phenomenon dependent on the coordination of growth, proliferation and differentiation between large numbers of cells. Cell growth refers to the size of individual cells, and proliferation is a process by which cell numbers are increased, defined by relative rates of cell division and death. Together, cell growth and proliferation determine the overall size of tissues and organs. Signaling between cells define and reinforce the identities of unique populations, leading to the generation of a tissue with the correct cell types in the appropriate locations.

In the early 20<sup>th</sup> century, the embryologist Theodor Boveri observed that the eggs of both sea urchins and nematodes had a noticeable polarity. When eggs were fertilized and embryos began development, cell divisions occurred at reproducible locations, partitioning the cytoplasm of the egg along its polar axis. Boveri wondered if there were substances within the egg cytoplasm that were distributed unevenly, and if uneven inheritance of these substances might impart unique identities upon cells of the early embryo. Although the mechanisms of such signaling events remained unknown, the concept of graded signals, and their ability to impart increasingly refined patterns upon fields of cells, became an intellectual tenant of developmental biology. Implicated in the process of morphogenesis, these signals became known as “morphogens”.

Decades of embryology, biochemistry, and genetics have solidified the concept of morphogens. In 1924, Hans Spemann and Hilde Mangold demonstrated that a population of cells in the salamander embryo could impart specific fates upon neighboring cells, suggesting that privileged regions of the embryo acted as “organizers”, able to influence the behaviors of cells in their surroundings to drive large-scale developmental patterning events (Spemann & Mangold, 2001). A seminal genetic screen undertaken by Christiane Nüsslein-Volhard and Eric Wieschaus in 1979 uncovered the identities of genes responsible for patterning the *Drosophila* embryo (Nüsslein-Volhard & Wieschaus, 1980). This work electrified the field of cell and developmental biology, providing a genetic handle with which to dissect the complexities of organismal patterning. Although identified by their requirement in *Drosophila* embryogenesis, the genes characterized in Nüsslein-Volhard and Wieschaus' screen were found to be important for the development and patterning of other fly organs, and conserved across metazoa.

Among these genes were the fly orthologues of Hedgehog (Hh), Bone Morphogenic Protein (BMP) and Wingless-related integration site (Wnt). When characterized

molecularly, they were found to share similar properties: each gene was expressed in restricted populations of cells during development, and gene products were released, forming an extracellular concentration gradient as they diffused across the tissue. Patterns of gene expression in cells surrounding the signal-producing population were dictated by the concentration of gene product they were exposed to. Thus, complex patterns were set up across a field of cells by the formation and interpretation of gradients of these vital signaling genes. Incredibly, it was discovered that the same signaling molecules were deployed over and over again in development, to organize and pattern many disparate tissues across developmental time. The “French Flag Model”, proposed by Lewis Wolpert, posited that cells interpreted concentrations of morphogens to derive a positional identity (Wolpert, 1969). It seemed as if the problem of patterning would be solved by producing a simple catalogue of morphogens.

However, as theoretically parsimonious as the morphogen model of patterning seemed, there arose numerous mechanistic questions that remain unsolved today. For one, it is unclear how many of the well-characterized morphogens are produced and transported *in vivo* to form gradients across a tissue. Many morphogens are modified prior to secretion by glycosylation or lipidation, resulting in extremely hydrophobic molecules which would not be predicted to readily diffuse through extracellular space (Miura & Treisman, 2006). Direct tagging of the molecules dramatically diminished their biological activity, rendering attempts to track diffusion *in vivo* futile. Alternative modes of morphogen transport, through signaling projections like cytonemes (F.-A. Ramírez-Weber & Kornberg, 1999), or within extracellular vesicles or lipoprotein particles, were also described, adding to the suite of mechanisms by which morphogens could be distributed, but complicating the simple diffusion paradigm.

An additional problem concerned interpretation of morphogen signal. When the protein distributions of morphogens were assessed in fixed tissues, they were found to be distributed in shallow concentration gradients. However, these shallow gradients led to the demarcation of remarkably sharp domains of downstream gene expression. How cells amplify small changes in the concentration of a morphogen into meaningful binary fate outcomes remains unknown. The growing power of synthetic biology is promising to address this question, and many groups are beginning to take a bottom-up approach to morphogen signal interpretation, engineering synthetic signaling molecules in culture to describe dynamics quantitatively.

A further complication to the morphogen model of patterning has come in the last few decades, as cell and developmental biologists have come to appreciate instructive signals that arise from physical phenomena. Patterns of force that are produced and interpreted by tissues are required for developmental patterning (Desprat, Supatto, Pouille, Beaupaire, & Farge, 2008; Hiramatsu et al., 2013), as are electrical signals (Pai et al., 2015) and proper regulation of the extracellular material properties of tissues (Daley & Yamada, 2013). Together, these results suggest that morphogenesis may be a multimodal process, in which chemical and physical signals are both instructive, and are integrated to drive pattern formation.

## 1.2 *Drosophila* imaginal discs as model tissues for studying organ growth and morphogenesis

An understanding of cell signaling during morphogenesis has been greatly facilitated by the utility of the vinegar fly *Drosophila melanogaster* as a genetically tractable model system. Spearheaded by the lab of Thomas Hunt Morgan at Columbia, the study of fly genetics took off in the early 20<sup>th</sup> century. The size and culture of collaboration within the *Drosophila* research community have produced many technical methods which facilitate cell and developmental biology research. Among these are binary expression systems and the generation of mosaic tissues.

Binary expression systems allow for overexpression or knockdown of genes of interest with both spatial and temporal control. The most popular of these systems utilizes the Gal4 transcription factor and Upstream Activating Sequence (UAS) derived from yeast (reviewed in (M. D. Adams & Sekelsky, 2002)). Expression of Gal4 protein can be controlled by inserting the sequence encoding Gal4 protein downstream of promoters or enhancers of interest. When expressed, Gal4 binds to an UAS sequence, driving transcription of downstream genetic elements. Plasmids containing UAS sequences upstream of RNAi constructs, or the coding sequences of genes, can be integrated into the *Drosophila* genome to allow for gene knockdown or overexpression, respectively. The *Drosophila* research community has generated an enormous collection of transgenic stocks, allowing for rapid RNAi screens, overexpression of genes of interest, and exploration of unique gene expression patterns. More recently, adaption of CRISPR/Cas9-mediated genomic editing techniques in flies has allowed for conditional mutagenesis (Xue et al., 2014) and endogenous tagging of gene products.

A second impactful method available in *Drosophila* is the generation of mosaic tissues, or tissues in which clones of cells mutant for a gene of interest are generated in an otherwise wild-type tissue. Mosaic analysis allows for the study of essential genes, whose loss of function would otherwise be lethal, as well as the investigation of heterotypic interactions between cells of disparate genotypes, and can be carried out using FLP/FRT-mediated mitotic recombination (Golic, 1991), or FLP-mediated excision of a stop codon upstream of Gal4 (reviewed in (Griffin, Binari, & Perrimon, 2014)). The combination of targeted binary expression systems and mosaic analysis, along with derivatives of these systems that allow for lineage tracing, clonal overexpression, or mutagenesis, has endowed the *Drosophila* research community with a wealth of research tools to deploy in a complex model system.

Although *Drosophila* are utilized to study a wide variety of biological phenomena, they have been particularly useful in the characterization of developmental morphogenesis. The larval organs that give rise to adult structures, called imaginal discs, are epithelial tissues that undergo a defined program of growth and patterning to produce adult organs of stereotyped size and shape. As the organization of cells within imaginal discs is similar to that of human epithelial tissues, imaginal discs make tractable models in which to study epithelial tissue biology (Beira & Paro, 2016).

The wing imaginal disc is composed of three regions of tissue: the wing pouch, which will evert during metamorphosis to produce the adult wing blade, the hinge, which forms the structure connecting the wing blade to the body of the fly, and the notum, which gives rise to portions of the thorax (Figure 1.1 B). The wing disc forms from a cluster of roughly 30-40 embryonic ectodermal cells (Garcia-Bellido & Merriam, 1971; Mandaravally Madhavan & Schneiderman, 1977; Worley, Setiawan, & Hariharan, 2013), which straddle a parasegment boundary in the second thoracic segment of the animal. This cluster invaginates to form a flat disc, which, over the course of a few days prior to pupariation, undergoes roughly ten rounds of cell division to grow to 30,000-40,000 cells (Martin, Herrera, & Morata, 2009; Milan, Campuzano, & Garcia-Bellido, 1996; Worley et al., 2013). This rapid growth and concomitant patterning, along with the sophisticated genetic toolkit available in *Drosophila*, make the wing imaginal disc one of the most well-studied systems in which to interrogate cell signaling in morphogenesis, and the regulation of organ growth (Beira & Paro, 2016; Hariharan, 2015).

By the time the wing disc is specified, it is already a non-homogenous tissue, comprised of two populations of cells which express unique selector genes. Gene expression differences across parasegment boundaries are set up during early embryogenesis, as a result of a complex cascade of mutually-regulating patterning genes (the “segment polarity network”). In tissue which will give rise to the wing disc, cells to the anterior of the parasegment boundary express the gene *wingless* (Baker, 1987), and cells to the posterior of the boundary express the transcription factor *engrailed* (Kornberg, Siden, O'Farrell, & Simon, 1985). This expression pattern is retained during the specification, invagination, and development of the wing imaginal disc. Over the course of larval development, regions of wing disc tissue are further specified by the expression of selector genes that drive differentiation into the major cell types of the wing, hinge, and notum.

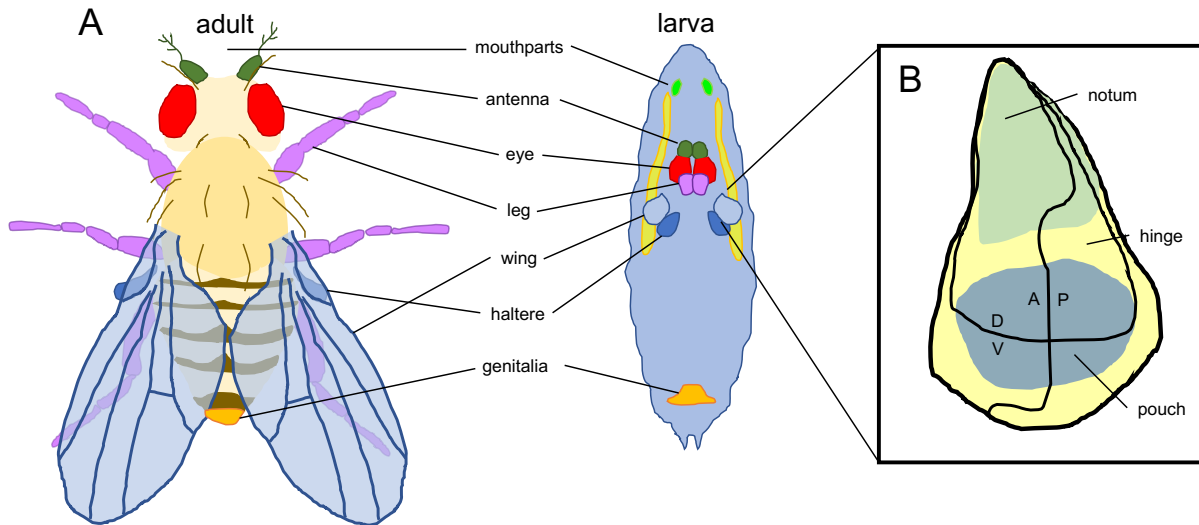


Figure 1.1: ***Drosophila* development and wing imaginal disc anatomy.**

(A) The larval imaginal discs that give rise to adult structures. (B) *Drosophila* larval wing imaginal disc. Black lines show the anteroposterior and dorsoventral compartment boundaries. The notum gives rise to portions of the dorsal thorax, the hinge gives rise to tissue that connects the adult wing to the body wall, and the pouch gives rise to the wing blade.

One fascinating property of the wing imaginal disc is its compartmentalization into anterior, posterior, dorsal, and ventral lineage-restricted populations. The phenomena of compartmentalization was first described by Antonio Garcia-Bellido and colleagues (Garcia-Bellido, Ripoll, & Morata, 1973), who generated marked clones in the wing. Across most of the wing, neutral clones displayed wiggly boundaries, suggesting that cells within the clones were able to intermingle with surrounding tissue. However, in some locations, clones displayed remarkably smooth, and sharp boundaries, indicating the cells in the clone were not intermixing with neighbors. Careful characterization of these clones resulted in the definition of boundaries in the tissue across which cells could not cross. These “compartment boundaries” ran through the center of the wing disc, and divided it into anterior and posterior compartments, and dorsal and ventral compartments. Cells respect the boundary even if they are given growth advantages, and cell competition does not occur across the boundary (reviewed in (Morata, 2021)). Importantly, compartment boundaries have now been described in diverse systems, including the hindbrain of vertebrate embryos (Lumsden & Keynes, 1989), and the abdomen of invertebrates (Lawrence, Green, & Johnston, 1978), suggesting that they may be a conserved mechanism of tissue organization.

The generation and maintenance of compartment boundaries is vital to the growth and patterning of the wing imaginal disc, as they represent signaling centers within the tissue. Cells of the posterior compartment produce the morphogen Hedgehog, which is a target of the transcription factor *engrailed* (Tabata, Eaton, & Kornberg, 1992). Hh is received by cells in the anterior compartment, which express the transcriptional co-effector *Cubitus interruptus* (Ci) (Figure 1.2 A). Due to its low diffusability, only cells just anterior to the compartment boundary receive detectable concentrations of Hh ligand, and respond to the signal by stabilizing the transcriptional co-effector Ci. Stabilization of Ci results in the expression of Hh target genes, like Decapentaplegic (Dpp), the fly homologue of BMP2/4, which diffuses across the tissue and acts as a pro-growth signal, as well as to further specify domains of the disc (Tanimoto, Itoh, ten Dijke, & Tabata, 2000). The dorsoventral compartment boundary is defined after the anteroposterior boundary, and is the site of Wingless (Wg), the fly homologue of Wnt, expression.

### *The Hedgehog pathway*

Hedgehog signaling, a potent developmental signaling pathway with high activity at the anteroposterior compartment boundary in the wing disc, has been implicated in patterning and fate specification, and hyperactivation of the pathway has been shown to lead to overgrowth and neoplasia (reviewed in (Jiang & Hui, 2008)). Although the Hh pathway is evolutionarily conserved and required for patterning in vertebrates, its components and their distribution within the cell differ significantly in flies. Currently, central unanswered questions for researchers studying the Hh pathway include how Hh is released and transported across a tissue, and the mechanism by which Hh activates the GPCR-like activator Smoothed (Smo) in signal-receiving cells. I will discuss recent efforts and progress towards addressing these two questions.

While Hh signaling is compartmentalized in primary cilia in vertebrate cells, signaling takes place on the cell surface in flies. Hh is modified with cholesterol and palmitic acid before it is released from cells of the posterior compartment (Ducuing, Mollereau, Axelrod, & Vincent, 2013). Release of Hh from posterior cells occurs basolaterally, and is dependent specifically on the 12-transmembrane protein Dispatched (Callejo et al., 2011). In the absence of Dispatched, cholesterol modified, but not cholesterol-free, Hh is retained in posterior cells (Burke et al., 1999). Intriguingly, it is not known how exactly Dispatched mediates Hh release. Dispatched bears homology to a family of proton gradient-driven transporters (the resistance nodulation-division family), suggesting that it may be involved in directly mediating the translocation of the hydrophobic Hh molecule across membranes.

Due to its hydrophobic nature, it is unclear to what extent Hh freely diffuses across extracellular space after its release. Multiple models of long-range Hh transport have been proposed, buttressed by compelling experimental evidence, suggesting that there may be more than one route Hh takes between producing and releasing cells. In a variety of systems, Hh has been shown to be released in exovesicles (Tanaka, Okada, & Hirokawa, 2005), lipoproteins (M. H. Chen, Li, Kawakami, Xu, & Chuang, 2004), or multimers (Goetz, Singh, Suber, Kull, & Robbins, 2006). These higher-order structures may shield hydrophobic Hh domains and mediate long-range diffusion (Palm et al., 2013). In wing discs, Hh has also been shown to be transported along thin cellular projections called cytonemes. Cytonemes are specialized signaling filopodia which mediate interactions between multiple cell types in the wing disc. Live imaging studies have shown that many Hh pathway components, including Hh itself, its receptor Patched (Ptc), and proteins involved in Hh release and reception, are transported between anterior and posterior cell populations, and that this transport is dependent on a number of proteins canonically associated with synaptic transmission (W. Chen, Huang, Hatori, & Kornberg, 2017) (González-Méndez, Seijo-Barandiarán, & Guerrero, 2017). Complicating the picture further is the observation that distinct pools of Hh protein, localized to the apical and basal surfaces of disc epithelium respectively, may contribute independently to long- and short-range signaling (Ayers, Gallet, Staccini-Lavenant, & Therond, 2010). Therefore, a coherent model of Hh transport across tissues has yet to be established.

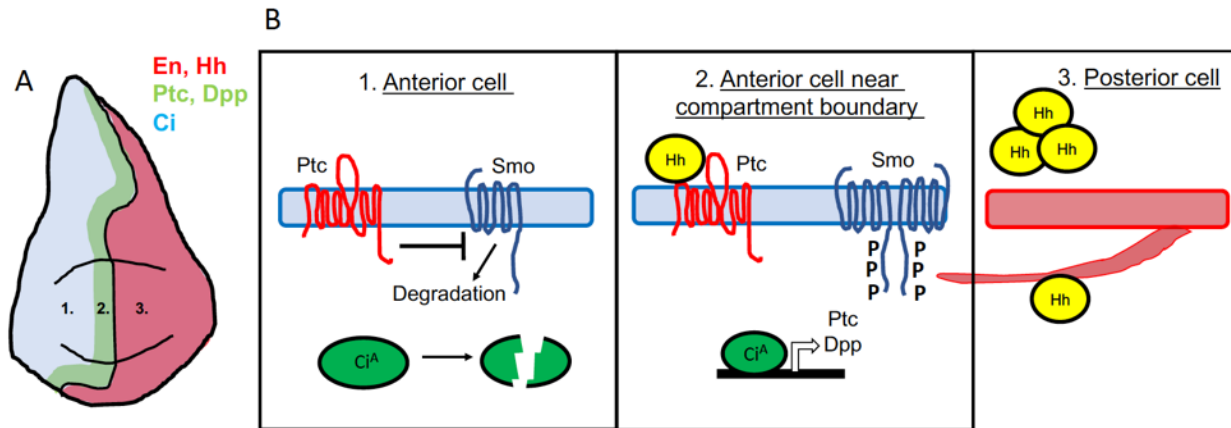


Figure 1.2: **Hedgehog signaling in the wing disc.**

(A) Patterns of expression of Hedgehog (Hh) pathway components in the third instar wing imaginal disc. Hh expression is regulated in the posterior compartment by the transcription factor Engrailed (En) (red). Cells of the anterior compartment express the transcriptional co-effector Cubitus interruptus (Ci) (light blue). In cells just anterior to the compartment boundary, Hedgehog target genes including Patched (Ptc) and Decapentaplegic (Dpp) are expressed (green). (B) Hedgehog signal transduction in cells of the imaginal wing disc. In cells of the anterior compartment which do not receive Hh morphogen, the transmembrane protein Ptc represses the GPCR-like protein Smo. Smo is ubiquitinated, and degraded. In the absence of activated Smo, the transcriptional co-effector Ci is cleaved from an active to inactive form, and Hh target genes are not expressed. Cells just anterior to the compartment boundary receive Hh morphogen from the posterior compartment. Hh binds to the extracellular domain of Ptc, which represses Ptc, and relieves Smo from Ptc-mediated repression. Smo is phosphorylated on intracellular residues, and is stabilized in multimers at the cell membrane. Activation of Smo results in accumulation of the active, full-length isoform of Ci, which drives expression of Hh target genes, like Ptc and Dpp. Posterior cells release Hh morphogen via multiple mechanisms, including lipoprotein particles, multimers, and via cytonemes.

In the wing disc, Hh signal is received by cells just anterior to the anteroposterior compartment boundary. However, the molecular mechanism by which Hh activates downstream pathway components has remained elusive. It is known that Hh binds to an extracellular domain of Patched (Ptc), a transmembrane transporter protein expressed in a domain of cells just anterior to the compartment boundary, and whose activity depends on a gradient of sodium across the cell membrane (Myers, Neahring, Zhang, Roberts, & Beachy, 2017). Hh binding relieves Ptc-mediated inhibition of the Hh activator Smo, which is then phosphorylated by Protein Kinase A and stabilized at the cell membrane. Smo stabilization results in reduced proteolytic cleavage of the transcriptional co-effector Ci from its active to inactive form. Active Ci mediates expression of Hh target genes, among which is the Hh receptor Ptc (Figure 1.2 B).

A central unanswered question in the field regards the mechanism by which Ptc inhibits Smo in the absence of Hh ligand, and how this repression is alleviated upon Hh reception. It is known that in the absence of Hh, Smo is ubiquitinated at intracellular residues, endocytosed, and degraded (Li et al., 2012). Surprisingly, no physical interaction between Ptc and Smo has been convincingly demonstrated in *Drosophila* (Ingham et al., 2000). Additionally, Ptc-mediated inhibition is sub-stoichiometric; one molecule of Ptc can inhibit more than one molecule of Smo (Taipale, Cooper, Maiti, & Beachy, 2002). Therefore, leading models propose that Ptc inhibits Smo indirectly, perhaps by modulating the abundance of an inhibitor or activator.

An attractive candidate for such a second-messenger is cholesterol, which has been shown to be both necessary and sufficient for Smo activation (Luchetti et al., 2016). Recent structural studies have identified a hydrophobic pore within Ptc, which could mediate the transport of sterols (Gong et al., 2018). Given the homology of Ptc with ion-driven transporters, its potential to transport cholesterol, and the Smo-activating functions of cholesterol, it is possible that Ptc acts to regulate the abundance of cholesterol in the cell membrane, thereby indirectly repressing Smo. Binding of Hh may repress this transporter function, resulting in a local increase in cholesterol.

Due to its organizing activity at the anteroposterior compartment boundary, investigation of mechanisms of compartment boundary formation and maintenance have focused on Hh pathway components, as well as cell-cell adhesion molecules, cortical tension, and innate immunity molecules. Preferential cell adhesion was an early and attractive model of compartment segregation, but efforts to identify anteroposterior compartment-specific cell-cell adhesion molecules *in vivo* have been largely unsuccessful. However, experiments in culture suggest that cells expressing Ihog and Ptc (mimicking anterior cells) preferentially aggregate together when mixed *in vitro* with cells expressing Ihog and Hh (mimicking posterior cells) (Hsia et al., 2017). Self-aggregation was proposed to be due to Hh-mediated degradation of Ihog in anterior cells, but the mechanisms linking Ihog to known cell adhesion molecules are unknown.

It has also been observed that cortical tension at the anteroposterior compartment boundary is increased roughly 2.5-fold relative to cells within the compartments, an effect that is dependent on Myosin II (Landsberg et al., 2009). Modeling suggests that

increased tension may bias cell divisions in order to reduce cross-boundary intercalations. Interestingly, reducing Hh signaling results in decreased cortical tension, although direct connections between Hh signaling components and actomyosin structures have not been established.

Compartment boundary maintenance depends on Hh signal transduction across the boundary. Clones of cells mutant for the Hh activator Smo, when generated in wild-type tissue, form smooth boundaries with both the anterior and posterior compartments, and sort out to locations between the two compartments (Blair & Ralston, 1997; Rodriguez & Basler, 1997). Recent work has also demonstrated that Eph/Ephrin molecules are involved in boundary maintenance (Umetsu, Dunst, & Dahmann, 2014). However, although more than fifty years have passed since the discovery of the imaginal disc anteroposterior compartment boundary and its associated signaling center, we are still without a complete mechanistic understanding of how cell populations are segregated with such fidelity through the tumult of developmental morphogenesis.

### **1.3 Ion channels in developmental morphogenesis**

Although the bulk of developmental studies in the twentieth century focused on morphogen signaling and developmental genetics, work in the last twenty years has highlighted the role of biophysical inputs in patterning and growth. It is now well appreciated that cells and tissues can both produce and respond to patterns of mechanical force, and in many cases, these forces are instructive in driving patterning. However, another biophysical parameter of cells, the electrochemical potential maintained across the plasma membrane, is increasingly understood to be both dynamic and patterned in developing tissues, suggesting that electrical signaling may also play a role in morphogenesis.

Membrane potential is defined as the difference in concentration of charged species across an insulating membrane, and is set up and maintained by the action of ion channels and pumps. Chemical gradients of sodium and potassium across the cell membrane are driven by Na<sup>+</sup>/K<sup>+</sup> ATPases, a class of ion pumps that hydrolyzes ATP to pump three sodium ions out of the cell, and two potassium ions into the cell, for each cycle of activity. The resting membrane potential of a cell is a function of the abundance and gating of numerous ion channels, which mediate flux of particular ions into or out of the cell according to the relationship between current membrane potential and the resting potential of the ionic species. While excitable cells like neurons and muscle undergo well-characterized, dramatic changes in membrane potential following stimulation, non-excitable cells also display changes in membrane potential over time. For example, the membrane potential of many cell types is correlated with cell cycle stage; cells are generally hyperpolarized preceding S phase, followed by membrane depolarization throughout mitosis (Blackiston, McLaughlin, & Levin, 2009; Cone, 1969).

Given that the behavior and function of peripheral and integral membrane proteins are directly impacted by the electrical environment, changes in membrane potential are likely to impact many aspects of cell biology. Clustering of K-ras molecules depends on

particular values of membrane potential (Zhou et al., 2015), and membrane potential has been shown to reversibly influence the polymerization and bundling of actin fibers (Chifflet, Hernandez, Grasso, & Cirillo, 2003; Nin, Hernandez, & Chifflet, 2009). At the level of cell behavior, maintenance of particular values of membrane potential correlate with biological characteristics. In general, cells that are more depolarized tend to be more proliferative and un-differentiated, and include cells of the early embryo, many cancer cell lines, and iPSCs (reviewed in (Abdul Kadir, Stacey, & Barrett-Jolley, 2018)). Terminally differentiated and quiescent cells tend to be more hyperpolarized. The connection between membrane potential and gene expression programs is an area of active investigation, but evidence exists that membrane potential could directly impact gene expression through modulating calcium flux, and downstream activation of calcium-responsive transcription factors (Barbado, Fablet, Ronjat, & De Waard, 2009).

Channelopathies, or lesions in ion channels, are the cause of many heritable birth defects. Mutations in inwardly rectifying potassium channels induce abnormal craniofacial development in mice and humans, and aberrant wing vein and eye development in flies, phenomena linked to regulation of BMP signaling (Belus et al., 2018; Dahal et al., 2012; Donaldson, Yoon, Fu, & Ptacek, 2004). Timothy syndrome, which results in digit abnormalities, is caused by mutations in the CaV1.2 calcium channel (Dixon, Cheng, Mercado, & Santana, 2012), and TRPV4 channel disruption causes dramatic skeletal defects (Nishimura et al., 2012).

In addition to genetic evidence linking the action of ion channels to morphogenesis, dynamic patterns of membrane potential across fields of cells in developing systems have been recently described. These studies largely employ voltage-reporting dyes, which allow for visualization of subtle changes in membrane potential across fields of hundreds or thousands of non-excitable cells. Culturing *Xenopus* tadpoles in a membrane potential reporting dye uncovered dynamic patterns of membrane potential that emerged during craniofacial morphogenesis, as a result of patterned expression of H<sup>+</sup>-V-ATPase pumps (Vandenberg, Morrie, & Adams, 2011). Ablation of those pumps resulted in significant craniofacial defects. Membrane potential is also patterned in the *Drosophila* ovarian follicle, where it impacts the polarization of the cytoskeleton in the follicle epithelium (Weiss & Bohrmann, 2019a, 2019b). More recently, chondrocyte precursors in the developing vertebrate limb have been shown to be more depolarized relative to surrounding tissues, by virtue of increased expression of epithelial sodium channels. Pharmacological blockade or genetic ablation of epithelial sodium channels in the chondrocyte precursor population resulted in failure to differentiate into osteoblasts, and subsequent altered limb development (Atsuta, Tomizawa, Levin, & Tabin, 2019). Taken together, these data suggest that, like morphogen production or patterns of physical force, membrane potential may be dynamically patterned during development, and an instructive signal in morphogenesis.

#### *Piezo channels in development and differentiation*

Mechanosensitive ion channels are emerging as regulators of many cell behaviors central to morphogenesis. Piezo, a well-characterized mechanosensitive cation

channel, has recently been implicated in numerous morphogenic processes. Piezo channels are large, and possess an incredible number of transmembrane domains (thirty eight in mouse). Recently published cryo-EM studies have shown that Piezo channels form homotrimers. Each monomer contains a blade, which emanates from the central pore of the channel via a beam structure, and deforms the membrane surrounding the channel (Zhao et al., 2018). Current models propose that the blades and beams transduce changes in membrane curvature to the pore, resulting in channel opening following stretch or compression (Fang et al., 2021).

In zebrafish, the development of the heart outflow tract valve is regulated by mechanical forces. Piezo channels expressed in the outflow tract sense mechanical signals, and modulate the activity of Hippo and Notch pathway components to coordinate outflow tract morphogenesis (Duchemin, Vignes, & Vermot, 2019). Piezo channels are also key mediators of hydrostatic pressure-induced odontoblast differentiation, and control the translocation of the transcription factor RUNX2 to the nucleus in these cells (Miyazaki et al., 2019). In the *Drosophila* gut, Piezo expression marks an enteroendocrine precursor population, and mechanical signal transduction via the channel is responsible for differentiation into enteroendocrine cells (He, Si, Huang, Samuel, & Perrimon, 2018). Additionally, Piezo channels regulate pressure-induced blebbing migratory behaviors, via a mechanism that involves modulating intracellular calcium concentration (Srivastava, Traynor, Piel, Kabla, & Kay, 2020). Taken together, these data suggest that mechanosensitive ion channels comprise a conserved signaling mechanism which transduces extrinsic mechanical forces to changes in cell physiology and transcriptional state.

An outstanding challenge in the field of developmental bioelectricity concerns linking ion channel expression, membrane potential, and downstream cell biology. Advances in imaging conditions and voltage-reporting dye development, as well as the increased genetic tractability of previously intractable model systems, promise to usher in a more complete understanding of the role of membrane potential in patterning and growth.

#### **1.4 Summary of dissertation work**

Due to its experimental tractability, *Drosophila* is an ideal model system in which to study the effects of membrane potential on patterning and growth. It has previously been reported that expression of Kir2.1 channels is required for the regulated release of the developmental morphogen Decapentaplegic (Dpp, the *Drosophila* TGF- $\beta$ /BMP family proteins) in the wing imaginal disc, and that ablation of this channel results in undergrowth and mispatterning of the wing (Dahal, Pradhan, & Bates, 2017). Building off of this observation, I combined live imaging, genetic manipulation, and optogenetics to dissect the role of membrane potential and ion channel expression in the morphogenesis of a model epithelium, the third instar wing imaginal disc.

Early in the course of my thesis research, I discovered that membrane potential was patterned in the wing imaginal disc. Cells anterior to the compartment boundary, a region of high Hh signal transduction, are more depolarized than surrounding tissue.

Using published comparative gene expression datasets, I identified sets of differentially expressed ion channels and pumps across the compartment boundary, and demonstrated that the increased expression of epithelial sodium channels, specifically the channel Ripped Pocket, in anterior cells is required for patterned depolarization. The expression of these endogenous channels is dependent on high levels of Hh signal transduction. Using optogenetics in the salivary gland as well as the wing disc, I demonstrated that membrane potential facilitates Hh signaling by increasing the abundance of the Hh activator Smo at the cell membrane, an effect that is independent of Ptc. This work, described in Chapter 2, describes a novel physiological input into the regulation of developmental signaling in a model epithelium.

While exploring expression patterns of ion channels and pumps in the wing imaginal disc, I discovered that Piezo, a mechanosensitive cation channel, was expressed in a subset of cells distributed throughout the disc. Knockdown of Piezo in that cell subset resulted in overgrowth of the larval wing disc, as well as larger adult wings. I validated this effect in Piezo mutants, and found that it was due to an increase in cell size, as opposed to increased numbers of cells, an effect potentially due to increased insulin/Pi3K signaling. Chapter 3 describes this work, which represents an intriguing new model for sensation and control of organ size.

Heterotypic interactions between cells of different properties abound during development. Given that the wing disc is comprised of populations with different values of membrane potential, I set out to explore mechanisms mediating interactions between cells of disparate membrane potential. With Riku Yasutomi, I found that clones of depolarized cells are preferentially recovered in the anterior compartment of the wing disc. Clones in the posterior compartment are eliminated via a mechanism reminiscent of cell competition. Chapter 4 describes this work, which suggests that membrane potential is sensed in non-autonomous manner, and is an important input in relative cell fitness.

A previous graduate student in the laboratory, Jo Bairzin, discovered that clones of cells which express a constitutively active allele of the Hippo pathway co-effector Yorkie overgrow, and misexpress developmental selector genes. Yki-expressing clones of cells in the posterior compartment express the Hh pathway co-effector Ci, a gene whose expression is normally constrained to the anterior compartment. This misexpression of Ci results in developmental signaling interactions between the overgrowing cell population and wild-type neighbors. I contributed to this work by defining the requirement of Scalloped in Yki-mediated misexpression of Ci, and validating other results. This work, presented in Chapter 5, highlights transcriptional plasticity in tumor models, as well as identifies the tumor boundary as an important signaling center.

## Chapter One

### Membrane potential modulates Hedgehog signaling in the wing imaginal disc.

This chapter is a reproduction of the following paper:

Emmons-Bell M., Hariharan I.K. (2021). Membrane potential modulates Hedgehog signalling in the wing imaginal disc. *EMBO Reports* 2021(22), e51861

I contributed to study design, designed and executed all experiments, collected and analyzed data, and wrote and edited the manuscript with IKH.

## Abstract

While the membrane potential of cells has been shown to be patterned in some tissues, specific roles for membrane potential in regulating signalling pathways that function during development are still being established. In the *Drosophila* wing imaginal disc, Hedgehog (Hh) from posterior cells activates a signalling pathway in anterior cells near the boundary which is necessary for boundary maintenance. Here, we show that membrane potential is patterned in the wing disc. Anterior cells near the boundary, where Hh signalling is most active, are more depolarized than posterior cells across the boundary. Elevated expression of the ENaC channel Ripped Pocket (Rpk), observed in these anterior cells, requires Hh. Antagonizing Rpk reduces depolarization and Hh signal transduction. Using genetic and optogenetic manipulations, in both the wing disc and the salivary gland, we show that membrane depolarization promotes membrane localization of Smoothened and augments Hh signalling, independently of Patched. Thus, membrane depolarization and Hh-dependent signalling mutually reinforce each other in cells immediately anterior to the compartment boundary.

## Introduction

During the development of multicellular organisms, cell–cell interactions have an important role in regulating cell proliferation and cell fate specification. In both invertebrates and vertebrates, the Hedgehog (Hh) signalling pathway has been implicated in patterning a number of tissues during development (Lee, Zhao, & Ingham, 2016). Alterations of this pathway have been implicated in human diseases. Reduced Hh signalling can result in congenital abnormalities such as holoprosencephaly (Xavier et al., 2016), and increased activity of the pathway has been implicated in multiple types of cancer (Raleigh & Reiter, 2019; Wu, Zhang, Sun, McMahon, & Wang, 2017). In recent years, this pathway has been targeted pharmacologically with the goal of reducing its activity in cancers where the pathway is excessively active. Identifying all the ways that this conserved pathway is regulated is of importance in understanding its role in regulating development and for devising ways to alter its activity in disease states.

Initially discovered for its role in regulating segment polarity in *Drosophila* (reviewed in (Ingham, 2018)), Hh signalling has since been implicated in a multitude of developmental processes. Among the best characterized is the signalling between two populations of cells that make up the *Drosophila* wing imaginal disc, the larval primordium of the adult wing and thorax. The wing disc consists of two compartments of lineage-restricted cells separated by a smooth boundary. Posterior (P) cells make the morphogen Hedgehog, which binds to its receptor Patched (Ptc), which is expressed exclusively in anterior (A) cells. Hh has a relatively short range either because of its limited diffusion (Strigini & Cohen, 1997; Tabata & Kornberg, 1994), or because it is taken up by nearby target cells via filopodia-like protrusions known as cytonemes (González-Méndez et al., 2017). Hh alleviates the repressive effect of Ptc on the seven-transmembrane protein Smoothened (Smo) in A cells near the boundary, initiating a signalling cascade that culminates in the stabilization of the activator form of the transcription factor Cubitus

interruptus (Ci), and expression of target genes such as the long-range morphogen Dpp (Jiang & Hui, 2008; Lee et al., 2016; Petrov, Wierbowski, & Salic, 2017). In turn, Dpp regulates imaginal disc patterning and growth in both compartments (Hamaratoglu, Affolter, & Pyrowolakis, 2014).

While the role of cell–cell interactions, diffusible morphogens and even mechanical forces have been studied in regulating the growth and patterning of the wing disc, relatively little attention has been paid to another cellular parameter, membrane potential or  $V_{mem}$ .  $V_{mem}$  is determined by the relative concentrations of different species of ions across the cell membrane, as well as the permeability of the membrane to each of these ions. These parameters are influenced by the abundance and permeability of ion channels, the activity of pumps, and gap junctions. While changes in  $V_{mem}$  have been studied most extensively in excitable cells, there is increasing evidence that the  $V_{mem}$  of all cells, including epithelial cells, can vary depending on cell-cycle status and differentiation status (Blackiston et al., 2009; Sundelacruz, Levin, & Kaplan, 2009). Mutations in genes encoding ion channels in humans (“channelopathies”) can result in congenital malformations (Plaster et al., 2001). Similarly, experimental manipulation of ion channel permeability can cause developmental abnormalities in mice as well as in *Drosophila* (Belus et al., 2018; Dahal et al., 2017). Only more recently has evidence emerged that  $V_{mem}$  can be patterned during normal development. Using fluorescent reporters of membrane potential, it has been shown that specific cells during *Xenopus* gastrulation and *Drosophila* oogenesis appear more depolarized than neighbouring cells (Krüger & Bohrmann, 2015; Pai et al., 2015). A recent study established that cells in the vertebrate limb mesenchyme become more depolarized as they differentiate into chondrocytes, and that this depolarization is essential for the expression of genes necessary for chondrocyte fate (Atsuta et al., 2019). However, in many of these cases, the relationship between changes in  $V_{mem}$  and specific pathways that regulate developmental patterning have not been established.

Here we investigate the patterning of  $V_{mem}$  during wing disc development and show that the regulation of  $V_{mem}$  has an important role in regulating Hh signalling. We show that the cells immediately anterior to the compartment boundary, a zone of active Hh signalling, are more depolarized than surrounding cells, and that Hh signalling and depolarized  $V_{mem}$  mutually reinforce each other. This results in an abrupt change in  $V_{mem}$  at the compartment boundary.

## Materials and Methods

### *Drosophila* strains and husbandry

Animals were raised on standard medium as used by the Bloomington *Drosophila* Stock Center. All animals were raised at 25°C, except *ap>rpk-RNAi* crosses, which were raised at 18°C to reduce lethality. Crosses using GAL80<sup>TS</sup> and the hh<sup>TS2</sup> allele were raised at 18°C and then upshifted to 30°C at the reported timepoints.

Stocks used in this study include the following: *hsFLP*; *act<stop<Gal4*, *UAS-RFP/S-T*, *yw;ap-Gal4/Cy0*; *TM2/TM6B*; *ap-Gal4*; *ptc>RFP*; *w*; *UAS-Ci3 M*; *71B-Gal4*, and *w;UAS-Kir2.1*; *UAS-Kir2.1/TM6B* (from Kristin Scott, UC Berkeley, USA).

Stocks obtained from the Bloomington Stock Center (Bloomington, IN, USA) include *UAS-ArcLight* (BL:51056), *UAS-rpk-RNAi*; (BL:39053, 25847—data using BL:39053 are shown and confirmed with BL:25847), *UAS-NaChBac*; (BL:9466), *UAS-ChR2::mCherry*; (BL:28995), *UAS-ReaChR::Citrine*; (BL:53741), *UAS-ChloC::tdTom* (BL:76328), *en-Gal4*; (BL:6356); *UAS-Ptc-RNAi*; (BL:55686).

### *Live imaging and optogenetics*

Larvae were washed with 70% EtOH and PBS prior to dissection. Live tissue was dissected in Schneider's media (#21720001, Gibco), and care was taken to not damage or stretch tissue. For DiBAC staining, imaginal discs were incubated in 1.9  $\mu$ M DiBAC<sub>4</sub>(3) (bis-(1,3-dibutylbarbituric acid) trimethine oxonol; DiBAC<sub>4</sub>(3); Molecular Probes)) in Schneider's media for 10 min with gentle rotation. A small amount media was used to mount the discs, such that the addition of a coverslip did not destroy the tissue, and discs were imaged right away. 100  $\mu$ M amiloride (#A7419, Sigma-Aldrich) and 100  $\mu$ M ouabain (#O3125, Sigma-Aldrich) were added to DiBAC solution for pharmacology experiments. Discs imaged in FM4-64 dye (#T13320, Thermo Fisher) were incubated in 9  $\mu$ M FM4-64, and imaged without washing, to preserve staining of the cell membrane.

For optogenetics experiments in the salivary gland, carcasses were dissected and cleaned (fat body removed) in Schneider's medium. Carcasses were loaded onto a glass cover slip in a large drop of Schneider's, and either kept in the dark (control condition) or exposed to activating light (480 nm for ChR2 and ChloC experiments, 647 nm for ReaChR experiments). After exposure, carcasses were immediately fixed and prepared for immunohistochemistry. For optogenetics experiments using the ChR2 channel in the wing imaginal disc, carcasses were dissected and cleaned (fat body removed) in Schneider's medium, then either fixed (0 min activating light condition), or loaded onto a glass cover slip in a large drop of Schneider's, and exposed to 25 min of activating light (480 nm). Following activation, discs were fixed and prepared for immunohistochemistry. For experiments using the ReaChR channel in the wing imaginal disc, flies were raised on a 12-h light/dark cycle, and imaginal discs were harvested and prepared for immunohistochemistry during the third larval instar.

### *Immunohistochemistry*

Imaginal discs were dissected in phosphate-buffered saline, fixed for 20 min in 4% PFA at room temperature, permeabilized in phosphate-buffered saline with 0.1% Triton X-100, and blocked in 10% Normal Goat Serum. Primary antibodies used were: rat anti-Ci (1:10, #2A1; Developmental Studies Hybridoma Bank, DSHB), mouse anti-Smo (1:10, #20C6; DSHB), rabbit anti-Rpk (1:500) (gift from Dan Kiehart), mouse anti-ATP $\alpha$  (1:100, #a5; DSHB), mouse anti-Cut (1:100, #2B10; DSHB), mouse anti-Wg (1:100, #4D4

DSHB), and mouse anti-Ptc (1:50, #Apa1; DSHB). Secondary antibodies used were: goat anti-rabbit 488 (#A32731; Invitrogen), goat anti-mouse 488 (#A32723; Invitrogen), goat anti-mouse 555 (#A32727; Invitrogen), goat anti-rat 555 (#A-21434; Invitrogen), goat anti-mouse 647 (#A32728; Invitrogen), goat anti-rabbit 647 (#A32733; Invitrogen) and goat anti-rat 647 (#A-21247; Invitrogen). Nuclei were stained with DAPI (1:1,000, Cell Signaling). Samples were imaged on a Zeiss Axio Imager.M2 with Apotome.2.

### *Quantification and statistical analysis*

Fluorescence intensity measurements were recorded using FIJI software (NIH, Bethesda, USA). P values were obtained using ANOVA and unpaired Student's t-tests (GraphPad). Error bars in all graphs are standard deviation. P value significance < 0.001: \*\*\*; 0.001 to 0.01: \*\*; 0.01 to 0.05: \*; > 0.05: not significant.

### *Mosaic tissue generation*

To generate clones expressing *ci3m* or *ptc<sup>RNAi</sup>*, *hsFLP;;act<STOP<UAS-RFP/S-T* virgin females were crossed to *UAS-Ci3m* or *UAS-Ptc<sup>RNAi</sup>* males. Larvae were collected as described above, and vials were subjected to a 10 min heat shock in a 37°C water bath 48 h before dissection and live imaging in DiBAC, or fixation and preparation for immunohistochemistry.

## **Results**

We began by asking whether or not  $V_{mem}$  is patterned in the wing imaginal disc. Wing imaginal discs from third-instar larvae were dissected and incubated in Schneider's medium containing the  $V_{mem}$  reporting dye DiBAC<sub>4</sub>(3) (hereafter DiBAC) at a concentration of 1.9 μM for 10 min. DiBAC is an anionic, membrane-permeable, fluorescent molecule that accumulates preferentially in cells which are relatively depolarized compared to surrounding cells due to its negative charge and has been used to investigate patterns of endogenous  $V_{mem}$  in non-excitable cells in a variety of organisms (D. S. Adams & Levin, 2012; Atsuta et al., 2019; Krüger & Bohrmann, 2015). In contrast to patch-clamp electrophysiology, utilizing DiBAC allowed us to make comparisons of membrane potential across a field of thousands of cells.

A stripe of cells running through the middle of the pouch of the wing disc appeared more fluorescent, thus indicating increased DiBAC uptake (Figure 2.1A and 2.1B), suggesting that these cells are more depolarized than surrounding cells. This pattern of fluorescence was observed in more than 35 individual wing imaginal discs and was not observed when imaginal discs were cultured in the voltage-insensitive membrane dye FM4-64 (Figure 2.1C-E). Patterned DiBAC fluorescence was observed at both apical (Figure 2.1 A-A') and basal (Figure 2.1 B-B') focal planes. Addition of the Na<sup>+</sup>/K<sup>+</sup> ATPase inhibitor ouabain to the cultured discs, which depolarizes cells by collapsing transmembrane Na<sup>+</sup> and K<sup>+</sup> gradients, resulted in increased, and more uniform, DiBAC fluorescence (Figure 2.1 F and G), indicating that patterned DiBAC

fluorescence in wing disc tissue was contingent upon mechanisms that normally maintain  $V_{mem}$ .

The position of the stripe of altered  $V_{mem}$  is reminiscent of the anteroposterior (A-P) compartment boundary in the wing disc, which separates two lineage-restricted populations—the A cells and the P cells. In order to identify the population of depolarized cells with respect to the compartment boundary, we examined discs expressing *UAS-RFP* under the control of *patched-Gal4* (*ptc>RFP*) that had been incubated in DiBAC. *ptc>RFP* is expressed in those cells that express the highest levels of endogenous *ptc*, which are immediately anterior to the compartment boundary. The cells in which DiBAC accumulated at higher levels correlated with expression of RFP throughout the third larval instar (Figure 2.1 H-H’), indicating that cells anterior to the compartment boundary are more depolarized than cells across the compartment boundary in the posterior compartment. *ptc*-expressing cells in the hinge also were more fluorescent upon DiBAC staining (Figure 2.1 H, yellow arrowheads), but for the purposes of this work we focused on the wing pouch (Figure 2.1 H, white arrowhead). As with *ptc-Gal4* expression, the domain of relative depolarization was broader in early third-instar wing discs, becoming more and more restricted to cells just anterior to the compartment boundary over the course of developmental time (Figure 2.1 I-I’).

#### *Expression and function of endogenous ion channels anterior to the compartment boundary*

The resting potential,  $V_{mem}$ , results from the activity of a large number of different transporters of charged molecules, as well as the permeability of the membrane to each of those molecules. Thus, the relative depolarization of the region immediately anterior to the compartment boundary is unlikely to result simply from a change in the activity of a single pump or channel. However, by identifying transporters expressed in this region, it should be possible to manipulate  $V_{mem}$  by altering their expression or properties. To that end, we examined a published transcriptome data set (Willsey et al., 2016), comparing the abundance of transcripts in *ptc*-expressing cells with those of cells in the posterior compartment. In this data set, we noticed several ion channels with differential expression between the two populations of cells. Among these are two members of the Degenerin Epithelial Na<sup>+</sup> Channel (DEG/ENaC) family of channels, *ripped pocket* (*rpk*) (C. M. Adams et al., 1998), and *pickpocket 29* (*ppk 29*) (Thistle, Cameron, Ghorayshi, Dennison, & Scott, 2012). DEG/ENaC channels are members of a diverse family of amiloride-sensitive cation channels. An antibody that recognizes the Rpk protein has been characterized previously (Hunter, Crawford, Genkins, & Kiehart, 2014), which allowed us to examine its pattern of expression. In late L3 wing discs, we found that Rpk was indeed expressed anterior to the compartment boundary, in a stripe of cells that also express *ptc>RFP* (Figure 2.2 A-A’). In addition, we observed expression of Rpk in cells near the dorsoventral (D-V) boundary. Expression was most obvious in two rows of cells flanking the D-V boundary in the anterior compartment, which are likely to be the two rows of cells arrested in the G2 phase of the cell-cycle (Johnston & Edgar, 1998). Indeed, the pattern of DiBAC uptake in this portion of the wing disc also suggests a very thin stripe of low-fluorescence flanked by two regions of higher fluorescence (see inset

in Figure 2.1 D). This is consistent with previous work showing that cells in culture become more depolarized as they progress through S-phase and peaks at the onset of mitosis (Cone, 1969), reviewed in (Blackiston et al., 2009). Thus, at least in principle, the increased expression of Rpk could contribute to the depolarization observed in these regions of the wing disc.

Since Rpk, and possibly Ppk29, are expressed anterior to the compartment boundary, we tested the effect of blocking these channels by treating discs with amiloride. Amiloride is predicted to reduce the permeability of DEG/ENaC family channels (Garty, 1994). Addition of amiloride did not alter the pattern of Rpk protein expression (Figure 2.2 C-C'). However, amiloride addition abolished the stripe of increased DiBAC fluorescence anterior to the compartment boundary (Figure 2.2 B-B''). These findings suggest that a conductance mediated by one or more channels of the DEG/ENaC family contributes to the relative depolarization of this region. Amiloride addition did not, however, seem to affect the increased DiBAC fluorescence observed at the D-V boundary (Figure 2.2 B''). Since amiloride likely targets multiple ENaC channels, we also depleted Rpk using an RNAi transgene expressed in cells anterior to the compartment boundary using *dpp-Gal4* and *Gal80<sup>TS</sup>*, allowing us to express RNAi in only the 48 h prior to dissection. In these discs, we no longer observed the stripe of increased DiBAC fluorescence that ran along the A-P compartment boundary (Figure 2.2 D and E white arrowhead), while increased fluorescence at the D/V boundary was preserved (Figure 2.2 E, yellow arrowhead). Additionally, we knocked down *rpk* in the wing pouch during the last 48h of larval development using *rotund-Gal4* and *Gal80<sup>TS</sup>*. *rpk* knockdown reduced anti-Rpk antibody staining (Figure 2.8 B and D), validating the efficacy of the dsRNA, and it also reduced DiBAC staining in the wing pouch (Figure 2.8 A and C). From these experiments, we conclude that reducing either the expression or permeability of endogenous DEG/ENaC family channels, notably Rpk, can abolish the region of depolarization anterior to the A-P compartment boundary. Hence, Rpk, and possibly other DEG/ENaC channels, contribute to this local alteration in  $V_{mem}$ .

In most cells, the  $\text{Na}^+/\text{K}^+$  ATPase is primarily responsible for setting a negative  $V_{mem}$ , since it uses ATP hydrolysis to extrude three  $\text{Na}^+$  ions and bring in two  $\text{K}^+$  ions per cycle of activity (Morth et al., 2007). RNA of *ATP $\alpha$*  (Lebovitz, Takeyasu, & Fambrough, 1989), which encodes a subunit of the  $\text{Na}^+/\text{K}^+$  ATPase, was also detected at higher levels in *ptc*-expressing cells (Willsey et al., 2016). Using an antibody to *ATP $\alpha$*  (Roy, Sivan-Loukianova, & Eberl, 2013), we once again observed elevated expression anterior to the compartment boundary, with a hint of increased expression at the D-V boundary (Figure 2.3 A'''). While it is difficult to predict the contribution of patterned expression of each channel to the patterning of  $V_{mem}$ , detection of these channels at the anteroposterior compartment boundary of the wing disc allowed us to manipulate their expression or to pharmacologically alter their properties.

*Patterned expression of rpk and ATP $\alpha$  is regulated by Hedgehog signalling*

Since the increased expression of Rpk and ATP $\alpha$  anterior to the compartment boundary occurs precisely within the region of increased Hh signalling (Figure 2.3 A-A'''), we tested whether manipulating components of Hh signalling pathway could alter expression of Rpk or ATP $\alpha$ . We used a temperature-sensitive *hh* allele (*hh<sup>TS2</sup>*) (C. Ma, Zhou, Beachy, & Moses, 1993) in order to decrease Hh signalling for a short period of time. Larvae were raised at a permissive temperature (18°C) to permit normal *hh* function during early development and then shifted to a restrictive temperature (30°C) during the third larval instar in order to reduce *hh* function and dissected 12 h after the temperature shift. Under these conditions, increased expression of either ATP $\alpha$  or Rpk was not observed anterior to the compartment boundary (Figure 2.3 B-C', controls in Figure 2.9 A-A''), indicating that a normal level of *hh* activity is necessary for the increased expression of these proteins anterior to the compartment boundary. Interestingly, some expression of Rpk is still visible near the D-V boundary in the anterior compartment which is likely *hh*-independent. We then examined the effects of increasing Hh signalling. Since Hh-dependent gene expression in this region typically results from stabilization of the activator form of Cubitus interruptus (Ci) (Aza-Blanc, Ramírez-Weber, Laget, Schwartz, & Kornberg, 1997), we generated clones of cells expressing a constitutively active version of Ci (*ci3m* (Price & Kalderon, 1999)). The *ci3m* allele has S to A mutations at PKA-phosphorylation sites 1–3, rendering the protein more resistant to proteolytic cleavage. These clones had modest increases in expression of both of Rpk and ATP $\alpha$  (Figure 2.3 D-E'''). Additionally, these clones showed increased DiBAC fluorescence (Figure 2.3 F-F'), as did clones expressing RNAi against *ptc* (Figure 2.3 G-G'). *ci3m*-expressing clones showed increased DiBAC fluorescence in both the anterior and posterior compartments (Figure 2.10 A and A'), consistent with the ability of constitutively active Ci to activate Hh target genes in both compartments. Clones expressing *ptc*-RNAi only showed increased DiBAC fluorescence in the anterior compartment, as *ptc* is not expressed in the posterior compartment (Figure 2.10 B and B'). There was not always perfect concordance of increased DiBAC staining with clones, so to describe this variability we quantified the ratio of DiBAC staining in *ci3m*-expressing clones to DiBAC staining to control tissue (Figure 2.10 C). Thus, Hh signalling appears to promote expression of both Rpk and ATP $\alpha$ , as well as relative depolarization of  $V_{mem}$ .

### *Manipulating expression of endogenous ion channels modulates Hedgehog signalling*

We then investigated whether a depolarized  $V_{mem}$  is required for the high levels of Hh signal transduction that occur immediately anterior to the compartment boundary. To that end, we reduced *rpk* expression in the dorsal compartment of the wing imaginal disc using *ap-Gal4* (Figure 2.11 A) and *UAS-rpk<sup>RNAi</sup>*. The Hh signal transducer *smo* is transcribed throughout the *Drosophila* wing imaginal disc, but immunostaining for Smo protein reveals that it is most abundant on cell membranes in the posterior compartment, and in cells directly anterior to the compartment boundary (Figure 2.4 A-A'''). Membrane localization of Smo in the anterior compartment is thought to depend on high levels of Hh signalling (Zhu, Zheng, Suyama, & Scott, 2003). The Hh signalling pathway is active in several rows of cells immediately anterior to the compartment boundary that receive Hh. Additionally, several components of the Hh signalling

pathway are active in the entire posterior compartment, possibly because the absence of Ptc renders Smo constitutively active (F. A. Ramírez-Weber, Casso, Aza-Blanc, Tabata, & Kornberg, 2000). However, target genes are not activated in posterior cells because Ci is only expressed in the anterior compartment. Knockdown of *rpk* resulted in a reduction in membrane staining of Smo in the dorsal compartment, as compared to ventral cells (Figure 2.4 B'). This was observed in both posterior cells which do not express *ptc* and in anterior cells which do. Thus, at least in posterior cells, the effect on Smo localization does not require *ptc* function. In anterior cells near the compartment boundary, Hh signalling also results in stabilization of the activator form of Ci. In *ap>rpk<sup>RNAi</sup>* discs, the level of activated Ci in the dorsal compartment was reduced (Figure 4B''). We also examined the expression of *ptc*, which is a direct transcriptional target of Ci (Alexandre, Jacinto, & Ingham, 1996). The stripe of staining with anti-Ptc was much fainter in the dorsal part of the disc (Figure 4C). Thus, expression of *rpk<sup>RNAi</sup>* reduces Hh signalling in cells anterior to the compartment boundary. Knockdown of ATP $\alpha$  using *ap>ATP $\alpha$ <sup>RNAi</sup>* resulted in severely altered tissue morphology (Figure 2.11C and D), and a reduction in anti-Ptc staining (Figure 2.11 D), suggesting that expression of *ATP $\alpha$ <sup>RNAi</sup>* also reduces Hh signalling. We have shown earlier that antagonizing the function of the Na/K-ATPase, of which ATP $\alpha$  is a component, with ouabain completely abolishes the patterned depolarization in this disc (Figure 2.1 G).

To examine the effect of altering *rpk* expression on pathways other than Hh, we reduced *rpk* expression in the wing pouch using *rotund-Gal4* and *Gal80<sup>TS</sup>* (hereafter *rn<sup>TS</sup>*) (Figure 2.11 B). Larvae were raised at 18°C and then shifted to 30°C for 48 h before dissection and staining. In these discs, anti-Smo and anti-Ci staining were clearly reduced in the wing pouch (Figure 2.11 E-F''). Anti-Ptc staining was also clearly reduced (Figure 2.11 G-H'). All of these observations were consistent with reduced Hh signalling. We also observed a modest reduction in the width of the dorsoventral stripe of Wingless expression in discs expressing *rpk*-RNAi (Figure 2.11 I-J''). More obvious was the absence of expression of the Notch and Wingless target gene, *cut* along the dorsoventral margin (Figure 2.11 K-L'). Thus, in addition to Hh signalling, altering *rpk* impacts other pathways as well.

#### *Manipulating V<sub>mem</sub> regulates Smoothened localization in salivary glands*

Cells of the wing imaginal disc are quite small and columnar, posing a challenge for subcellular imaging. Cells of the salivary gland are much larger than those of the wing disc, allowing for easier visualization of subcellular protein localization. Additionally, much work characterizing the regulation of Smo has been carried out in this tissue (Zhu et al., 2003). To directly test whether or not altering *V<sub>mem</sub>* can modulate Hh signalling, we used the bacterial sodium channel NaChBac, which can be used to cause membrane depolarization in insect cells by overexpression (Luan et al., 2006; Nitabach et al., 2006; Ren et al., 2001). Expression of NaChBac in the salivary gland using the *Gal4* driver line *71B-Gal4* showed a clear increase in membrane-associated staining with anti-Smo (Figure 2.5 A, B and D) as well as increased expression of Ptc (Figure 2.5 E and F). Correspondingly, increased expression of the mammalian potassium channel Kir2.1, which would be predicted to hyperpolarize *Drosophila* cells (Baines, Uhler,

Thompson, Sweeney, & Bate, 2001; Hodge, 2009), reduces fluorescence at the cell surface and increases intracellular fluorescence (Figure 2.5 C and D). Thus, sustained alteration in  $V_{mem}$  modulates Hh signalling as assessed by Smo localization and Ptc expression.

In order to investigate the short-term consequences of altering  $V_{mem}$ , we used channelrhodopsin ChR2, which when exposed to blue light causes membrane depolarization (Nagel et al., 2003; Schroll et al., 2006). In addition to providing a second independent way of depolarizing cells, this approach allowed us to examine short-term changes in Hh signalling that occur in response to depolarization. Dissected, ChR2-expressing salivary glands were either kept in darkness or exposed to activating light for variable intervals of time. Compared to glands kept in the dark, light-exposed glands had higher levels of Smo at the cell membrane (Figure 2.5 G-I), suggesting that even relatively short-term depolarization can facilitate Smo accumulation at the cell surface. A time course showed that an increase in Smo membrane abundance was detectable as early as 10 min and appeared maximal after 25 min of activating light (Figure 2.5 M-Q). A red light-activated depolarizing channelrhodopsin ReaChR (Inagaki et al., 2014; Lin, Knutsen, Muller, Kleinfeld, & Tsien, 2013) also elicited a similar effect (Figure 2.12 A-C). Activation of ChR2 did not alter membrane abundance of the integrin component Mys (Bunch et al., 1992) or the integrin-associated protein Talin (Brown et al., 2002) (Figure 2.12 D-G'). In contrast, expression and activation of ChloC, a blue light-activated anion channel which hyperpolarizes cells (Wietek et al., 2017; Wietek et al., 2014), resulted in a reduction of Smo on the plasma membrane as well as in internal compartments (Figure 2.5 J-L). This suggests that short-term hyperpolarization generally reduces Smo levels, perhaps due to the fact that inactivated Smo is targeted for proteasome-mediated degradation following internalization, as has been reported previously (Li et al., 2012).

#### *$V_{mem}$ regulates Smo membrane localization independently of Ptc in the wing disc*

Since a chemiosmotic mechanism has been hypothesized to drive Ptc-mediated inhibition of Smo (Myers et al., 2017), we wondered if depolarization might reduce the inhibitory effect of Ptc on Smo. If this were the case, ectopically depolarizing cells of the posterior compartment of the wing disc should have no effect on Smo membrane localization, since Ptc is not expressed in these cells (Hooper & Scott, 1989; Nakano et al., 1989). To test this, we expressed ChR2 in the dorsal compartment of the wing disc and exposed dissected wing discs to 25 min of activating light. Smo membrane abundance was increased in the anterior dorsal compartment of these discs as compared to discs not exposed to light (Figure 2.6 A-C), indicating that depolarization has a similar effect on Smo membrane localization in the wing imaginal disc as in the salivary gland. A change in the dorsal portion of the posterior compartment was not readily apparent.

To test the effects of sustained depolarization during development, we expressed the red light-activated optogenetic channel ReaChR, which is activatable through the larval cuticle, in the dorsal compartment of the wing disc. Animals were raised on a 12-h

light/dark cycle, and imaginal discs were harvested in the third larval instar and stained with an anti-Smo antibody. Under these conditions, membrane abundance of Smo was markedly increased in the dorsal portion of both anterior and posterior compartments in these discs, as compared to the ventral compartments (Figure 6 D and D'), indicating that depolarization can mediate increased Smo membrane abundance independently of Ptc. The tissue was also overgrown, in line with other reported phenotypes of Hh pathway hyperactivation (Christiansen, Ding, & Bergmann, 2012). In the wing pouch, expression of the Hh target gene *ptc* was increased in the dorsal compartment of discs expressing *ap>ReaChR* (Figure 6 E and E'). Thus, optogenetic manipulation of  $V_{mem}$  *in vivo* can regulate Smo localization and abundance even in cells that do not express Ptc.

## Discussion

In this study, we show that  $V_{mem}$  is patterned in a spatiotemporal manner during development of the wing disc of *Drosophila* and that it regulates Hedgehog signalling at the compartment boundary. First, we have shown that cells immediately anterior to the compartment boundary are relatively more depolarized than cells elsewhere in the wing pouch. This region coincides with the A cells where Hh signalling is most active, as evidenced by upregulation of Ptc. Second, we found that the expression of at least two regulators of  $V_{mem}$ , the ENaC channel Rpk and the alpha subunit of the Na<sup>+</sup>/K<sup>+</sup> ATPase are expressed at higher levels in this same portion of the disc. Third, by altering Hh signalling, we demonstrate that the expression of both Rpk and ATP $\alpha$  is increased in cells with increased Hh signalling. Fourth, by manipulating Hh signalling in the disc and using optogenetic methods, both in the salivary gland and wing disc, we show that membrane depolarization promotes Hh signalling as assessed by increased membrane localization of Smo, and expression of the target gene *ptc*. Thus, Hh-induced signalling and membrane depolarization appear to mutually reinforce each other and thus contribute to the mechanisms that maintain the segregation of A and P cells at the compartment boundary.

### *Developmentally regulated patterning of $V_{mem}$ in the wing disc*

We have observed two regions of increased DiBAC fluorescence in the wing imaginal disc. We did not observe obvious upregulation of Rpk and ATP $\alpha$  in other discs, and therefore, our studies have focused on the region immediately anterior to the A-P compartment boundary in the wing disc. In the late L3 wing disc, we observed a region of increased DiBAC fluorescence in the A compartment in the vicinity of the D-V boundary. This corresponds to a “zone of non-proliferating cells” (ZNC) (O'Brochta & Bryant, 1985). Interestingly, the ZNC is different in the two compartments. In the A compartment, two rows of cells are arrested in G2 while in the P compartment, a single row of cells is arrested in G1 (Johnston & Edgar, 1998). Our observation of increased DiBAC fluorescence in the DV boundary of only the A compartment is consistent with previous reports that cells become increasingly depolarized as they traverse S-phase and enter G2 (Cone, 1969), reviewed in (Blackiston et al., 2009). In contrast, cells in G1 are thought to be more hyperpolarized. Additionally, we observed increased expression of the ENaC channel Rpk in two rows of cells at the D-V boundary in the anterior

compartment (Figure 2.2 A''), indicating that increased expression of Rpk could contribute to the depolarization observed in those cells. We note, however, that the increased DiBAC fluorescence in these cells was not entirely eliminated by exposing discs to amiloride, indicating that other factors are also likely to contribute.

#### *How does membrane depolarization relate to Hh signalling?*

Our data are consistent with a model where membrane depolarization and Hh-induced signalling mutually reinforce each other in the cells immediately anterior to the compartment boundary. Both membrane depolarization and the presence of Hh seem necessary for normal levels of activation of the Hh signalling pathway in this region; neither alone is sufficient (Figure 2.7). First, we have shown that Hh signalling promotes membrane depolarization. We have also shown that the expression of Rpk just anterior to the A-P compartment boundary is dependent upon Hh signalling. Elevated Rpk expression is not observed when a *hh<sup>ts</sup>* allele is shifted to the restrictive temperature, and cells become more depolarized when Hh signalling is constitutively activated through expression of the *ci3m* allele. Previously published microarray data suggest that Rpk as well as another ENaC family channel Ppk29 are both enriched in cells that also express *ptc* (Willsey et al., 2016). However, there is no antibody to assess Ppk29 expression currently. The sensitivity of the depolarization to amiloride indicates that these and other ENaC channels make an important contribution to the membrane depolarization.

Second, we have shown that the depolarization increases Hh signalling. The early stages of Hh signalling are still incompletely understood (reviewed by (Petrov et al., 2017)). Hh is thought to bind to a complex of proteins that includes Ptc together with either Ihog or Boi. This alleviates an inhibitory effect on Smo, possibly by enabling its access to specific membrane sterols. Interestingly, it has recently been proposed that Ptc might function in its inhibitory capacity by a chemiosmotic mechanism where it functions as a Na<sup>+</sup> channel (Myers et al., 2017). An early outcome of Smo activation is its localization to the membrane where its C-terminal tail becomes phosphorylated and its ubiquitylation and internalization are prevented (Li et al., 2012; Zhang, Williams, Guo, Lum, & Beachy, 2004). By manipulating channel expression in the wing disc, and by optogenetic experiments in both the salivary gland and wing disc, we have shown that membrane depolarization can promote Hh signalling as assessed by increased Smo membrane localization and increased expression of the target gene *ptc*. The time course of Smo activation is relatively rapid (over minutes) and is therefore unlikely to require new transcription and translation. In the P compartment, membrane Smo levels are elevated likely because of the complete absence of Ptc, and some downstream components of the Hh signalling pathway are known to be activated (F. A. Ramírez-Weber et al., 2000). However, since Ci is not expressed in P cells, target gene expression is not induced. In the cells just anterior to the boundary, the partial inhibition of Ptc by Hh together with membrane depolarization seem to combine to achieve similar levels of Smo membrane localization. More anteriorly, the absence of this mutually reinforcing mechanism appears to result in Smo internalization (Figure 2.7).

Our experiments do not point to a single mechanism by which depolarization promotes Hh signalling. It is possible that depolarization results in increased  $\text{Ca}^{2+}$  levels by opening  $\text{Ca}^{2+}$  channels at the plasma membrane or by promoting release from intracellular sources (e.g. the ER or mitochondria). Indeed, there is evidence that  $\text{Ca}^{2+}$  entry into the primary cilium promotes Hh signalling, and recent work shows that targets of Sonic Hedgehog (Shh) signalling during mammalian development is augmented by  $\text{Ca}^{2+}$  influx (Delling, DeCaen, Doerner, Febvay, & Clapham, 2013; Klatt Shaw et al., 2018). A second possibility is that membrane depolarization could, by a variety of mechanisms, activate the kinases that phosphorylate the C-terminal tail of Smo and maintain it at the plasma membrane in an activated state. Depolarization could also impact electrostatic interactions at the membrane that make the localization of Smo at the membrane more favourable. Since Rpk and  $\text{ATP}\alpha$  are expressed at higher levels in the cells that receive Hh, which have been postulated to make synapse-like projections with cells that produce Hh (González-Méndez et al., 2017), it is conceivable that these channels could modulate synapse function. Additionally, while our work was under review, it has been reported that reducing glycolysis depletes ATP levels and results in depolarization in the wing imaginal disc, reducing the uptake of Hh pathway inhibitors and stabilizing Smo at the cell membrane (Spannl et al., 2020). Importantly, all these mechanisms are not mutually exclusive and their roles in Hh signalling are avenues for future research.

It is now generally accepted that both cell–cell signalling and mechanical forces have important roles in cell fate specification and morphogenesis. Our work here adds to a growing body of literature suggesting that changes in  $V_{mem}$ , a relatively understudied parameter, may also have important roles in development. Integrating such biophysical inputs with information about gene expression and gene regulation will lead to a more holistic understanding of development and morphogenesis.

## Figures

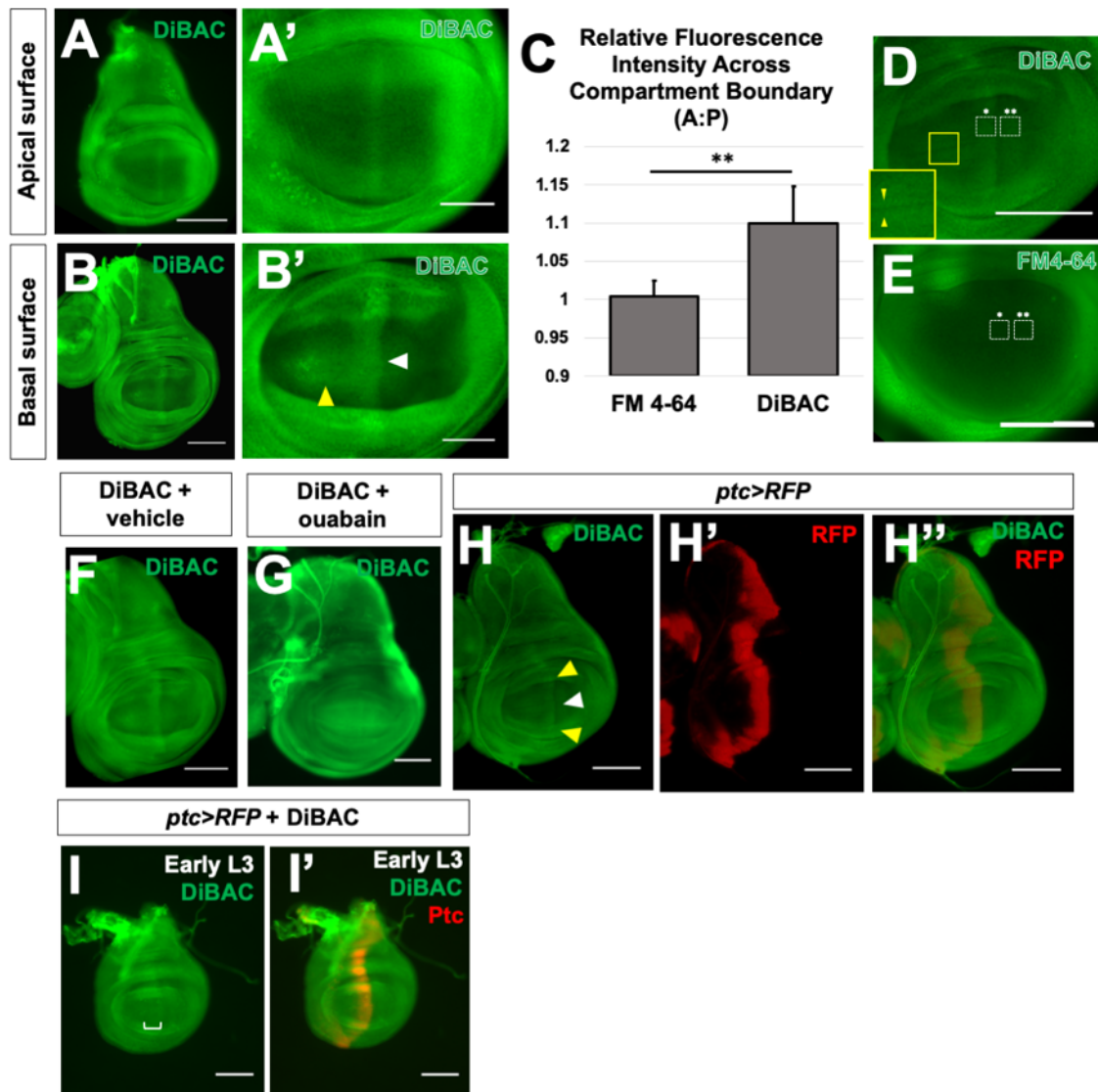


**Figure 2.1: Membrane potential is patterned in the third-instar wing imaginal disc.**

(A, B) Live third-instar discs incubated in DiBAC. DiBAC fluorescence is observed in the wing imaginal disc in both apical (A–A') and basal (B–B') optical sections. Increased fluorescence is observed in the centre of the pouch (white arrow, B') and at the dorsoventral (D–V) compartment boundary in the anterior compartment (yellow arrow, (B'), and inset, (D)). (C–E) Comparison of DiBAC with the voltage-insensitive dye FM4-64. Incubation of live discs in FM4-64 (E) shows more uniform fluorescence when compared to DiBAC (D). Quantitative comparison of fluorescence in the two white boxes in each panel is shown in (C).  $N = 7$  discs for each treatment, data compared using an unpaired  $t$ -test, \*\* indicates  $P < 0.001$ , error bars are standard deviations. The region boxed in yellow in (D) is shown at higher magnification to show DiBAC

fluorescence at the D-V compartment boundary. (F, G) Incubation in ouabain results in brighter and more uniform DiBAC fluorescence. (H–H'') Live wing discs expressing *UAS-RFP* anterior to the compartment boundary, under the control of *ptc-Gal4*, were incubated in DiBAC, showing that the stripe of increased DiBAC fluorescence coincides with the posterior edge of *ptc* expression. White arrowhead in (H) indicates the stripe in the wing pouch; yellow arrowheads indicate the stripe in the dorsal and ventral hinge. (I, I') Early L3 discs incubated in DiBAC. Patterned depolarization is evident throughout the third larval instar, with the stripe of increased fluorescence becoming narrower in more mature discs with developmental time (Compare I with A, bracket in I indicates width of increased DiBAC fluorescence). Data information: Scale bars are 100  $\mu\text{m}$  in all panels, except for (A' and B'), where scale bars are 50  $\mu\text{m}$ .

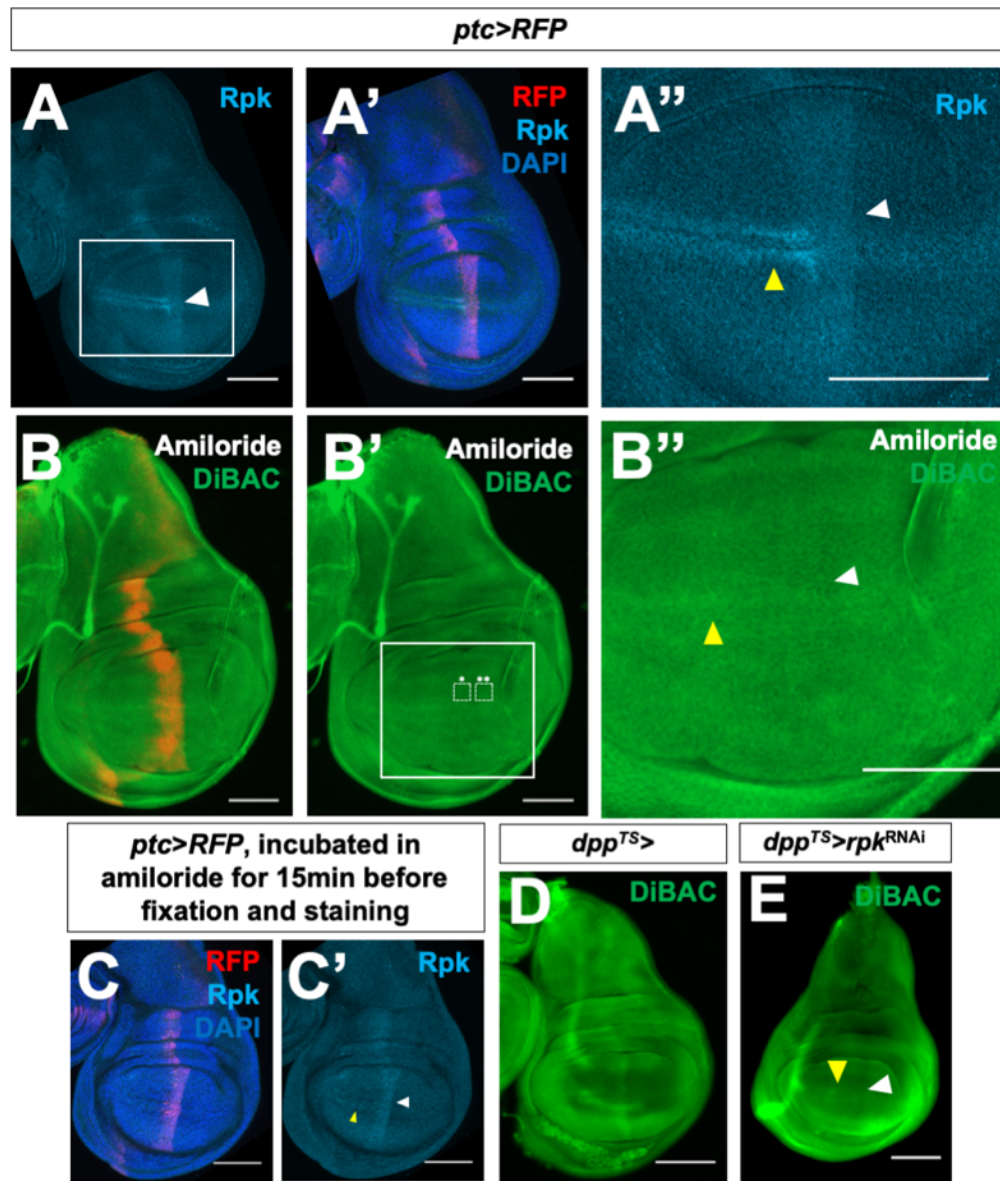


**Figure 2.2: Expression of endogenous channels is patterned and contributes to depolarization anterior to the compartment boundary**

A–A'') Expression of Rpk is increased anterior to the A-P compartment boundary and in two rows of cells flanking the D-V compartment boundary in the A compartment. (B–B'') Blockade of DEG/ENaC channels by incubation in amiloride abolishes the stripe of increased DiBAC fluorescence along the A-P compartment boundary (white arrowhead). White boxes indicate regions used to calculate the average DiBAC fluorescence intensity ratio across the compartment boundary = 0.98, standard deviation = 0.05,  $n = 5$  discs. Increased fluorescence at the D-V boundary in the A compartment is still observable (yellow arrowhead). The same vehicle was used as in

experiments with ouabain, and the control is in Fig [1E](#). (C, C'). Amiloride incubation does not diminish Rpk expression. White arrowhead indicates approximate position of the A-P compartment boundary, yellow arrowhead indicates approximate position of the D-V compartment boundary. (D, E) Expression of *rpk*-RNAi using *dpp-Gal4* results in diminished DiBAC fluorescence along the A-P compartment boundary (white arrowhead), while increased fluorescence at the D-V boundary in the A compartment is still observable (yellow arrowhead). Data information: Scale bars are 100  $\mu\text{m}$ , except in (B''), where scale bar is 50  $\mu\text{m}$ .

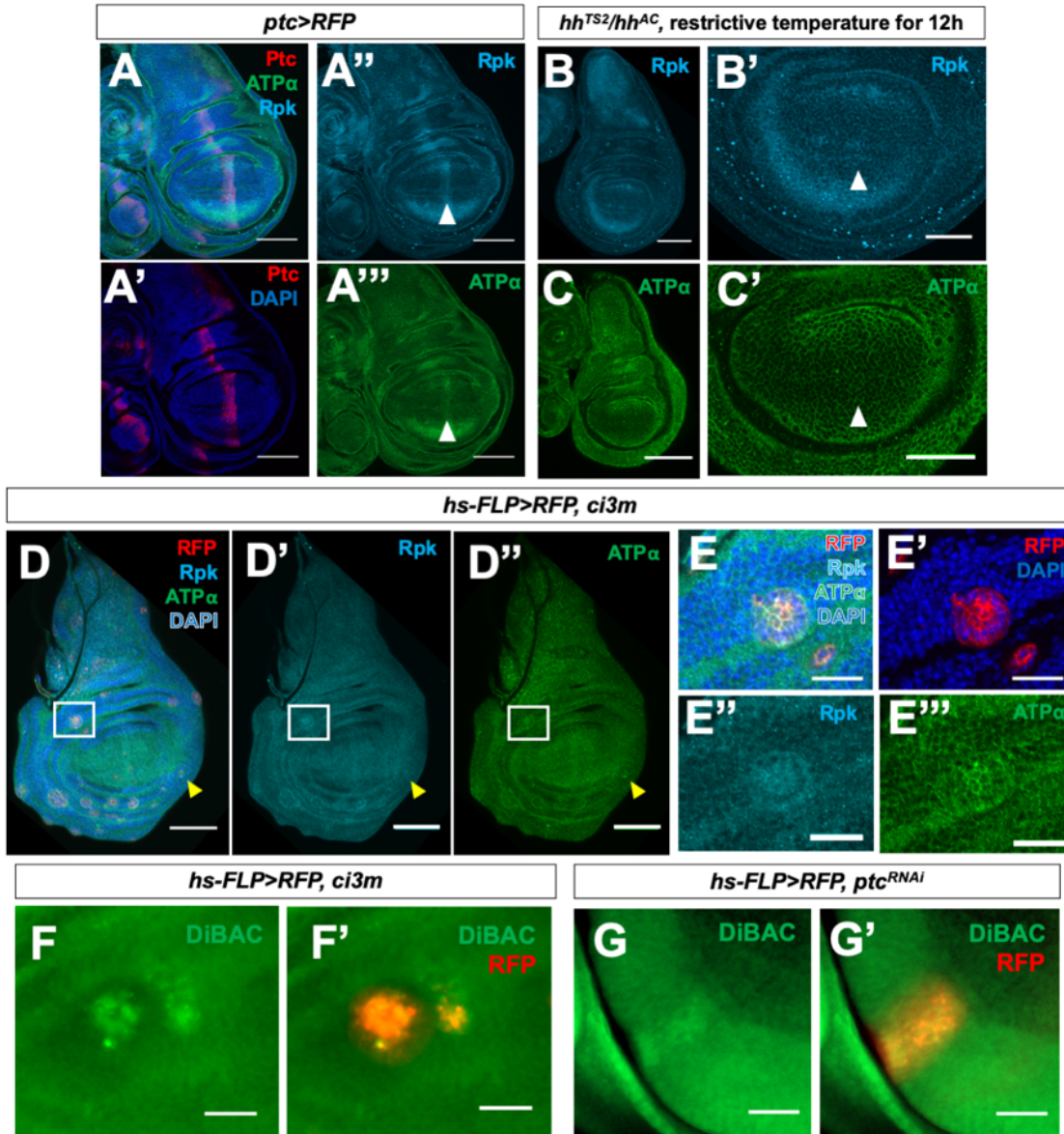


**Figure 2.3: Patterned Rpk and ATP $\alpha$  expression and membrane depolarization require Hh signaling**

(A–A''') Immunostaining of discs expressing *ptc>RFP* with antibodies to Rpk and ATP $\alpha$  showing elevated levels of both proteins anterior to the compartment boundary. White arrowheads indicate approximate position of the A-P compartment boundary. (B–C') L3 discs that are temperature-sensitive for *hh* following shift to the restrictive temperature for 12 h show loss of increased expression of Rpk (B, B') and ATP $\alpha$  (C, C') anterior to the compartment boundary. Controls shown in Fig. EV2. White arrowheads indicate approximate position of the A-P compartment boundary. (D–E''') Clones of cells expressing an activated form of the transcription factor Ci show elevated Rpk and ATP $\alpha$  expression in the anterior compartment (white box) as well as the posterior

compartment (yellow arrowhead). (E–E'') A single clone in the A compartment is shown at higher magnification. (F–F') A clone of cells in the anterior compartment expressing *ci3M* following incubation in DiBAC. (G–G') A clone of cells in the anterior compartment expressing *ptc*-RNAi following incubation in DiBAC. The clones also express RFP. Data information: All scale bars are 100  $\mu\text{m}$ , except for (B'), (C') and (F–G') where scale bars are 50  $\mu\text{m}$  and (E–E'') where scale bars are 25  $\mu\text{m}$ .

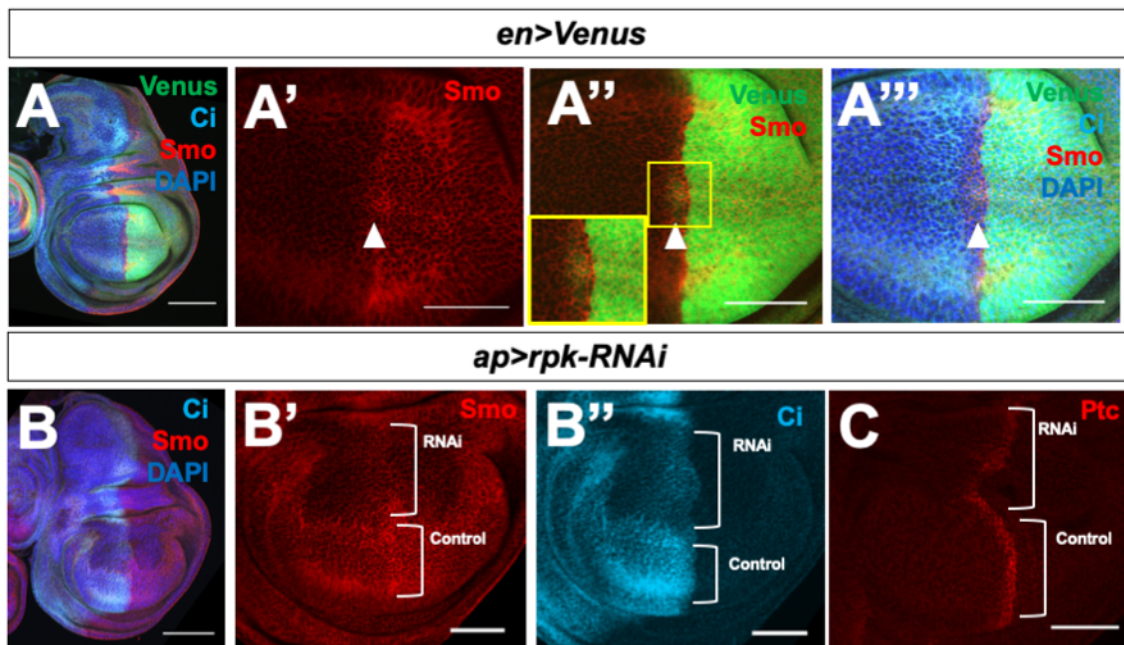


**Figure 2.4: The ENaC channel Rpk is required for Hh signal transduction**

(A–A''') Immunostaining of Smo protein (red) and full-length Ci (light blue) in discs expressing *en-Venus*. Smo is expressed at higher levels in the P compartment and in a stripe 5–10 cells wide just anterior to the A-P compartment boundary. White arrowhead indicates cells just anterior to the A-P compartment boundary. (B, C) Effect of expressing an RNAi against the ENaC channel *rpk* in the dorsal compartment of the disc using *ap-Gal4*. Knockdown of Rpk in the dorsal compartment results in decreased accumulation of the Hh signal transducer Smo (B, B') and the activator form of Ci (B, B''). The expression of *ptc*, visualized using an anti-Ptc antibody (C), a downstream target gene of Hh signalling, is also diminished. The *rpk*-RNAi line BL:39053 is used in all panels shown, but the phenotype was validated with a second RNAi line (BL:25847). Data information: All scale bars are 50  $\mu\text{m}$ , except for (A) and (B), where scale bars are 100  $\mu\text{m}$ .

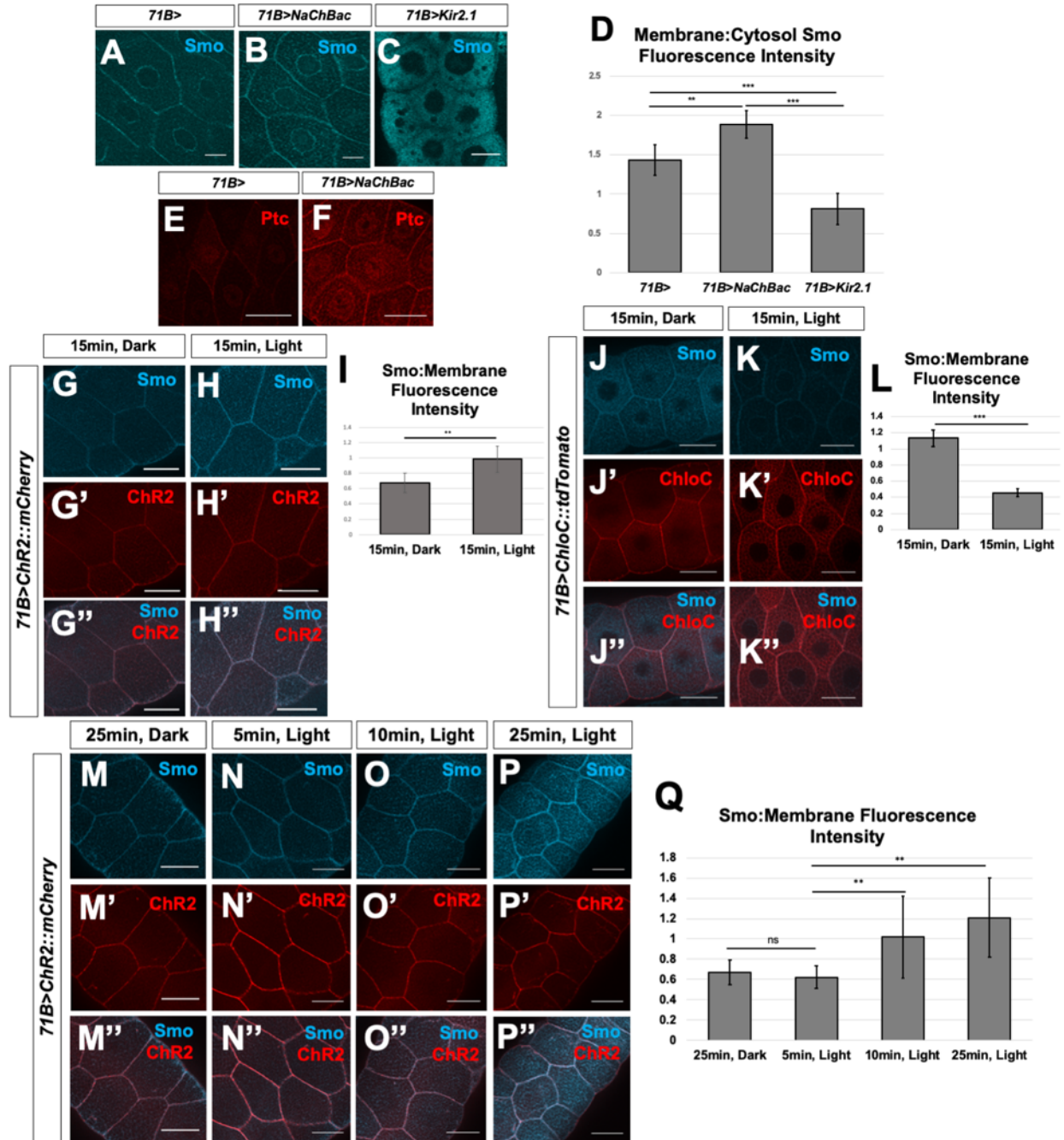


**Figure 2.5: Membrane potential modulates Smo membrane abundance and downstream Hh signal transduction in larval salivary glands**

(A–Q) Manipulation of  $V_{mem}$  in salivary glands dissected from third-instar larvae. (A–C) Localization of Smo protein (blue) following expression of *71B-Gal4* (A), *71B-Gal4* and *UAS-NaChBac* (B) or *71B-Gal4* and *UAS-Kir2.1* (C). Expression of the sodium channel *NaChBac* increases membrane localization of Smo while expression of the potassium channel *Kir2.1* reduces membrane localization and increases cytosolic Smo (B, C). (D) Quantification of the ratio of membrane Smo fluorescence to cytosol

fluorescence.  $N = 7$  salivary glands per genotype. Data were compared using ANOVA followed by Tukey's test for significance (\*\* indicates  $P < 0.01$ , \*\*\* indicates  $P < 0.001$ ), error bars are standard deviations. (E, F) Expression of the Hh target gene *ptc* is visualized using anti-Ptc immunostaining. Compared to *71B-Gal4* (E), Ptc expression is increased in glands expressing *71B-Gal4* and *UAS-NaChBac* (F). (G-I) Effect of expression and activation of the depolarizing channelrhodopsin ChR2 on Smo protein membrane abundance. After dissection, glands were kept in either dark conditions (G) or exposed to 15 min of blue light (H). (I) Quantification of membrane fluorescence;  $N = 13$  glands, data compared using an unpaired *t*-test (\*\* indicates  $P < 0.01$ ), error bars are standard deviations. (J-L) Effect of expression and activation of the Cl<sup>-</sup>-selective channelrhodopsin ChloC. An overall reduction in Smo immunostaining was observed following channel activation (K), as compared to control glands kept in the dark (J). (L) Quantification of membrane fluorescence;  $N = 10$  glands, data were compared using an unpaired *t*-test (\*\*\* indicates  $P < 0.001$ ), error bars are standard deviations. (M-Q) Time course of change in Smo localization. Salivary glands expressing the channelrhodopsin ChR2 were subjected to increasing intervals of activating light, then fixed and stained for Smo protein (M-P). (Q) Quantification of membrane-associated fluorescence;  $N = 7$  glands/timepoint, data were compared using ANOVA followed by Tukey's test for significance (\*\* indicates  $P < 0.01$ ), error bars are standard deviations. Scale bars are 50  $\mu\text{m}$ , except for (A-C), where scale bars are 25  $\mu\text{m}$ .

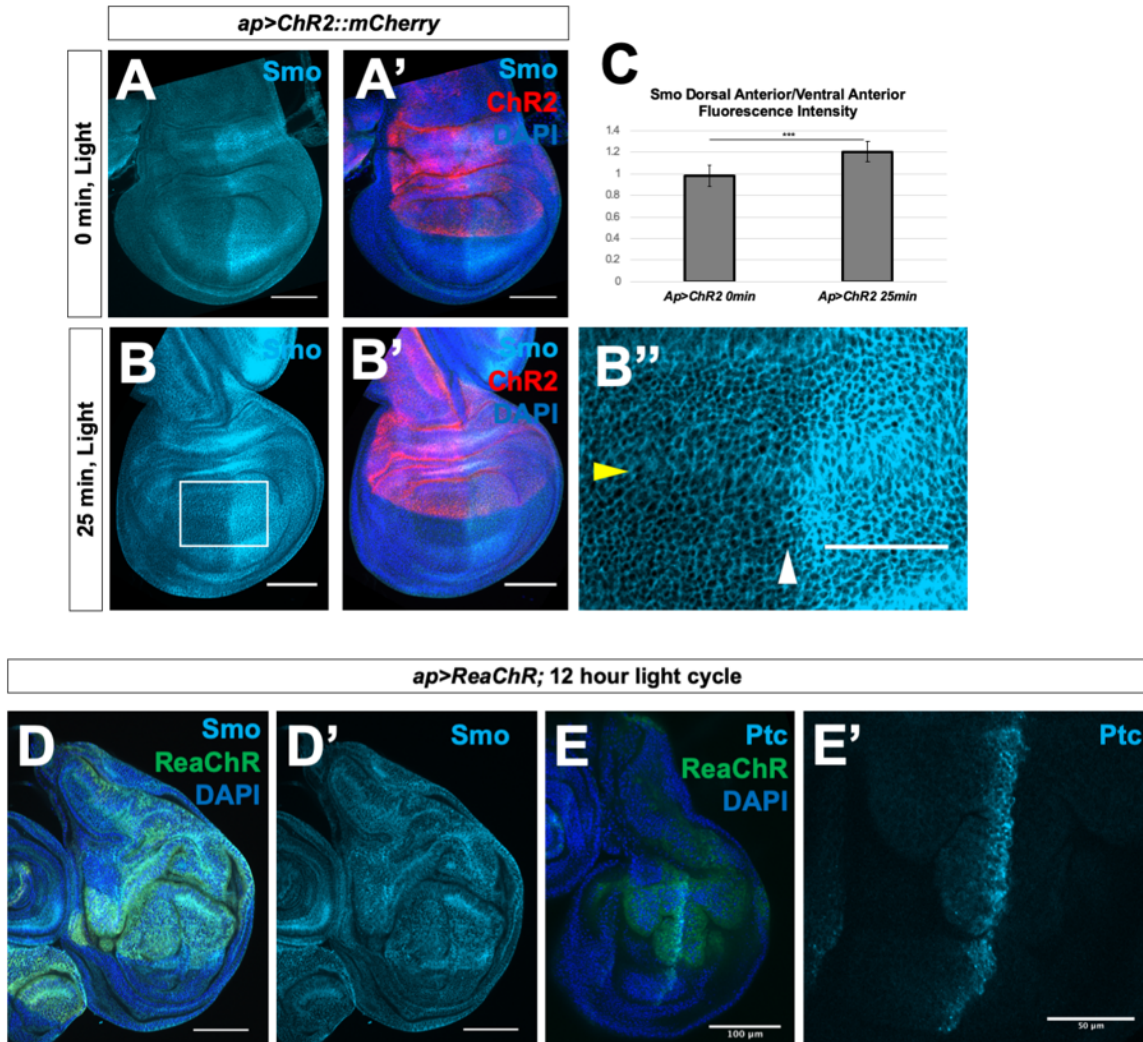


**Figure 2.6:  $V_{mem}$  regulates Smo membrane localization independently of Ptc in the wing imaginal disc**

(A–B'') Wing discs expressing the channelrhodopsin ChR2 were subjected to 0 min or 25 min of activating light in culture, then fixed and stained for Smo protein. In (B''), the yellow arrowhead indicates dorsoventral compartment boundary, and the white arrowhead indicates anteroposterior compartment boundary. (C) Quantification of the ratio of mean Smo fluorescence intensity in 25  $\mu\text{m}^2$  regions in the dorsal anterior compartment compared to the ventral posterior compartment.  $N = 5$  for 0 min discs,  $n = 9$  for 25 min discs, data were compared using an unpaired  $t$ -test ( $***P < 0.001$ ), error bars are standard deviations. Identical analyses were carried out comparing dorsal posterior fluorescence to ventral posterior fluorescence ( $P = 0.132$ ), dorsal posterior fluorescence to dorsal anterior fluorescence ( $P = 0.12$ ) and ventral posterior fluorescence to ventral anterior fluorescence ( $P = 0.36$ ). (D–E') Discs expressing the red light-activated channelrhodopsin ReaChR under control of *ap-Gal4* were raised on a 12-h light/dark cycle, dissected and stained for Smo protein (D,

D') or Ptc protein (E, E'). Data information: Scale bars are 100  $\mu\text{m}$  in all panels except (B'') and (E'), where scale bars are 50  $\mu\text{m}$ .

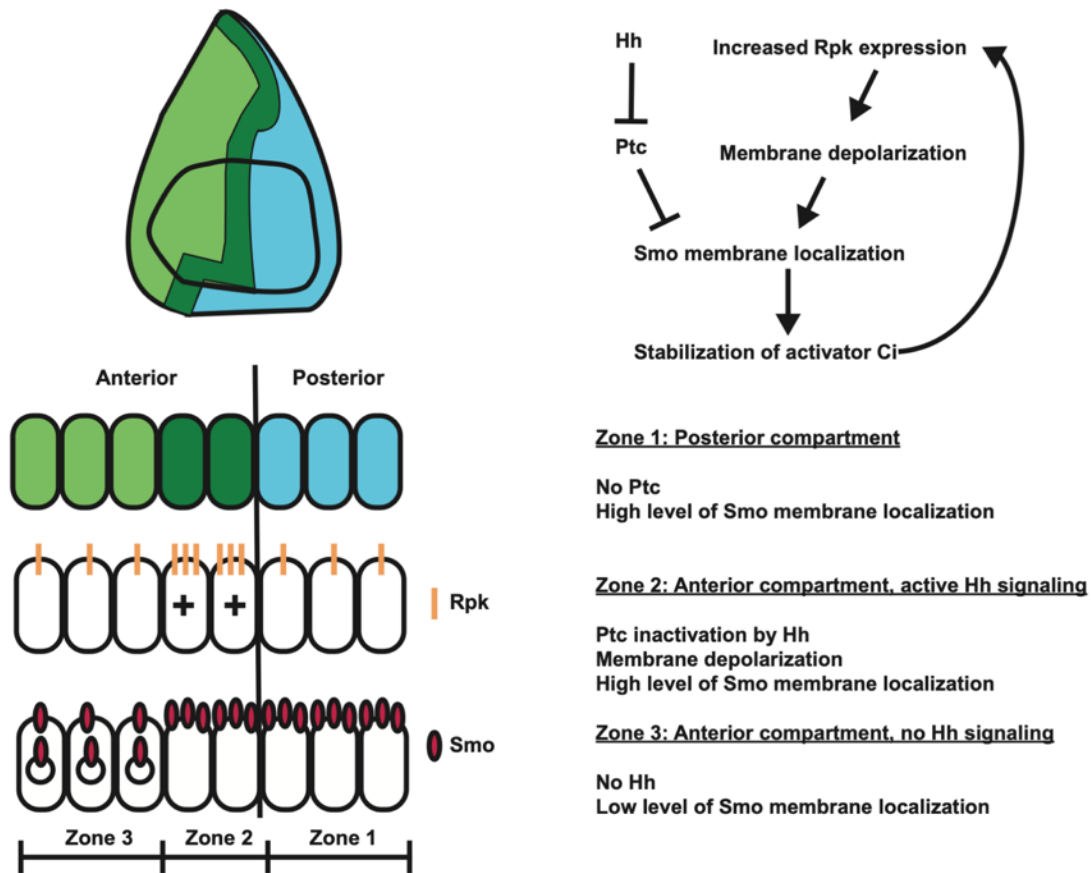


**Figure 2.7: Membrane potential modulates Hh signalling at the anteroposterior compartment boundary**

Cells in the posterior compartment (blue) produce the short-range morphogen Hedgehog, which is received by cells immediately anterior to the compartment boundary, in the anterior compartment (dark green). Hh signal releases Ptc-mediated inhibition of Smo, allowing for the stabilization of the transcriptional co-effector Ci, and increased expression of the ENaC channel Rpk, which depolarizes cells immediately anterior to the compartment boundary. Depolarization results in increased membrane abundance of the Hh activator Smo and increased transduction of Hh signal. This, in turn, increases expression of Rpk, reinforcing high levels of Hh signal transduction in the region immediately anterior to the compartment boundary.

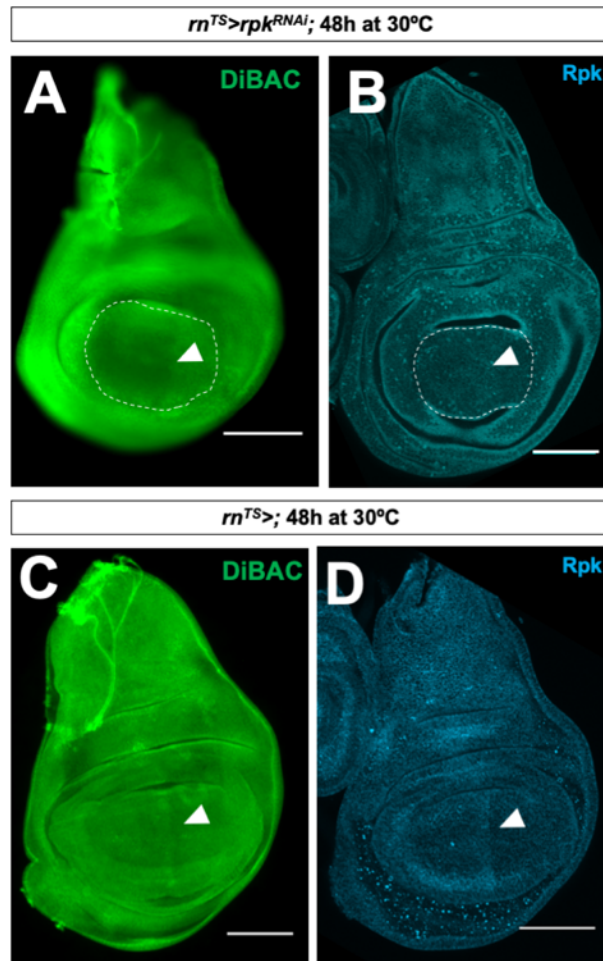


**Figure 2.8: *rpk* knockdown decreases DiBAC staining and Rpk expression at the A-P compartment boundary**

(A) Expression of *rpk*-RNAi in the wing pouch decreases patterned DiBAC staining (white arrowhead). (B) Expression of *rpk*-RNAi in the wing pouch decreases anti-Rpk staining anterior to the A-P compartment boundary (white arrowhead). (C, D) Control discs. Increased DiBAC staining and anti-Rpk staining are visible in the centre of the wing pouch (white arrowheads). Data information: Scale bars are 100  $\mu$ m.

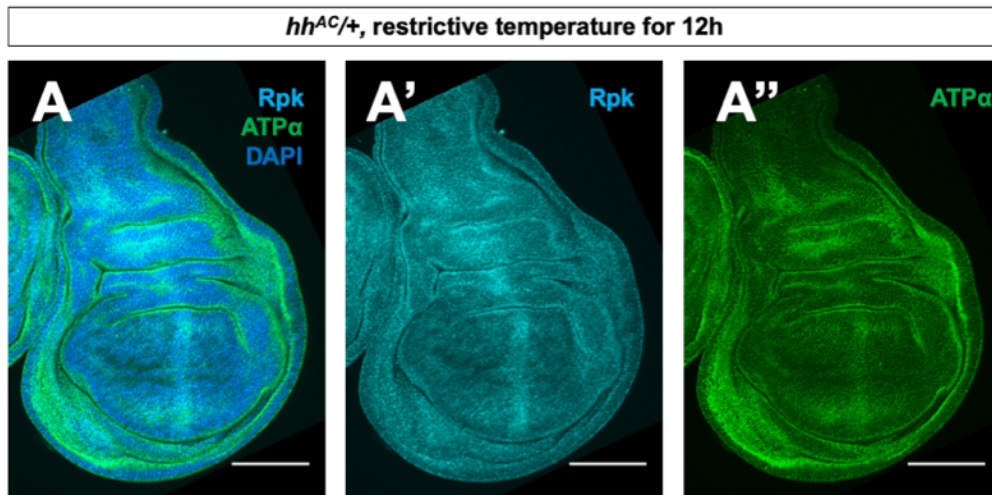


**Figure 2.9: Patterned Rpk and ATP $\alpha$  expression and membrane depolarization require Hh signaling**

(A–A'') Immunostaining of discs heterozygous for the *hh<sup>AC</sup>* allele and upshifted to 30°C for 12 h with antibodies to Rpk and ATP $\alpha$  showing elevated levels of both proteins anterior to the A-P compartment boundary. All scale bars are 100  $\mu$ m.

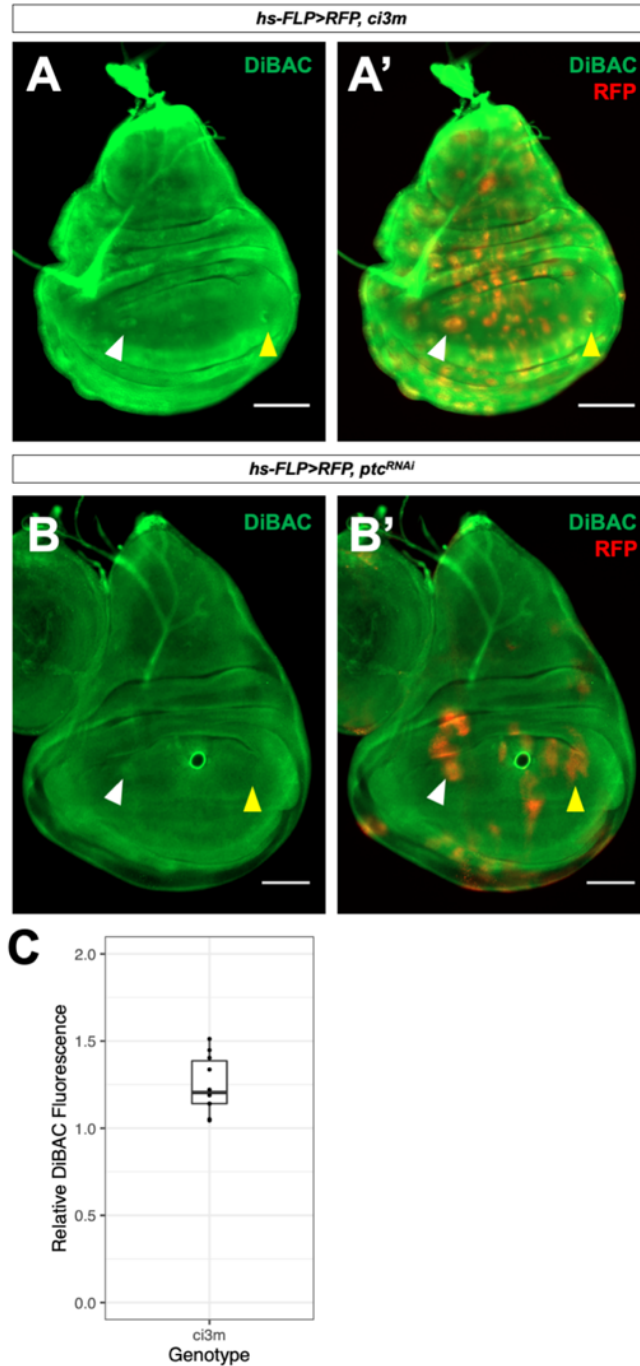


**Figure 2.10: Hh pathway activation results in depolarization**

(A–A') Clones of cells expressing *ci3m* accumulate more DiBAC relative to surrounding tissue in both the anterior (white arrow) and posterior (yellow arrow) compartments. (B–B') Clones of cells expressing *ptc*-RNAi accumulate more DiBAC relative to surrounding tissue in the anterior compartment (white arrow), but not the posterior compartment

(yellow arrow). (C) The ratio of DiBAC fluorescence in *ci3m*-expressing clones to equally-sized regions of tissue not expressing *ci3m*.  $N = 10$  clones from three imaginal discs. Individual data points are shown, as well as a box plot showing descriptive statistics. Bounds of the box show lower and upper quartiles, bar within the box shows the median of the data, and whiskers show minimum and maximum bounds of data. Data information: All scale bars are 100  $\mu\text{m}$ .

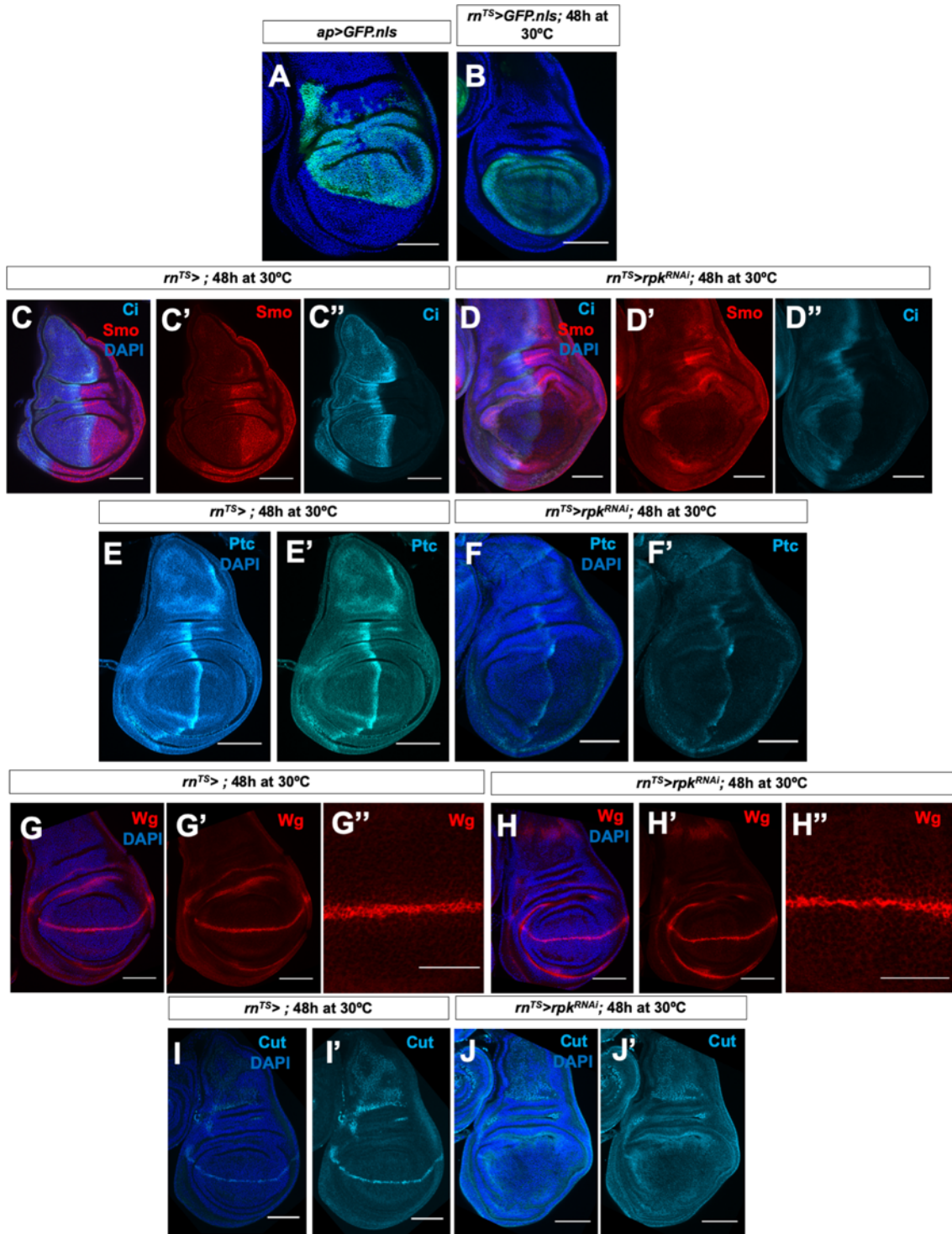
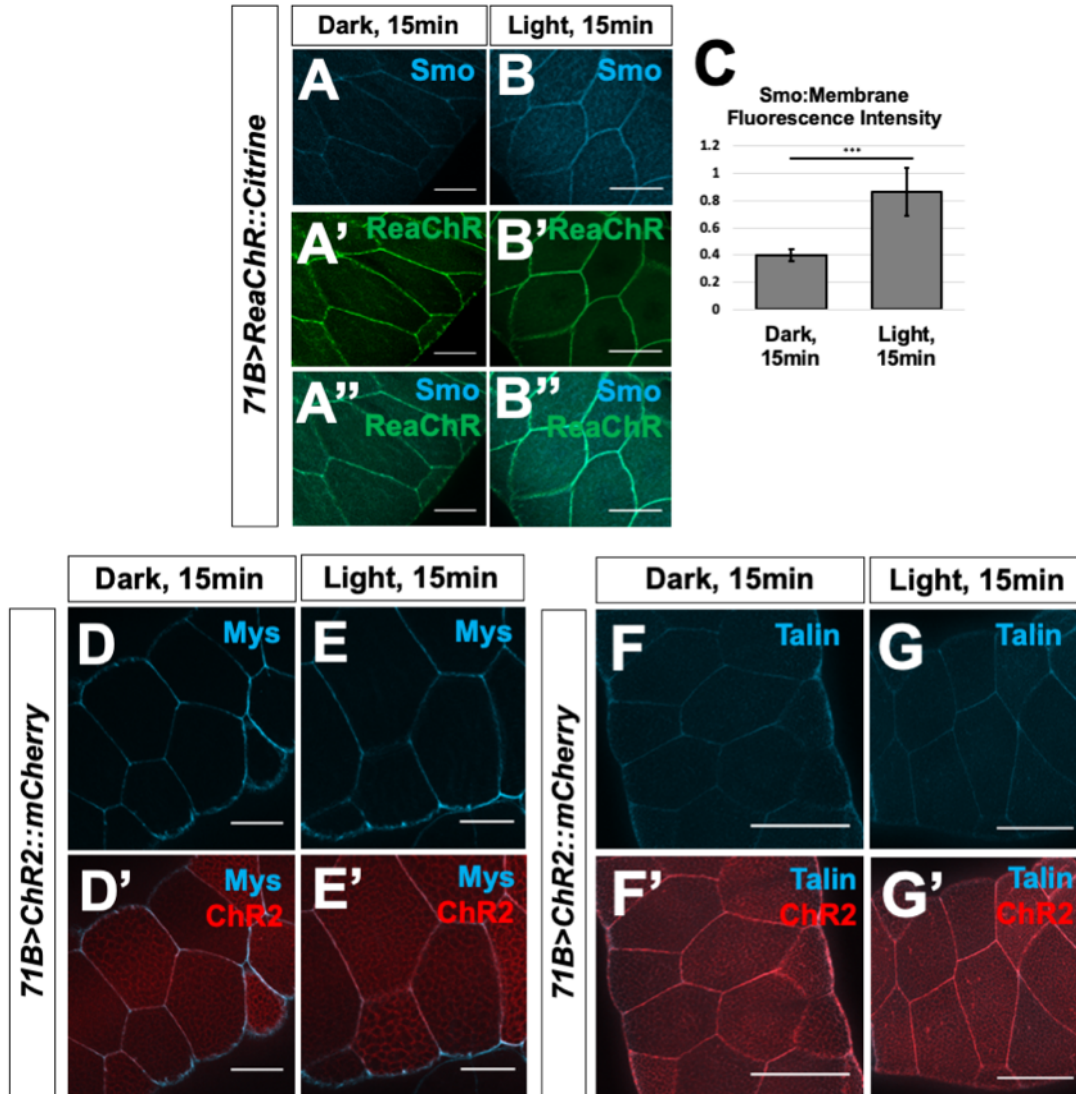


Figure 2.11: Manipulating levels of the ion channel Rpk impacts both Hh and Wg signal transduction

(A, B) Expression patterns of *ap-Gal4* (A) and *rn-Gal4* (B). (C, D) Immunostaining of Smo protein (red), full-length Ci (light blue) (C–C'') and Ptc protein (D) in discs expressing *ATPα<sup>RNAi</sup>* in the dorsal compartment. Brackets indicate tissue expressing RNAi and control tissue. (E–F'') Immunostaining of Smo protein (red) and full-length Ci (light blue) in (E–E'') control discs and (F–F'') discs expressing *rpK<sup>RNAi</sup>* for 48 h before dissection. (G–H') Immunostaining of Ptc protein in (G, G') control discs and (H, H') discs expressing *rpK<sup>RNAi</sup>* for 48 h before dissection. (I–J'') Immunostaining for Wg protein in (I–I'') control discs and (J–J'') discs expressing *rpK<sup>RNAi</sup>* for 48 h before dissection. (K–L') Immunostaining for Cut protein in (K, K') control discs and (L, L'), discs expressing *rpK<sup>RNAi</sup>* for 48 h before dissection. Data information: All scale bars are 100 μm except (D), where scale bar is 50 μm.



**Figure 2.12: Optogenetic manipulation of  $V_{mem}$  in *Drosophila* salivary glands**

(A–G') Salivary glands expressing the channelrhodopsin ReaChR were subjected to 15 min in activating light, then fixed and stained for Smo protein (A–C).  $N = 9$  glands, data were compared using an unpaired  $t$ -test ( $***P < 0.001$ ), error bars are standard deviations. Membrane abundance of the beta integrin subunit Mys and the integrin-associated protein Talin are not altered upon ChR2 activation (D–G'). Scale bars are 50  $\mu\text{m}$  in all panels.

## **Chapter Two**

### **Piezo-expressing cells regulate organ size in the wing imaginal disc**

## Abstract

During development, organisms generate tissues and organs of astoundingly reproducible size. The regulation of growth involves both tissue-intrinsic and -extrinsic mechanisms, including the interpretation of secreted chemical signals and patterns of mechanical force. The intriguing discovery that many growth-regulatory signaling pathways are modulated by mechanical signals has led to increasing interest in the role of mechanical force in size regulation. Here, we describe a role for the mechanosensitive ion channel Piezo in organ growth in the *Drosophila* wing imaginal disc. Piezo is expressed in a sparse population of cells in the wing disc, and reduction of Piezo expression in this population, or loss of function of the Piezo gene, results in larger larval and adult organs. Larger organ size is due to an increase in the size of individual cells, rather than an increase in cell proliferation. These data implicate a force-sensing ion channel in the regulation of cell size.

## Introduction

Many models of organ size regulation center around diffusible signals (reviewed in (Hariharan, 2015; Schwank & Basler, 2010)). In these models, pro-growth molecules are produced in source cells, and are received by neighboring cells. The identity and concentration of these molecules informs fate and proliferation decisions. It is thought that as the tissue grows, pro-growth signals are diluted, and as a result, proliferation ceases at a prescribed organ size. Evidence supporting diffusible signal models of growth regulation include the roles of secreted molecules like Decapentaplegic (Dpp, the *Drosophila* TGF-B/BMP family protein) and Wingless (Wg, the *Drosophila* Wnt family protein) in regulating wing size. However, there are many unanswered questions regarding the mechanisms by which tissue-wide gradients of secreted signaling molecules orchestrate organ size. For example, it is unknown to what extent every cell in a tissue is able to respond to pro-growth signals, and if cells are able to detect subtle changes in signal concentration and amplify these changes into meaningful growth outcomes.

Increasing attention has been paid to cell-intrinsic sensors of mechanical signals as potential mediators of organ size. Recent evidence suggests that cells have the capacity to sense tension and compression, a readout of how tightly packed they are within a tissue, and transduce that information into decisions about proliferation or growth (Bosveld et al., 2012; Discher, Janmey, & Wang, 2005; Ulrich, de Juan Pardo, & Kumar, 2009; Wozniak & Chen, 2009). Components of the Hippo pathway, a well-known growth regulatory signaling pathway, have been shown to be mechanosensitive (Irvine & Harvey, 2015), and cells cultured in different mechanical conditions display different propensities toward proliferation. Patterns of force also exist in the developing wing disc. As the wing disc grows, cells in the center of the disc become more and more compacted, and it has been proposed that this compaction is responsible for slowing organ growth at the end of the larval life stage (Legoff, Rouault, & Lecuit, 2013).

Mechanosensitive ion channels are emerging as important transducers of biophysical signals, and have been implicated in the growth of tumors, the regulation of cell volume, homeostatic cell extrusion, and organogenesis. Perhaps the most well characterized mechanosensitive channel is Piezo, a non-selective cation channel (Coste et al., 2010; Coste et al., 2012). Piezo channels are highly curved, with arms that extend away from the channel pore and deform the cell membrane. This unique structure amplifies the sensitivity of the channel to membrane tension. Upon deformation, the channel pore opens, facilitating inward cationic current and transiently depolarizing the cell membrane. Piezo activity modulates the morphogenesis of the zebrafish heart outflow tract, through positive regulation of both the Notch and Hippo pathways (Duchemin et al., 2019), and is required for the differentiation of progenitors from a stem cell population in the *Drosophila* gut (He et al., 2018). Piezo has also been linked to the release of pro-growth factors, including Wnt and insulin (Deivasikamani et al., 2019; Miyazaki et al., 2019). Recent work has shown that Piezo is upregulated in many cancers, promoting overgrowth through activation of the mTOR pathway (Han et al., 2019).

An outstanding question concerns the downstream mechanisms that link Piezo channel activation to changes in gene expression, cell shape, or cell behavior. In many, but not all cases, calcium signaling has been shown to be downstream of Piezo activation. Piezo activation transiently depolarizes the cell membrane, resulting in the opening of voltage-sensitive calcium channels in the plasma membrane or endoplasmic reticulum. Increased cytosolic calcium activates differentiation and proliferation programs, in a mechanism thought to be mediated by calcium-sensitive transcription factors. For example, in the *Drosophila* midgut, Piezo is expressed in an enteroendocrine precursor population, and is required for the generation of differentiated enteroendocrine cells (He et al., 2018). Manipulation of cytosolic calcium levels in these cells rescues Piezo loss of function, suggesting that calcium is downstream of Piezo in the mechanical regulation of stem cell fate.

While screening expression patterns of mechanosensitive ion channels in the *Drosophila* third instar wing imaginal disc, I found that a cloned enhancer of Piezo drove expression in a sparse subset of cells distributed evenly throughout the wing disc. Analysis of an enhancer trap at the endogenous *Piezo* locus showed more widespread expression of the channel. Surprisingly, knockdown of Piezo in Piezo-expressing cells resulted in larger larval wing discs and larger adult wings, a phenotype that was also observed in Piezo mutants. The increased wing size was due to an increase in individual cell size. Reduction of Piezo expression resulted in increased cell size, while overexpression of Piezo resulted in decreased cell size. The insulin signaling pathway is a known regulator of cell size, and insulin signaling was modestly increased in Piezo mutants. Taken together, these data comprise preliminary evidence that mechanosensation via the Piezo cation channel is a core component of organ size regulation in the wing imaginal disc.

## Materials and Methods

### *Drosophila stocks and husbandry*

Crosses were maintained on standard fly food at 25C unless otherwise noted.

The following stocks were obtained from the Bloomington Stock Center: *Df(2L) BSC227* (BL9704), *Df(2L) BSC228* (BL9705), *Df(2L)BSC229* (BL9706), *Piezo<sup>KO</sup>* (BL58770), *UAS-Piezo::GFP* (BL58772), *Piezo-Gal4* (BL59266), *Piezo-Gal4; UAS-Piezo::GFP* (BL78336), *UAS-Stim-RNAi* (BL51865), *Tmc-Gal4* (BL66557), *Trpy-Gal4* (BL25629), and *Mid1-Gal4* (BL73633).

The following stocks were obtained from the Vienna Stock Center: *UAS-Piezo-RNAi* (V105523).

Additional stocks used include: *w<sup>1118</sup>*, *OreR*, *hsFLP*; *Act>>RFP*, *tGHP*, *UAS-GFP::cd8*, *UAS-GTRACE*.

### *Analysis of adult wings*

Right wings from density-controlled adult female flies were mounted onto slides using Canadian Balsam medium (Gary's Magic Mount) and imaged on a Leica transmitted light microscope (TL RC, Germany). Wing area and wing hair density was quantified in Image J.

### *Immunohistochemistry*

Imaginal discs were dissected in phosphate-buffered saline, fixed for 20 min in 4% PFA at room temperature, permeabilized in phosphate-buffered saline with 0.1% Triton X-100, and blocked in 10% Normal Goat Serum. Primary antibodies used were: rat anti-Ci (1:10, #2A1; Developmental Studies Hybridoma Bank, DSHB), mouse anti-Smo (1:10, #20C6; DSHB). Secondary antibodies used were: goat anti-mouse 555 (#A32727; Invitrogen) and goat anti-rat 647 (#A-21247; Invitrogen). Nuclei were stained with DAPI (1:1,000, Cell Signaling), and F-actin was stained with Alexa Flour 647 Phalloidin (Thermo Fisher A30107). Samples were imaged on a Zeiss Axio Imager.M2 with Apotome.2.

### *Cell dissociation*

Imaginal discs were dissected in Schnieder's medium, and dissociated in 1X TrpLE dissociation reagent (Thermo Fisher #A1217701) for 45 minutes with gentle rocking. At the 20min mark, vials were subject to additional mechanical dissociation by flicking the tube ten times. Cells were then pelleted by centrifugation at 8,000rpm for five minutes. The pellet was resuspended in 200µL Schnieder's medium, and mounted onto a glass slide. Samples were imaged on a Zeiss Axio Imager.M2 with Apotome.2. Cell area was measured using ImageJ.

### *Mosaic tissue generation*

To generate clones expressing Piezo, *hsFLP;;act<STOP<UAS-RFP/S-T* virgin females were crossed to *UAS-Piezo::GFP* males. Larvae were collected as described above, and vials were subjected to a 10 min heat shock in a 37°C water bath 48 h before dissection and fixation and preparation for immunohistochemistry.

### *Statistical analysis*

P values were obtained using ANOVA and unpaired Student's t-tests (GraphPad). Error bars in all graphs are standard deviation. P value significance < 0.001: \*\*\*; 0.001 to 0.01: \*\*; 0.01 to 0.05: \*; > 0.05: not significant.

## **Results**

### *A sparse cell population in the wing imaginal disc expresses the mechanosensitive ion channel Piezo.*

To explore a role for mechanosensitive ion channels in the development of the *Drosophila* wing, we began by characterizing expression patterns of known mechanosensitive channels. While Gal4 reporter lines for the channels Tmc, Trpy, and Mid1 did not show patterned expression (Figure 3.2 A-C), a cloned enhancer of the mechanosensitive channel Piezo was expressed in a sparse cell population throughout the disc proper (Figure 3.1 A-C) and peripodial epithelium (Figure 3.1 E, E'). The density of Gal4-expressing cells within the tissue decreased over developmental time, and only very few GFP+ cells were detectable by the late third instar (Figure 3.1 D). Piezo-expressing cells were integral within the disc proper and peripodial epithelium (Figure 3.1 F), suggesting that they are not derived from neuronal cell types. Overall, more GFP+ cells were detected in the pouch of the wing disc, as compared to the hinge and notum (Figure 3.1 G). Lineage tracing of the cloned enhancer using the GTRACE system showed that Piezo-expressing progenitors gave rise to large regions of the disc (Figure 3.1 H). To validate these findings, we investigated the expression pattern of a Gal4 knock in construct and the endogenous Piezo locus (generated in (He et al., 2018)). This line produced much more abundant GFP expression, although the abundance of GFP+ cells also decreased over the course of the third instar (Figure 3.1 I-K). Taken together, these data suggest that Piezo is expressed in a subset of the cells of the *Drosophila* wing imaginal disc.

### *Loss of Piezo results in larger larval wing discs and adult wings.*

As Piezo had been implicated in morphogenesis in other systems, we wondered if it might be required for growth or patterning in the wing imaginal disc. To test this, we expressed RNAi against Piezo using the cloned enhancer line. Surprisingly, knockdown of Piezo in the Piezo-expressing population resulted in larger adult wings (Figure 3.3 A, B).

We next set out to characterize organ size in a Piezo mutant. Using a previously generated line in which all 31 coding exons of Piezo are deleted through FLPase

mediated recombination, we compared adult wing size between *Piezo*<sup>KO</sup> animals and both *w*<sup>1118</sup> and *OreR* control lines (Figure 3.3 C, D). In both cases, *Piezo*<sup>KO</sup> wings were significantly larger than controls. We further validated this finding by measuring the wing area of F1 progeny of *Piezo* mutants and three deficiency lines which lack genomic regions containing the *Piezo* coding sequence (Figure 3.4 A). All three heterozygote crosses had larger wings than both *w*<sup>1118</sup> and *OreR* controls. Further, we established that *Piezo* loss of function is a dominant effect, by crossing the *Piezo* mutant to *w*<sup>1118</sup> flies (Figure 3.3 D). Collectively, these data suggest that *Piezo* expression is required to regulate the size of the *Drosophila* adult wing, and that loss of *Piezo* function results in organ overgrowth.

We wondered if larval organs were affected by *Piezo* loss of function. Third instar discs from *Piezo*>*Piezo-RNAi* and *Piezo*<sup>KO</sup> animals were larger, and showed ectopic folds and excess tissue, suggesting that in the absence of *Piezo*, organ overgrowth occurs in the larval life stage (Figure 3.3 E-H).

#### *Loss of Piezo results in an increase in cell size.*

An increase in organ size could be the result of increased cell numbers, or larger cells. To distinguish between these two possibilities, we took advantage of the fact that each cell of the prospective wing blade generates a single bristle during pupariation, which can be easily distinguished in the adult wing using transmitted light microscopy. We quantified the number of wing hairs within a 200µm square area in *w*<sup>1118</sup> and *Piezo*<sup>KO</sup> adult wings (Figure 3.5 A-C). The density of wing hairs was significantly reduced in the *Piezo*<sup>KO</sup> wings, suggesting that cell size was larger in these flies. We then used paired bristle density and wing area measurements to quantify the total number of cells per wing. Total cell number was slightly increased in *Piezo* mutants, but the effect was not statistically significant (data not shown). Therefore, the increase in wing size observed in *Piezo*<sup>KO</sup> animals is primarily due to an increase in cell size.

To validate these findings in the larval wing imaginal disc, we dissociated wing discs from each genotype, and measured the circumference and cross-sectional area of individual cells (Figure 3.5 D-F). In this assay, *Piezo*<sup>KO</sup> cells were observed to be larger than *w*<sup>1118</sup> cells. Finally, we generated clones of cells overexpressing *Piezo*, and compared the cross-sectional area of these cells to clones expressing RFP (Figure 3.5 G-I). *Piezo*-overexpressing cells had a smaller cross-sectional area than neutrally-marked clones. Together, these data indicate that *Piezo* function constrains cell size; loss of *Piezo* results in larger cells, and ectopic *Piezo* expression results in smaller cells.

#### *Signaling downstream of Piezo activation in the wing disc.*

We next wondered what mechanisms link *Piezo* channels to cell size regulation. Calcium signaling had previously been shown to be downstream of *Piezo* in the fly gut. We decreased cytosolic calcium concentration in *Piezo*-expressing cells by expressing RNAi against the STIM calcium channel. Knockdown of STIM increased the size of third instar wing imaginal discs, although not as dramatically as knockdown of *Piezo* (Figure

3.6 A-C). Therefore, calcium signaling in *Piezo*-expressing cells may also modulate organ size.

Insulin signaling is also known to regulate cell size. In the fly, mutations in the insulin receptor (InR) result in a ~30% increase in individual cell size (C. Chen, Jack, & Garofalo, 1996; Shingleton, Das, Vinicius, & Stern, 2005). To ask whether or not insulin signaling was affected by *Piezo* activity, we made use of a fly line which ubiquitously-expressed a plextrin homology domain GFP fusion protein (tGPH, (Britton, Lockwood, Li, Cohen, & Edgar, 2002)). The plextrin homology domain of tGPH binds to PIP3, a second messenger of insulin signaling. In instances of high insulin signaling, the tGPH reporter localizes to the cell membrane, and in instances of low insulin signaling, it is primarily cytosolic. We crossed this line to either *w<sup>1118</sup>* flies, or *Piezo<sup>KO</sup>* flies. While the wing discs of *w<sup>1118</sup>/tGPH* heterozygotes showed subtle membrane staining of tGPH, *Piezo<sup>KO</sup>/tGPH* heterozygotes showed slightly increased membrane staining (Figure 3.6 D-E'). This suggests that insulin signaling may be slightly increased in *Piezo<sup>KO</sup>* animals.

## Discussion

Tissues integrate intrinsic and extrinsic signals in order to coordinate growth and patterning during development. Mechanosensitive ion channels are emerging as regulators of complex morphological behaviors, cell size and shape, and stemness. Here, we present evidence suggesting that the mechanosensitive channel *Piezo* plays a role in regulating organ growth by influencing cell size in the *Drosophila* third instar wing imaginal disc.

Two major outstanding questions remain about the role of *Piezo* in wing disc size development. The first concerns the identity of *Piezo*-expressing cells. Two *Gal4* lines exist to assess in which cells *Piezo* is expressed. The first is a cloned enhancer inserted outside of the endogenous locus. This line reports expression in very few cells, which are relatively evenly spaced throughout the disc. The second reporter line is located within the endogenous locus, and reports expression in a much larger number of cells. Discerning whether or not there is something unique about the sparse population of cells marked by the cloned enhancer line will be of great importance, as work in the *Drosophila* gut identified a sparse *Piezo*-expressing cell population that represented restricted-lineage stem cells. Lineage tracing of this enhancer-expressing population suggests that these cells give rise to many, but not all, cells of the wing disc.

Further work is also necessary to link *Piezo* activation to cell size regulation. Calcium signaling in cells expressing *Piezo-Gal4* seems to be involved in size regulation, but downstream calcium targets have yet to be elucidated, and it is unclear whether or not there are multiple *Piezo*-expressing populations that are marked by *Piezo-Gal4*. Bulk RNA sequencing comparing wild type and *Piezo* mutant imaginal discs 96 hours after egg deposition has been undertaken to identify differentially expressed genes downstream of *Piezo* inactivation.

It will also be of interest to assess the role of other known regulators of cell size, like dMyc and mTOR signaling in Piezo mutants. Insulin signaling, as assessed by tGPH membrane localization, is slightly increased in *Piezo*<sup>KO</sup> animals. Previous work has shown that loss of the insulin receptor InR decreases cell size in *Drosophila*. However, there are other regulators of cell size that have yet to be explored. Assaying dMyc activity and translational activity in mosaic tissue will provide more information about the mechanism by which Piezo mutant cells grow larger than wild type. Additionally, exploring potential interactions between Piezo and the Hippo pathway, a growth-regulatory signaling cascade known to be modulated by mechanical signaling, is an important future direction.

## Figures

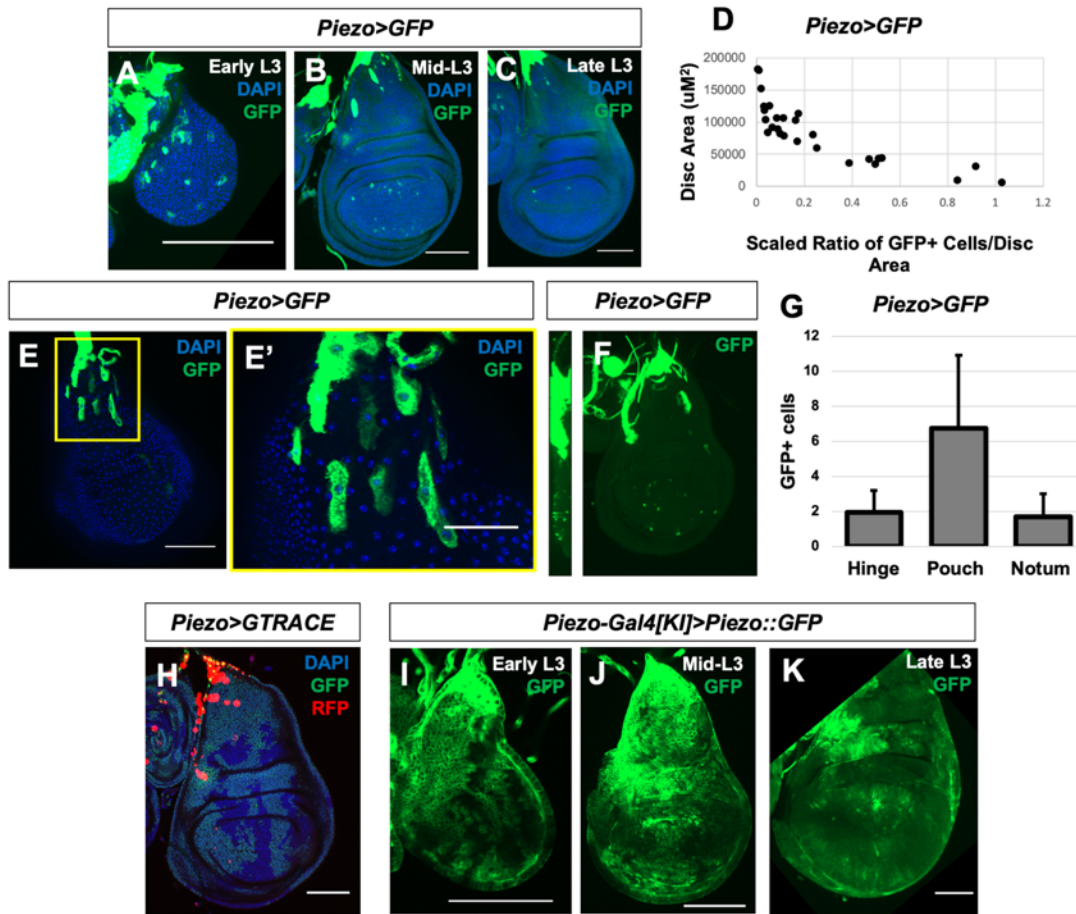


### Figure 3.1: A sparse population of Piezo-expressing cells in the wing imaginal disc.

(A–C) Expression pattern of a cloned Piezo enhancer (BL59266) in the disc proper throughout the third larval instar. (D) Density of GFP+ cells over increasing disc areas. Piezo is expressed in some peripodial epithelium cells in the notum (E), inset (E'). (F) Piezo-expressing cells in the disc proper are integral to the epithelium. (G) Distribution of Piezo-expressing cells across regions of the disc. (H) Lineage tracing of the Piezo-Gal4 cloned enhancer. (I) Expression pattern of Piezo-Gal4 at the endogenous locus (BL78336) in the disc proper throughout the larval instar. Scale bars are 100  $\mu\text{m}$  in all panels.

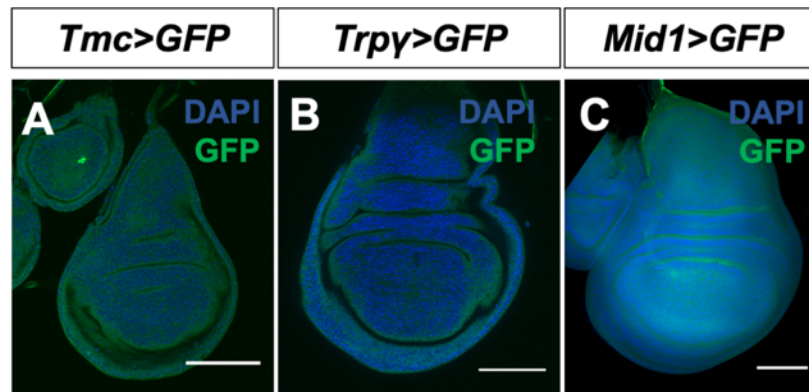


**Figure 3.2: Expression patterns of other mechanosensitive ion channels in the disc.**

Expression patterns of (A) *Tmc-Gal4*, (B) *Trpy-Gal4*, and (C) *Mid1-Gal4* in the third instar wing disc. Scale bars are 100  $\mu\text{m}$  in all panels.

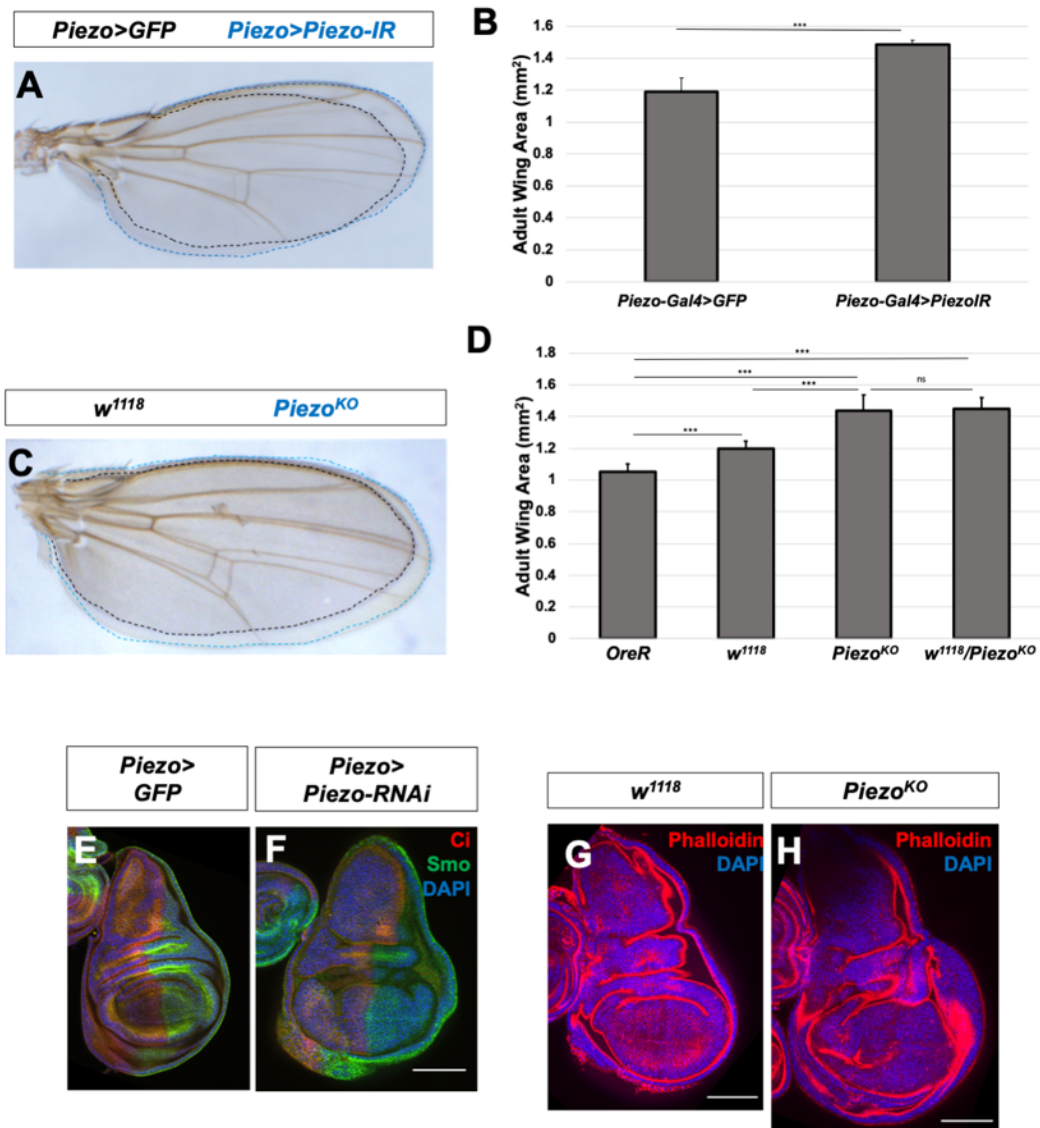


**Figure 3.3: Loss of Piezo results in larger adult organs and imaginal wing discs.** (A-B) Adult female right wing area measurements of flies in which *Piezo-RNAi* is driven with *Piezo-Gal4*. (C-D) Adult female right wing area measurements *OreR* and *w<sup>1118</sup>* wild-type flies, *Piezo* mutants, and heterozygotes. (E-F) Third-instar wing imaginal discs of control and *Piezo>Piezo-RNAi* animals. (G-H) *w<sup>1118</sup>* and *Piezo<sup>KO</sup>* third instar wing imaginal discs. Scale bars 100μm in all panels.

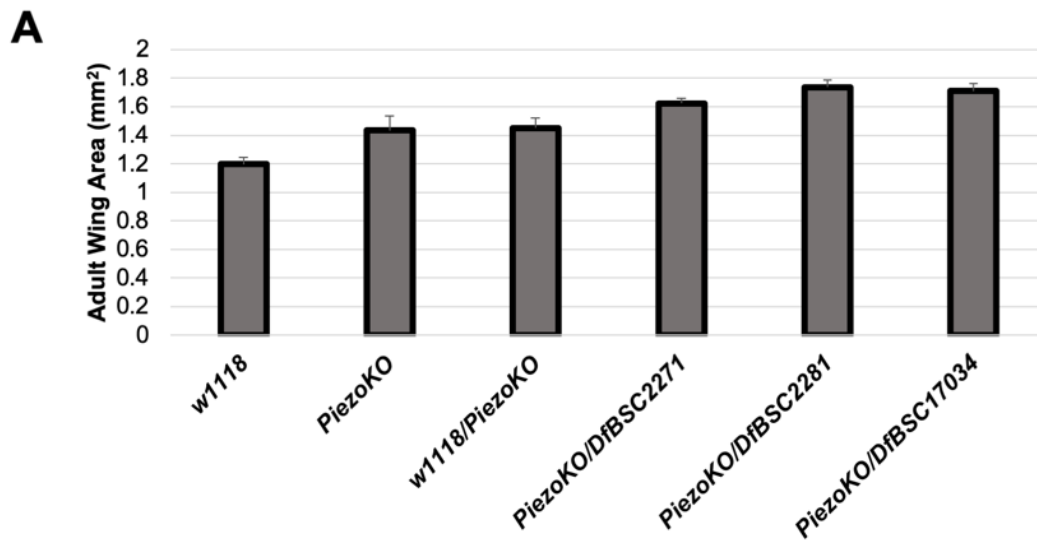


**Figure 3.4: Loss of Piezo results in larger adult organs.**

(A) Comparison of adult female fly right wing area in wild-type flies, Piezo mutants, flies heterozygous for Piezo loss of function, and F1 animals derived from crossing Piezo mutants with three deficiency lines in which the Piezo coding sequence is removed.

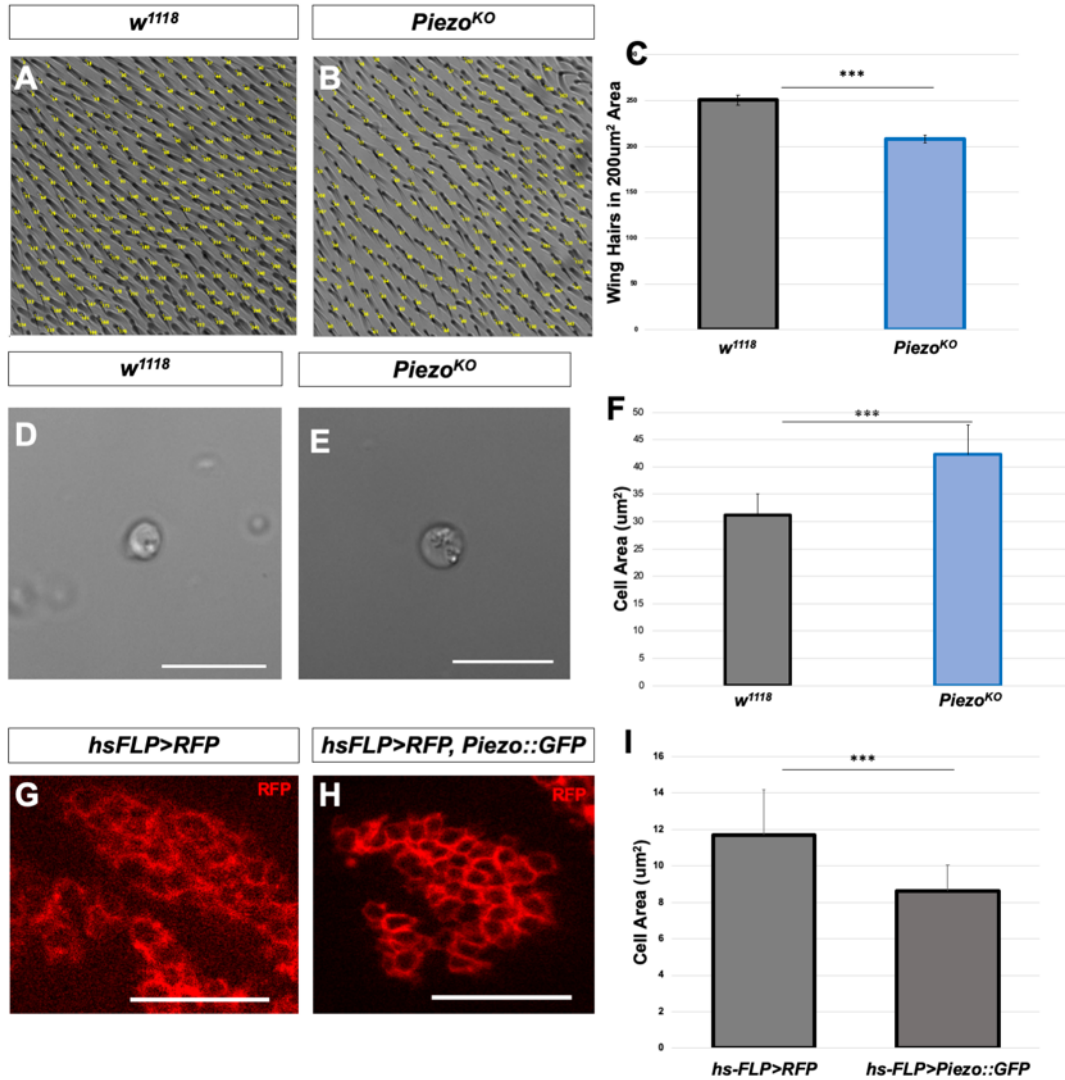
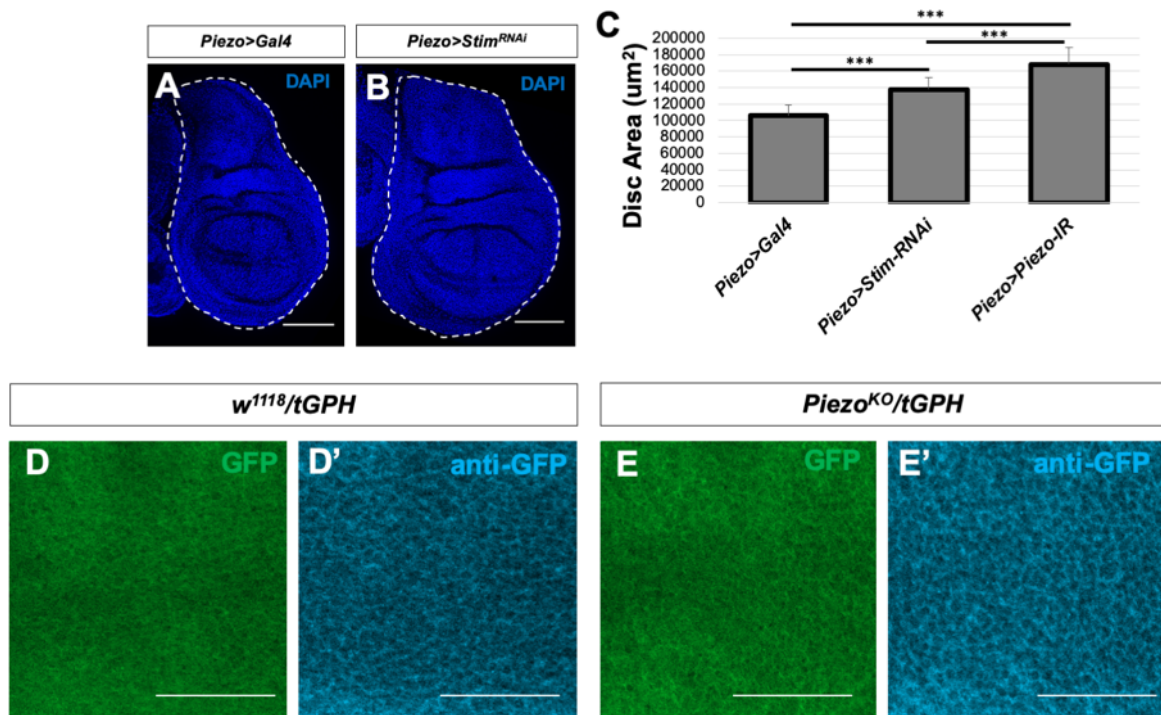


**Figure 3.5: Piezo modulates cell size.**

(A-C) Wing hair density in 200 $\mu\text{m}^2$  area sections in *w<sup>1118</sup>* wild-type flies and *Piezo* mutants. (D-F) Cell cross-sectional area measurements from dissociated wing disc tissue. (G-I) Cell area measurements in cells expressing *RFP*, or expressing *UAS-Piezo::GFP*. Scale bars 25 $\mu\text{m}$  in all panels.



## Chapter Four

### Membrane potential mediates compartment-specific cell competition in the wing disc.

This chapter is a partial reproduction of data from the preprint:  
Membrane potential regulates Hedgehog signaling and compartment boundary maintenance  
in the *Drosophila* wing disc. Emmons-Bell M, Yasutomi R, Hariharan IK. *BioRxiv*, 2020

I contributed Figures 4.1 C-G, supervised R. Yasutomi's generation of the remaining  
figures, and wrote the chapter.

## Abstract

During development, multi-cellular ensembles must tightly regulate their composition in order to form functional tissues. Aberrations in cellular growth rate, size, or differentiation status pose threats to the integrity of the developing organism, especially if they occur early in the course of development. Tissues employ mechanisms to surveil the composition of a tissue, and eliminate cells with altered behavior, a phenomenon called cell competition. Recently, electrochemical potential has been shown to be patterned in the *Drosophila* third instar wing imaginal disc, a model epithelium. We found that cells with values of membrane potential that deviate from the normal wild type pattern are eliminated through a mechanism reminiscent of cell competition. Clones of cells which overexpress the sodium channel NaChBac are eliminated from the posterior compartment, and cells expressing RNAi against the epithelial sodium channel Ripped Pocket are eliminated in the anterior compartment. This elimination is dependent on heterotypic interactions with wild-type cells, and is mediated by apoptosis. Our data suggests that membrane potential is a physiological parameter that is enforced at a tissue-wide scale by mechanisms of cell competition.

## Introduction

Although development relies on cooperation between cells, cellular interactions can also be competitive, resulting in the elimination of “loser” cells from a tissue by “winner” cells. Cell competition was first described by Gines Morata and Pedro Ripoll in 1975 (Morata, 2021; Morata & Ripoll, 1975). Morata and Ripoll were studying the behavior of a class of *Drosophila* mutants called Minutes, which although homozygous lethal, were viable as heterozygotes, and displayed delayed development due to decreased translation and a slower rate of cell division. When mosaic tissue comprised of cells heterozygous for a Minute mutation and wild type cells was generated, Minute mutant clones were rarely recovered in adult tissues. Morata and Ripoll suggested that the delayed rate of cell division in Minute mutant clones was sensed by surrounding wild-type cells, and that this led to the elimination of Minute mutants from the tissue

In the ensuing years, cell competition was documented in a variety of systems, including the developing nervous system (Jam et al., 2020), and in tumors (reviewed in (Pelham, Nagane, & Madan, 2020)). A diversity of cellular competitive mechanisms have been described. Cells with altered apicobasal polarity (Brumby & Richardson, 2003; Norman et al., 2012), inappropriate positional identity (Adachi-Yamada & O'Connor, 2002), and neoplastic behavior (Adachi-Yamada & O'Connor, 2002) have been shown to be eliminated from developing tissues. Reflecting the multitude of cell behaviors that induce competition, the mechanisms by which cell fitness is sensed in a tissue are varied. These include increased uptake of the tumor necrosis factor Eiger in “loser” cells (Igaki, Pastor-Pareja, Aonuma, Miura, & Xu, 2009), activation of Toll and NF- $\kappa$ B signaling in “winner” cells (Germani, Hain, Sternlicht, Moreno, & Basler, 2018), and downregulation of the Hippo pathway co-effector Yorkie in “loser” cells (Katsukawa, Ohsawa, Zhang, Yan, & Igaki, 2018). Therefore, cell competition is thought to be a phenomenon by which tissues suppress cells with broadly inappropriate properties,

including both overgrowing and undergrowing cells, and is carried out via numerous mechanisms that transduce cell-intrinsic phenomena to neighboring cells.

The wing imaginal disc of the *Drosophila* larvae has been fertile ground in the study of cell competition. Due to the fly's genetic tractability, mosaic tissue generation is rapid and easy, allowing scientists to assay competitive interactions between mutants of interest and wild-type tissue. Indeed, the vast majority of competitive mechanisms were first described in *Drosophila*.

The calcium channel protein *flower* (*fwe*) was recently proposed to mediate cell competition in the wing disc (Rhiner et al., 2010). Comparison of the transcriptomes of winner and loser cells resulted in the identification of multiple isoforms of *flower*, one of which was more highly expressed in loser cells, and one of which was more highly expressed in winner cells. The apposition of cells expressing different isoforms led to competitive elimination of the population expressing the loser isoform, by inducing the expression of the EF-hand protein Ahuizotl (*Azot*). Previously, we reported that membrane potential, a core physiological parameter in all cells, is patterned in the wing imaginal disc (Emmons-Bell & Hariharan, 2021). Cells anterior to the anteroposterior compartment boundary are more depolarized than cells in the posterior compartment. The domain of depolarized cells is broader early in the third instar, and is progressively refined as development progresses. Depolarized membrane potential serves to facilitate high levels of Hh signaling anterior to the compartment boundary.

We were interested in mechanisms that mediate interactions between cells of disparate membrane potential, as occurs across the compartment boundary. To investigate this, we generated clones of cells with altered membrane potential by virtue of overexpression or knockdown of particular ion channels. We found that cells with aberrantly depolarized membrane potential were recovered with lower frequency in the posterior compartment of the wing disc. We also found that cells expressing RNAi against the epithelial sodium channel Ripped Pocket were eliminated from the anterior compartment. This elimination was mediated by apoptosis, and was dependent on interactions with wild-type cells. Taken together, these data suggest that membrane potential is also sensed in a non-autonomous fashion, and cells with inappropriate values of membrane potential are subject to competitive interactions.

## Materials and Methods

### *Drosophila* strains and husbandry

Animals were raised on standard medium as used by the Bloomington *Drosophila* Stock Center. All animals were raised at 25°C.

Stocks used in this study include: *hsFLP*; *act<stop<Gal4, UAS-RFP/S-T, ), UAS-Rpk-RNAi*; (BL39053), *UAS-NaChBac*; (BL:9466), *en-Gal4*; (BL:6356), *UAS-p35* (BL5072).

### Mosaic Tissue Generation

Experiments using heat shock-controlled FLPase and *act<<Gal4* were maintained at 25°C. To generate clones overexpressing NaChBac, *ywhs-FLP*; *Act<<Gal4, UAS-RFP/S-*

*T* virgin females were crossed to *yw;;UAS-NaChBac* (BL:9466) males. Crosses were set up in cages, and females were allowed to lay eggs on grape plates with yeast paste for 8 hour increments. L1 larvae were picked and seeded into vials at a density of 50 larvae/vial. Vials were subjected to a 10 minute heat shock in a 37°C water bath 96, 72, and 48 hours prior to dissection. To generate clones expressing RNAi against Rpk, *hs-FLP;;act<STOP<UAS-RFP/S-T* virgin females were crossed to *yw;;UAS-Rpk-RNAi* (BL:39053, BL:25847) males. Larvae were collected as described above, but vials were subjected to five minute heat shocks in order to mitigate lethality associated with broad expression of Rpk-RNAi.

### *Quantification and statistical analysis*

Area measurements were recorded using FIJI software (NIH, Bethesda, USA). *P* values were obtained using ANOVA and unpaired Student's *t* tests (Graphpad). Error bars in all graphs are standard deviation. *P* value significance <0.001: \*\*\*; 0.001 to 0.01: \*\*; 0.01 to 0.05: \*; >0.05: not significant.

## **Results**

### *Compartment-specific recovery of cells with expressing NaChBac.*

The anteroposterior compartment boundary appears to represent not just the boundary between two lineage-restricted domains of cells, but also the boundary between two populations maintaining disparate  $V_{mem}$ . Although A cells just anterior to the boundary appear more obviously depolarized than neighboring P cells, the pattern of DiBAC fluorescence in younger discs suggests that the zone of depolarization could be broader at earlier stages of development. We therefore investigated the properties of clones of cells in each of the two compartments that are more depolarized or hyperpolarized than their neighbors. We first generated discs containing clones of cells that overexpressed the bacterial sodium channel NaChBac (Luan et al., 2006; Nitabach et al., 2006; Ren et al., 2001), which would be predicted to be more depolarized than their neighbors. When clones were induced late in development, and given only 48 hours to grow in the tissue before dissection, they were recovered with equal frequency in both compartments (Figure 4.1 A, B). However, when clones were induced at progressively earlier times in development, we observed fewer and fewer surviving clones in the P compartment (Figure 4.1 A'-B).

### *Elimination requires heterotypic cell interactions.*

The elimination of clones of cells over time in a context-dependent manner is reminiscent of cell competition (Baker, 2017; Johnston, 2009; Morata & Ripoll, 1975). Cell competition is a phenomenon by which cells of lower relative fitness are eliminated from a tissue due to heterotypic interactions with cells of higher fitness (Baker, 2017). We wondered whether cells expressing NaChBac were eliminated by a similar mechanism in the posterior compartment. We drove expression of NaChBac in the entire posterior compartment, forming a homotypic environment in which cells should survive if NaChBac expression is not cell-autonomously lethal. In these discs, we observed no increase in apoptosis in the NaChBac-expressing posterior compartments

as compared to control discs (Figure 4.1 C-E), suggesting that elimination of NaChBac expressing clones in the posterior compartment is dependent on heterotypic interactions with wild-type cells.

*Compartment-specific recovery of cells lacking Rpk.*

Our data suggest that ectopically depolarized clones are eliminated from the posterior compartment, which is relatively hyperpolarized as compared to the anterior compartment. In order to generate clones of cells that are predicted to be relatively hyperpolarized, we generated clones expressing *UAS-rpkRNAi*. Such clones were recovered preferentially in the P compartment, suggesting that these have lower relative fitness in the A compartment (Figure 4.1 F-G). Taken together, these data indicate that more depolarized cells survive better in the A compartment and that more hyperpolarized cells survive better in the P compartment.

*Eliminated cells undergo apoptosis.*

Elimination of cells from a tissue can occur via apoptosis, or via extrusion. We did not observe obvious extrusion of NaChBac-expressing cells from the disc. However, we did observe markers of cell death in NaChBac-expressing cells. Staining with an anti-DCP1 antibody showed clear death in clonal, but not homotypic situations (Figure 4.2 A, B). DCP1 staining was not dramatic in clones induced 24h before dissection, but was abundant in clones induced 48h before dissection, and slightly increased in the posterior compartment (Figure 4.2 C).

We next generated clones in which NaChBac was co-expressed with p35. These “undead” clones are unable to induce apoptotic programs, and were not eliminated from the posterior compartment when induced 72h prior to dissection, suggesting that normally elimination occurs via cell death (Figure 4.3 A-C). Interestingly, generation of these clones 48h prior to dissection proved lethal, and no clones were recovered in either compartment when clones were generated 96h prior to dissection. Additionally, many NaChBac clones co-expressing p35 displayed unusual morphology, and the wing discs containing these clones often displayed altered patterning with ectopic folds in the wing pouch and hinge (Figure 4.3 E, F).

## Discussion

Previous work has shown that cells with altered positional identity are eliminated via cell competition (Adachi-Yamada & O'Connor, 2004). This mechanism ensures the fidelity of morphogenetic fields, by reducing systemic noise and disruptions to patterning signals. Analogously, we have found a mechanism that could contribute to the segregation of A and P cells in the wing imaginal disc. Clones of cells that are more depolarized than their neighbors tend to survive preferentially in the A compartment while clones of hyperpolarized cells tend to survive preferentially in the P compartment. Thus, single cells from each compartment that enter the other compartment could be eliminated.

The compartment-specific mechanism of cell elimination that we have uncovered has some similarities to the group of phenomena referred to as cell competition that was first

described for clones of cells that were heterozygous for a Minute mutation (Morata & Ripoll, 1975). A gene that has been implicated in cell competition, *flower* (*fwe*) encodes a  $\text{Ca}^{2+}$  channel (Rhiner et al., 2010; Yao et al., 2009), but compartment specificity in the behavior of *fwe* clones has not been described thus far, and cells expressing a specific isoform of *fwe* are eliminated in both compartments (Rhiner et al., 2010). Thus, there is currently no simple way to connect the compartment-specific clone elimination phenomenon we have observed to existing models of cell competition.

The relationship between clone elimination caused by changes in  $V_{mem}$  and other types of cell competition therefore represent a fertile area for future research. For one, it remains unknown how altered membrane potential is sensed by neighboring cells. Gap junction channels are proteins that mediate electrical coupling between cells, and are able to rapidly transduce information about the physiological properties of cells. Cells within the anterior, posterior, dorsal and ventral compartments are coupled, likely via gap junctions, but compartments are electrically insulated from each other (Weir & Lo, 1984). Modulating the degree of electrical connectivity in the tissue and assaying compartment-specific elimination will help elucidate mechanisms which sense non-autonomous physiology.

It is also of interest that clones expressing NaChBac and p35 (and are therefore unable to initiate cell death programs) display altered morphology, and induce patterning disruptions in the rest of the wing disc. Future experiments assessing autonomous growth rates, as well secreted factors in these clones will further efforts to understand why altered membrane potential may be deleterious to the tissue. Overall, we have presented data which characterizes a novel, compartment-specific instance of cell competition, and highlights the importance of cellular membrane potential in development.

## Figures

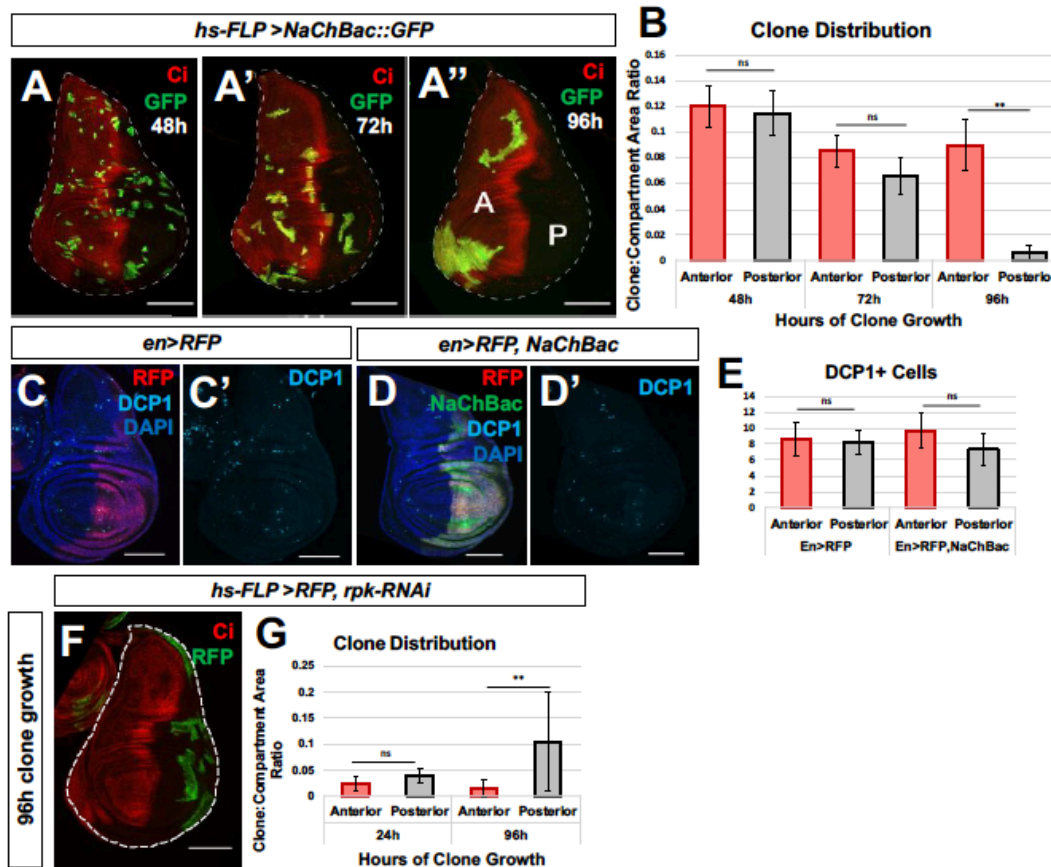


**Figure 4.1: Altered membrane potential induces compartment-specific cell elimination.** (A-A'') Clones of cells expressing the depolarizing bacterial sodium channel NaChBac were generated 48 hours, 72 hours, and 96 hours prior to dissection. (B) The amount of NaChBac-expressing tissue in a compartment was quantified by measuring the ratio of the total area of GFP+ tissue to the area of the compartment, to control for the difference in size between the anterior and posterior compartments. A striking preference for clone recovery in the anterior compartment was observed in clones induced 96 hours prior to dissection, while clones induced later in development survived with relatively equal frequency between compartments,  $n=12$  discs for each time point. Data were compared using an unpaired t test ( $**p<0.01$ ). (C-E) Elimination of clones from the posterior compartment is dependent on heterotypic interactions with wildtype cells. No difference in apoptosis was observed when NaChBac was expressed in the entire posterior compartment (E),  $n=6$  discs. Data were compared using an unpaired t test. (F-G) Clones of cells expressing RNAi against the ENaC *rpk* are recovered preferentially in the posterior compartment, using the quantification scheme described above,  $n=15$  discs, data were compared using an unpaired t test ( $**p<0.01$ ). Clone area ratios are lower in this experiment because the heat shock exposure was decreased in order to mitigate lethality associated with widespread knockdown of *rpk*. Scale bars are  $100\mu\text{M}$  in all panels.

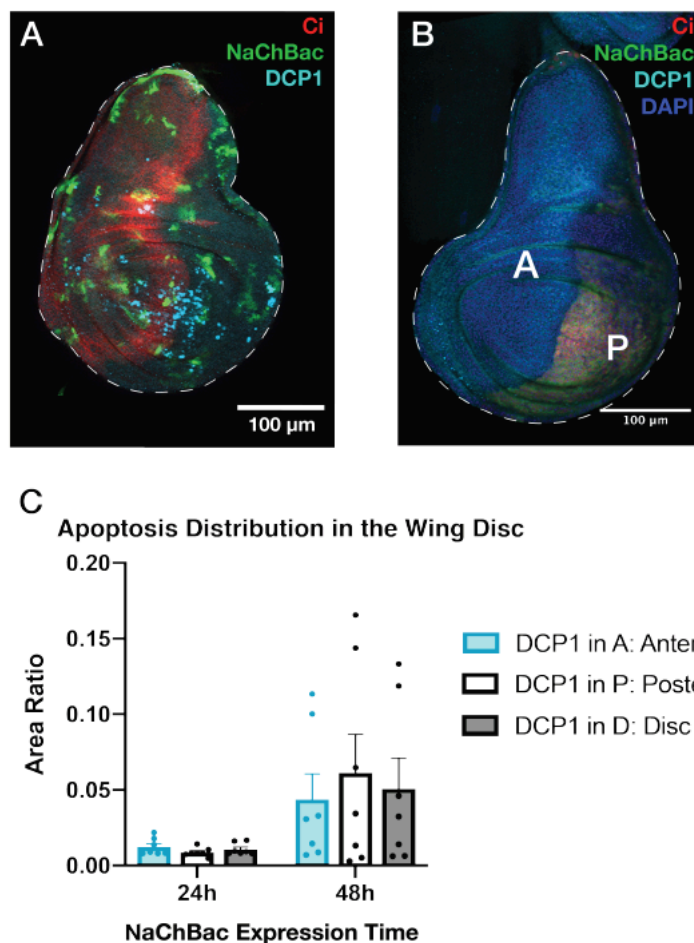


### Figure 4.2: Patterns of apoptotic death in NaChBac-expressing clones.

A) Apoptosis when clones are induced 54 hours after egg lay and NaChBac is expressed for 48 hours up to dissection, visualized by immunostaining for Death Caspase-1 (DCP1). Apoptosis of depolarized cells at the interface of clones and wild-type cells can be observed. (B) Generation of a homotypic environment. NaChBac is expressed in the entire posterior compartment, denoted by 'P' or red. No apoptosis is detected. (C) Quantification of apoptosis in the wing disc. Each dot represents a biological replicate wing disc and bars represent mean  $\pm$  SEM. Bars represent the ratio of area of DCP1 staining in the specified domain to the area of the entire domain. When NaChBac is expressed for 24 hours up to dissection, little apoptosis is observed. When NaChBac is expressed for 48 hours up to dissection, cells in the posterior undergo apoptosis, suggesting elimination by cell competition.

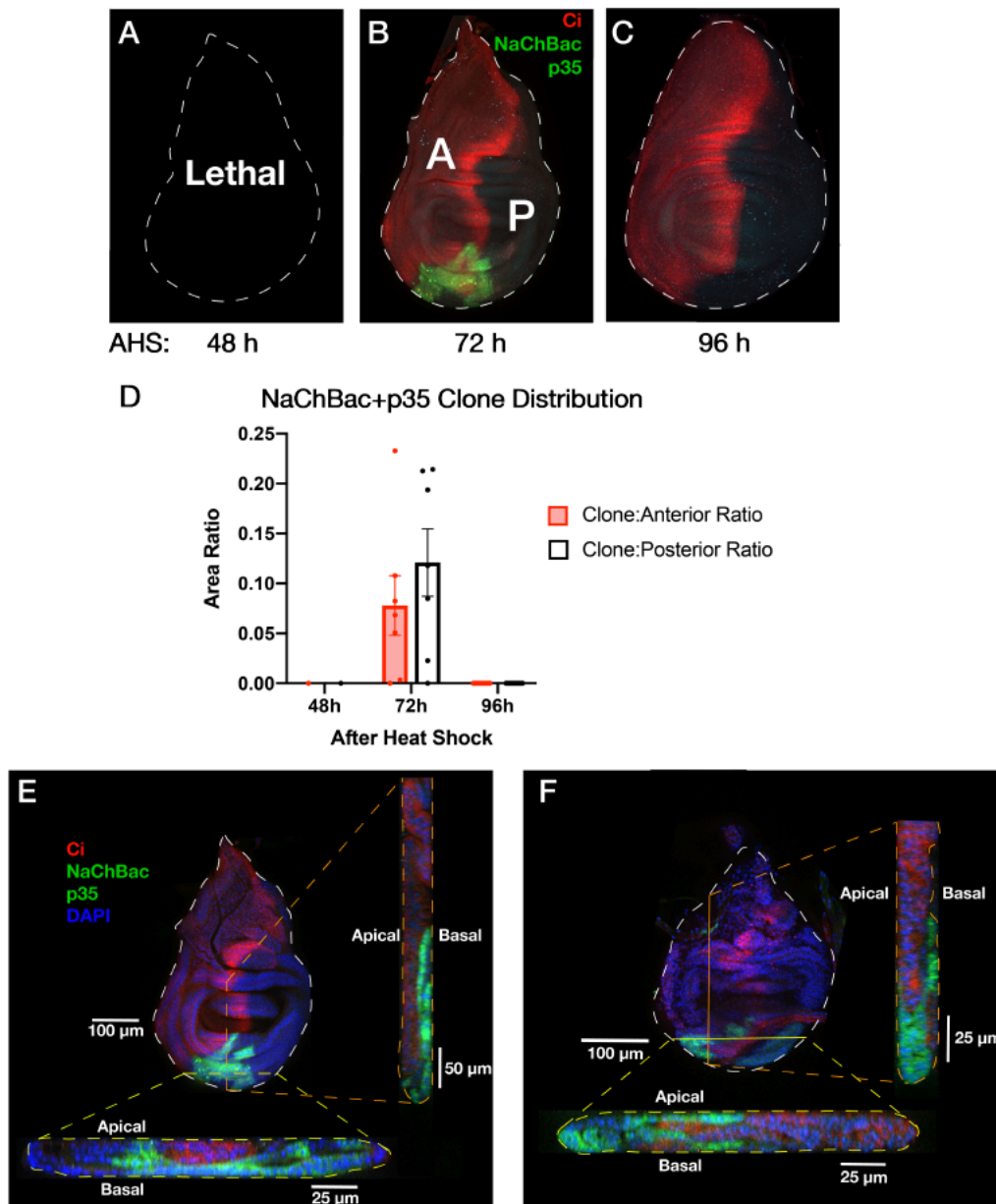


### Figure 4.3: Blockade of apoptosis in *NaChBac*-expressing clones.

(A-C) Distribution of clones expressing *NaChBac* and *p35* in the wing disc throughout development. The times denote hours after heat shock (AHS) until dissection. (D) Quantification of clone distribution in the wing disc. Each dot represents a biological replicate wing disc and bars represent mean  $\pm$  SEM. Red bars represent the ratio of anterior clone area to the anterior compartment area. White bars represent the ratio of posterior clone area to the posterior compartment area. Larvae heat shocked 48 hours prior to dissection did not survive. No clones were recovered in larvae heat shocked 96 hours prior to dissection. Larvae heat shocked 72 hours prior to dissection recovered clones in both compartments. (E-F) Wing discs of *NaChBac+p35* clones induced 72

hours prior to dissection. Clones are recovered preferentially in the ventral hinge. Cross section images anterior-posteriorly and dorsoventrally reveal unusual clone morphology.

## Chapter Five

### **The Hippo pathway coactivator Yorkie can reprogram cell fates and create compartment-boundary-like interactions at clone margins**

This chapter is a partial reproduction of the paper: Bairzin, J., Emmons-Bell M., Hariharan I.K. (2020). The Hippo pathway coactivator Yorkie can reprogram cell fates and create compartment-boundary-like interactions at clone margins. *Science Advances* 2020 (6), eabe8159.

I contributed Figures 5.2A-I", validated the experimental results presented in Figure 1, and assisted with the editing of the manuscript.

## Abstract

During development, tissue-specific patterns of gene expression are established by transcription factors and then stably maintained via epigenetic mechanisms. Cancer cells often express genes that are inappropriate for that tissue or developmental stage. Here, we show that high activity levels of Yki, the Hippo pathway coactivator that causes overgrowth in *Drosophila* imaginal discs, can also disrupt cell fates by altering expression of selector genes like *engrailed* (*en*) and *Ultrabithorax* (*Ubx*). Posterior clones expressing activated Yki can down-regulate *en* and express an anterior selector gene, *cubitus interruptus* (*ci*). The microRNA *bantam* and the chromatin regulator Taranis both function downstream of Yki in promoting *ci* expression. The boundary between Yki-expressing posterior clones and surrounding wild-type cells acquires properties reminiscent of the anteroposterior compartment boundary; Hedgehog signaling pathway activation results in production of Dpp. Thus, at least in principle, heterotypic interactions between Yki-expressing cells and their neighbors could activate boundary-specific signaling mechanisms.

## Introduction

As an organism develops from a fertilized egg, different portions of the embryo begin to exhibit specific patterns of gene expression. Those patterns of gene expression could be a consequence of the position of those cells in the embryo (e.g., Hox genes) or the specification of cells to the primordia of specific tissues (e.g., Pax6 for eye precursors). These patterns of gene expression are initially established by the expression of a specific combination of transcription factors and then stabilized by the attainment of specific chromatin states that make some genes more accessible to the transcription machinery, the so-called epigenetic landscape (Allis & Jenuwein, 2016; Britten & Davidson, 1969).

For many years, cancer cells have been known to display morphological characteristics that are inappropriate to their tissues of origin. One possible explanation is that cancer cells express tissue-inappropriate genes (Axelsen, Lotem, Sachs, & Domany, 2007; Flavahan, Gaskell, & Bernstein, 2017). Recent efforts at characterizing genomes of cancers have shown that a subset of human cancers have mutations in chromatin regulators and splicing factors, which would be predicted to cause changes in gene expression or alterations in the expression of certain splice isoforms (Vogelstein et al., 2013). However, it is also possible that the activation of a variety of oncogenes or inactivation of tumor suppressor genes could themselves cause tissue-inappropriate gene expression. Currently, we have a poor understanding of how oncogenesis can perturb mechanisms that preserve tissue-specific patterns of gene expression and the biological consequences of these perturbations.

The mechanisms that function during development to establish region-specific and tissue-specific patterns of gene expression have been studied extensively in *Drosophila*. A hierarchy of transcription factors acts during early embryogenesis to set up patterns of selector gene expression that specify individual regions of the embryo. Examples

include the Hox gene *Ultrabithorax (Ubx)*, which is expressed in specific embryonic segments, and the genes *engrailed (en)* and *cubitus interruptus (ci)*, which are expressed in the posterior and anterior compartments of each segment, respectively. Once their patterns of expression are established, they are maintained by epigenetic mechanisms that include the involvement of the Polycomb and Trithorax groups of genes (Kassis, Kennison, & Tamkun, 2017).

The pathways that promote tissue growth are conserved between humans and *Drosophila*. In *Drosophila* imaginal discs, the larval primordia of adult structures such as wings and eyes, increased activity of growth-promoting pathways can result in tissue overgrowth. This overgrowth can be elicited by expressing Myc (Johnston, Prober, Edgar, Eisenman, & Gallant, 1999), an activated form of Ras (RasV12) (Karim & Rubin, 1998; Prober & Edgar, 2000), or Yorkie (Yki) (Huang, Wu, Barrera, Matthews, & Pan, 2005), the coactivator downstream of the Hippo pathway (reviewed in (Pfleger, 2017)) in clones of cells. This allows us to investigate the effects of each of these genes on the patterns of selector gene expression that have been established in the imaginal discs.

Here, we show that among the genes tested, an activated form of Yki (*yki<sup>CA</sup>*) is especially potent in destabilizing established patterns of selector gene expression. Clones of *yki<sup>CA</sup>* cells in the posterior compartment of the wing disc express the anterior selector gene *ci* instead of the posterior gene *en* and sometimes inappropriately express *Ubx*. We present an investigation of these changes and also show that heterotypic interactions at the boundary between the overgrown clone and surrounding wild-type cells can acquire properties reminiscent of a compartment boundary, a phenomenon that could potentially occur at tumor margins in general.

## Materials and Methods

### *Experimental design*

We set out to characterize the ectopic expression of selector genes seen in some overgrown tissues and to investigate the role of this ectopic gene expression in the biology of overgrowth. To generate overgrown tissue, we used a system with heat shock–induced FLPase and actin-driven FLP-out Gal4 with UAS-ykiS168A. This system generated random overgrown clones throughout the larva, with clone frequency controlled by length of heat shock. All components of this system were contained within one stable stock that could be crossed to other stocks to test the role of candidate genes and use lacZ reporters.

### *Drosophila stocks*

Stocks used in this study include the following: hsFLP; act<stop<stopRFP, FRT40A, banΔ1, banGFP, en-Gal4, dpp-lacZ, UAS-RFP, AP-1-RFP (Chatterjee & Bohmann, 2012), and TIE-DYE (50). Stocks were obtained from the Bloomington Drosophila Stock Center (BDSC): UAS-ykiS168A.v5 (#28818), UAS-yki.v5 (#28819), UAS-yki::GFP (#28815), wtsX1 (#44251), smo3 (#3277), UAS-ciRNAi (#64928), tara1-lacZ (#6403), UAS-taraRNAi (#31634), nub-Gal4 (#42699), 30A-Gal4 (#37534), UAS-dMyc (#9674), UAS-rasv12 (#4847), and UAS-jnkDN (#9311). Ci-lacZ was a gift from D. Kalderon

(Columbia University, USA). UAS-bantamsponge and UAS-bantam.D were gifts from S. Cohen (University of Copenhagen, Denmark). hs-Pc-sensor was a gift from V. Pirrotta (Rutgers University, USA). UAS-myc::tara was a gift from R. Smith-Bolton [University of Illinois, UrbanaChampaign, USA (originally from M. Cleary, University of California, Merced, USA)]. MARCM FRT19A and sd47M, FRT19A were gifts from D. Pan.

#### *Temperature shift and clone induction experiments*

Experiments using heat shock–controlled FLPase and *act<<Gal4* were maintained at 25°C, heat shocked for 7 min at 37°C at 72 hours after egg lay (hAEL) ± 12 hours, and then dissected and analyzed at 144 hAEL ± 12 hours. TIE-DYE experiments were conducted under the same conditions. Because ascertaining clone boundaries in this system can be challenging, we attempted to score only clones where boundaries were reasonably clear. hsFLP-induced mosaic analysis with a repressible cell marker (MARCM) experiments were conducted under the same conditions but with 10- to 15-min heat shocks (except for MARCM 19A experiments in Figure 5.2, which were heat shocked for 1 hour). Discs in fig. S5D were dissected at 120 hAEL because of the lack of developmental delay in these larvae, while larvae expressing *ykiCA* are delayed by approximately 1 day and thus were dissected at 144 hAEL. Crosses using *nub-Gal4*, *30A-Gal4*, and *en-Gal4* were incubated at 25°C, and larvae were dissected at wandering third instar (approximately 120 to 144 hAEL).

#### *Immunohistochemistry*

Imaginal discs were dissected and fixed in 4% paraformaldehyde for 20 min, washed and permeabilized in phosphate-buffered saline with 0.1% Triton X-100, and blocked in 10% normal goat serum. Primary antibodies used were  $\alpha$ -Ci [1:25; Developmental Studies Hybridoma Bank (DSHB)],  $\alpha$ -Ubx (1:10; DSHB),  $\alpha$ -En (1:25; DSHB),  $\alpha$ - $\beta$ -galactosidase (1:500; Promega),  $\alpha$ -V5 (1:500; Sigma-Aldrich),  $\alpha$ -Wg (1:100; DSHB),  $\alpha$ -Cut (1:100),  $\alpha$ -Ptc (1:50; DSHB),  $\alpha$ -pMAD (1:500; Abcam),  $\alpha$ -Smo (1:10; DSHB),  $\alpha$ -MMP1 (1:100; a combination of 14A3D2, 3A6B4, and 5H7B11; DSHB),  $\alpha$ -Tara (1:700; K. Koh),  $\alpha$ -H3K27me3 (1:500; Active Motif),  $\alpha$ -H3K9me3 (1:500; Active Motif),  $\alpha$ -H3K4me1 (1:500; Active Motif),  $\alpha$ -H3K4me3 (1:500; Active Motif),  $\alpha$ -H4ac (1:500; Active Motif), and  $\alpha$ -Sd (1:500; K. Guss). Secondary antibodies were from Cell Signaling Technology and used at 1:400. Nuclei were stained with 4',6-diamidino-2-phenylindole (1:1000; Cell Signaling Technology). Samples were imaged on a Zeiss LSM 700 confocal microscope.

#### *Statistical analysis*

Images were processed using Fiji (54), and statistical analysis was completed with GraphPad Prism and VassarStats 2x2 Contingency Table. All scale bars are 100  $\mu$ m unless otherwise noted. For clone size comparisons in Figs. 2K and 4H, P values were generated through a one-way analysis of variance (ANOVA) with Tukey's multiple comparison test for wild-type clones, *ykiCA* clones in a wild-type background, *ykiCA* clones in a *ban $\Delta$ 1* /+ background, and *ykiCA* clones with *taraRNAi* (2K) or TIE-DYE *ykiCA* clones, TIE-DYE *ykiCA*, *dppRNAi* clones, or TIE-DYE wild-type clones (4H). Error bars are SDs. All comparisons between wild-type clones and other conditions had a P value of to 0.01, very significant; \*P = 0.01 to 0.05, significant; P > 0.05, not significant.

Anterior versus posterior clone size comparisons in fig. S5 (G, H, and J) P values were calculated with an unpaired Student's t test in GraphPad.

## Results

To test whether oncogenes can also affect the stability of selector gene expression, we created clones of cells expressing either Myc (Johnston et al., 1999), an activated form of *Ras* (*RasV12*) (Prober & Edgar, 2000), or an activated form of *yki* (*yki<sup>CA</sup>*) with a mutation in its critical serine-168 phosphorylation site, which negatively regulates nuclear localization (Dong et al., 2007; Huang et al., 2005; Oh & Irvine, 2008) in the wing imaginal disc. In third instar wing discs, Ci is expressed only in cells anterior to the compartment boundary (Figure 5.1 A), and Ubx is expressed in the squamous cells of the peripodial epithelium (Figure 5.1 B) but not in the disc proper. In discs containing multiple *yki<sup>CA</sup>*-expressing clones, we found clones in the posterior (P) compartment expressing Ci (74 of 76 discs) and clones in the disc proper expressing Ubx (23 of 28 discs) (Figure 5.1, C and D). Ectopic expression of two other Hox genes *Antennapedia* and *Abdominal-B* was not observed in these clones. Many of these clones appear to be extruding from the epithelium, as has been described when patterning gene expression has been altered within clones of cells (Bielmeier et al., 2016; Gibson & Perrimon, 2005; Shen & Dahmann, 2005). To rule out the possibility that the posterior Ci-expressing clones had originated in the anterior (A) compartment, we generated *ykiCA* clones using mitotic recombination that marked both the *ykiCA*-expressing clone and its wild-type sister clone. We observed Ci-expressing *ykiCA* clones in the posterior compartment adjacent to wild-type twin spots, thus confirming that they originated in the posterior compartment (Figure 5.1, E to E"). We did not observe a similar misexpression of these genes in discs expressing either *Myc* or *RasV12* (Figure 5.5 A, A', B, B', and C). Thus, of the oncogenes tested, *yki* appears especially capable of altering expression patterns of selector genes. We also observed Ci expression in *ykiCA* clones posterior to the morphogenetic furrow in the eye disc (Figure 5.1 F), in the posterior compartment of the leg disc, and in the central nervous system (Figure 5.1 G), indicating that *ykiCA* can promote Ci expression in diverse tissues. In addition to ectopic expression of Ci, we sometimes observed elevated Ci expression in tissues where Ci is normally expressed, such as in clones in the anterior compartment of the wing disc (Figure 5.1 C and H).

The induction of ectopic Ci expression was not observed in clones overexpressing wild-type *yki* or clones mutant for the Hippo pathway components *hippo* (*hpo*) or *warts* (*wts*), (Figure 5.5, D-F). Thus, ectopic Ci expression depends on especially high levels of Yki activity, caused by overexpression of a form of Yki that cannot be inhibited by Hpo and Wts and hence localizes efficiently to the nucleus. Furthermore, observing clones at different stages of development indicated that ectopic Ci expression required prolonged expression of *ykiCA* (Figure 5.6). Even within a given tissue, we observed regional differences in the level of ectopic Ci expression. In the wing disc, clones in the hinge typically expressed higher levels of Ci than clones in the pouch (Figure 5.1 H). When *ykiCA* was expressed using *nub-Gal4*, which is mostly expressed in the pouch, relatively little ectopic Ci was observed (Figure 5.1, I and J). In contrast, when the hinge driver *30A-Gal4* was used, ectopic Ci was consistently observed, especially in the

ventral hinge posterior to the compartment boundary (Figure 5.1, K and L). The hinge is a region of the disc that displays increased plasticity following damage and can be a tumor “hotspot” (Tamori, Suzuki, & Deng, 2016; Verghese & Su, 2016), suggesting that the underlying cause of these phenomena may be related.

*ci* is normally transcribed exclusively in anterior cells of the wing disc and is repressed in posterior cells by *en* (Chanas, Lavrov, Iral, Cavalli, & Maschat, 2004; Eaton & Kornberg, 1990; Schwartz, Locke, Nishida, & Kornberg, 1995). Clones of posterior cells that are mutant for both *en* and its adjacent paralog *invected* (*inv*) express Ci (Eaton & Kornberg, 1990). Posterior *ykiCA* clones up-regulate a transcriptional *ci* reporter, *ci-lacZ*, indicating that *ci* transcription is derepressed (Figure 5.1 M). Large Ci-positive posterior clones have reduced levels of staining with antibody 4D9, which recognizes both En and Inv (Patel et al., 1989), suggesting that the derepression of *ci* transcription could result from a reduction in En and Inv levels (Figure 5.1 N). En has also been shown to negatively regulate *Ubx* expression in the wing disc, although that mechanism is less well defined (Mann, 1994); consistent with this, we only observed ectopic *Ubx* in posterior *ykiCA* clones. Since Ci is expressed at elevated levels in anterior clones, where En is not normally expressed, *ykiCA* must also be capable of regulating *ci* expression by mechanisms that are independent of changes in En levels. Consistent with this notion, *ci* was identified as a Yki target, and *ci* RNA was elevated in tissue mutant for *wts*, which has higher Yki activity than wild-type tissue (Oh et al., 2013).

How does Yki regulate *ci* expression? Yki acts together with its binding partner Scalloped (Sd) to activate gene expression, with Sd binding directly to regulatory regions of target genes (Goulev et al., 2008). If Sd is the relevant binding partner, then alterations in gene expression would not occur in Yki-expressing clones that are mutant for *sd* (Yu & Pan, 2018). To determine whether Sd is required for expression of *ci*, we reduced *sd* expression in *ykiCA* clones (Figure 5.2, A-I). Anterior *ykiCA* clones did not show increased Ci expression (Figure 5.2, D-F, G-G", and H-H"), while posterior *ykiCA* clones no longer expressed ectopic Ci (Figure 5.2, D- F and I-I"), indicating that Sd is required for ectopic Ci up-regulation. Yki promotes growth, in large part, by activating expression of the microRNA *bantam* (*ban*) (Brennecke, Hipfner, Stark, Russell, & Cohen, 2003; Nolo, Morrison, Tao, Zhang, & Halder, 2006; Thompson & Cohen, 2006). To address a possible role for *ban* in mediating ectopic *ci* expression, we reduced *ban* levels by generating *ykiCA* clones in flies heterozygous for a null allele of *ban*, *banΔ1* (Figure 5.2, J and K; control in Figure 5.7 A) (Hipfner, Weigmann, & Cohen, 2002). In *banΔ1* /+ discs, discs appeared smaller overall, although clone size was unaffected (Figure 5.2 Q), yet the frequency of Ci-expressing *ykiCA* clones was reduced both overall and especially in the hinge (Figure 5.2 R). Thus, the ability of constitutively active Yki (YkiCA) to activate Ci expression in posterior clones is more sensitive to *ban* levels than its ability to promote overgrowth. We also used a “bantam sponge,” which encodes an RNA that has 10 optimal *ban*-binding sites upstream of the DsRed coding region; low DsRed expression likely correlates with clones with higher *ban* levels (Herranz, Hong, & Cohen, 2012). We found that clones expressing high levels of DsRed had low Ci levels and vice versa, suggesting a correlation between *ban* levels and induction of Ci (Figure 5.2, L and M).

We also investigated *taranis* (*tara*), originally classified as a TrxG gene, which is known to modulate homeotic gene expression by hitherto undefined mechanisms (Calgano, Boube, Cribbs, & Bourbon, 2002). A genome-wide chromatin immunoprecipitation screen for Yki targets found an enrichment of Yki binding in the *tara* promoter, as well as increased *tara* transcription in *wtsP2* discs (Oh et al., 2013). There is a putative binding site for Sd, Yki's primary binding partner, approximately 400 base pairs upstream of the *tara* transcriptional start site. In addition, *tara* negatively regulates *en* expression in embryos and in regenerating imaginal discs (Dutta & Li, 2017; Schuster & Smith-Bolton, 2015). We found that Taranis protein levels were increased in *ykiCA* expressing clones, as was the expression of a *tara-lacZ* transcriptional reporter (Figure 5.2, N and O). These findings are consistent with the possibility that an increase in Taranis in *ykiCA* clones reduces En levels and thus allows Ci expression. To examine this possibility, we reduced *tara* expression in *ykiCA* clones (Figure 5.2 P; control in Figure 5.7 B). These clones were slightly larger than *ykiCA* clones (Figure 5.2 Q), but the expression of ectopic Ci was reduced (Figure 5.2 R). This result implicates *tara* in the pathway by which YkiCA induces Ci expression and also shows that ectopic Ci expression does not simply correlate with the extent of overgrowth.

Since our results implicate both *ban* and *tara* in the pathway by which YkiCA activates ectopic Ci expression, we tested whether increasing *ban* and *tara* levels, either alone or in combination, could induce Ci expression in the posterior compartment. Posterior clones overexpressing either *ban* or *tara* alone in wild-type discs expressed very low levels of Ci at most (Figure 5.7, D and E). However, when expressed in combination with a wild-type version of *yki*, which normally does not induce Ci expression (Figure 5.7 C), either *ban* or *tara* could induce Ci expression, especially in the posterior ventral hinge (Figure 5.3, A and B). *tara* overexpression also enhanced Ci expression in YkiCA clones (Figure 5.3 C).

Furthermore, clones expressing *ban* and *tara* together could induce ectopic Ci at a low frequency and cause overgrowth reminiscent of *ykiCA* overexpression (Figure 5.3 D); anterior clones expressed a higher level of Ci than surrounding wild-type tissue (Figure 5.3 E). Clones expressing both *tara* and *ban* did not have an obvious decrease in En expression (Figure 5.3 E'), although a reduction in *tara* has previously been linked to result in increased En expression (Dutta & Li, 2017; Schuster & Smith-Bolton, 2015). Thus, *tara* likely regulates *ci* expression independently of *en*. We also found that anterior clones expressing *ban* and *tara* expressed ectopic En (Figure 5.3 E'), thereby generating clones that coexpress Ci and En, which indicates that, at least in this situation, the mere presence of En is insufficient to repress Ci expression and that *tara* in combination with *ban* can destabilize selector gene expression in multiple ways. When using the hinge *30A-Gal4* driver, combined expression of both *ban* and *tara*, but not either alone, induced a low but reproducible level of posterior Ci and Ptc expression in wild-type discs (Figure 5.7, H and I; control in Figure 5.7, F and G). The lower levels of ectopic Ci expression when compared to *ykiCA* clones and the absence of En down-regulation elicited by *ban* and *tara* coexpression indicate that YkiCA must also act via additional unidentified targets. Consistent with this idea, overexpression of *ban* and *tara*

together in *ykiWT* clones recapitulated the *ykiCA* clone phenotype to a greater extent, with consistent although often low-level ectopic Ci expression (Figure 5.3 F). A total of 77.2% of clones expressing YkiWT in combination with *ban* and *tara* expressed ectopic Ci versus 34.6% of clones expressing just *ban* and *tara* (Figure 5.3 G). In addition, while *tara* overexpression induced *ban* expression as assessed by a *ban-GFP* reporter (Figure 5.7, J and K) (Brennecke et al., 2003), *ban* overexpression did not induce *tara* (Figure 5.7, L and M), indicating that the increase in Tara levels does not result from the known ability of Yki to activate *ban* expression.

To look for evidence of alterations in chromatin in *ykiCA* clones, we used a panel of antibodies that recognize specific posttranslational modifications of histones. We found that *ykiCA* clones, especially in the hinge, show elevated levels of H3K27 trimethylation (H3K27me<sub>3</sub>), which typically correlates with increased Polycomb group (PcG)-mediated gene repression (Figure 5.3 H) (Muller et al., 2002; Vire et al., 2006). We observed less obvious increases in the level of H3K4me<sub>1</sub> and H3K4me<sub>3</sub>, but not H3K9me<sub>3</sub> or H4Ac (Figure 5.8 A to D). The increase in H3K27me<sub>3</sub> could potentially explain the decrease in *En* expression in *ykiCA* clones. However, the expression of *en* in the posterior compartment of imaginal discs is regulated by a particularly large region (approximately 79 kB) (Cheng et al., 2014) composed of multiple regulatory elements that sometimes function antagonistically, which makes it difficult to evaluate the relevance of local alterations in H3K27me<sub>3</sub>. The apparent global increase in H3K27me<sub>3</sub> levels did not always correlate with increased PcG-mediated repression; a reporter that is silenced by a Polycomb (Pc)-responsive element from the *bx<sub>d</sub>* locus (Dellino et al., 2004) is derepressed in *ykiCA* clones (Figure 5.3 I). Thus, the effects of YkiCA on chromatin state appear to be complex, and hence, effects on individual genes are not easy to predict. This is consistent with the notion that *ykiCA* activates Ci expression by multiple mechanisms, as demonstrated by effects on Ci in both anterior and posterior compartments.

To test whether the increases in *tara* and H3K27me<sub>3</sub> expression are specific to YkiCA activation or whether these phenomena occur in other overgrown tissue, we stained discs with clones expressing either *RasV12* or *Myc* with antibodies that recognize Tara and H3K27me<sub>3</sub>. Neither *RasV12*- nor *Myc*-expressing clones showed changes in Tara or H3K27me<sub>3</sub> relative to surrounding wild-type tissue (Figure 5.8, E and F), supporting the conclusion that these changes in chromatin regulation are specific to YkiCA activation.

What are the consequences of creating *ykiCA* clones that have down-regulated *en* and express *ci* in the posterior compartment? The juxtaposition of cells that express *en* and those that do not normally occurs at the anteroposterior compartment boundary. *ci* is expressed in anterior cells but repressed by *En* in posterior cells, which instead secrete the short-range morphogen Hedgehog (Hh) (Tabata et al., 1992). Activation of the Hh signaling pathway in cells anterior to the compartment boundary stabilizes the activator form of Ci and results in the transcription of multiple target genes including *patched* (*ptc*) and *dpp* (Aza-Blanc et al., 1997; Von Ohlen, Lessing, Nusse, & Hooper, 1997). *Dpp* is a long-range morphogen that diffuses widely from its source and regulates tissue growth

and gene expression in both compartments (Lecuit et al., 1996; Nellen, Burke, Struhl, & Basler, 1996). We found that the presence of Ci-expressing *ykiCA* clones in the posterior compartment generates ectopic sites of Hh pathway signaling near the clone boundary, possibly due to increased levels of the full-length activator form of Ci. The Hh target genes *dpp* and *ptc* were both expressed in these clones (Figure 5.4, A and B). Evidence of Dpp signaling, as assessed with the presence of the phosphorylated form of the signaling protein Mad (pMAD), was also observed (Figure 5.4 C). This is noteworthy given previous results showing that Mad and Yki cooperate to activate *ban* (Oh & Irvine, 2011), which we demonstrated is necessary for ectopic Ci activation (Figure 5.2, K-M and R). Thus, the clone boundary has indeed adopted anteroposterior compartment-boundary-like properties, at least with respect to Hh signaling. However, we did not see consistent evidence of clones establishing ectopic dorsoventral compartment boundaries. We did, however, observe some abnormalities in the pattern of dorsoventral gene expression (Figure 5.9, A-C). Some dorsal clones had reduced apterous expression (Figure 5.7 C', arrow), and some ventral clones expressed *cut* (Figure 5.7 B'), which is normally expressed at the dorsoventral compartment boundary. However, in these ventral clones, *cut* was expressed throughout the clone and not at the boundary.

What are the consequences of activating Hh signaling in *ykiCA* clones? When we inactivated *smo* in *ykiCA* clones, we found no impairment in growth, nor did we find growth impairment when we reduced Ci itself in *ykiCA* clones (Figure 5.7, D-F and I). We also observed no significant difference in anterior versus posterior clone size for *ykiCA* clones, *smo3*, *ykiCA* clones, or *ykiCA*, *ciRNAi* clones (Figure 5.7, G, H, and J). Thus, their overgrowth is not dependent on Hh signaling. This is consistent with the obvious overgrowth observed in *ykiCA* clones far from the compartment boundary in the anterior compartment, which are also far from an Hh source. Since the clones were overgrown and in the process of extrusion, it was difficult to ascertain whether clones close to the compartment boundary had crossed it (Figure 5.7 F). Clone overgrowth and changes in selector gene expression were also not dependent on c-Jun N-terminal kinase pathway activation, which has been previously linked to Hippo pathway signaling and thought to facilitate propagation of Yki activity to cells neighboring tumor cells (Figure 5.7, K to N) (Codelia, Sun, & Irvine, 2014; Enomoto & Igaki, 2013; Enomoto, Kizawa, Ohsawa, & Igaki, 2015; X. Ma et al., 2017). To investigate potential nonautonomous effects of *ykiCA* clones, we used the TIEDYE system (Worley et al., 2013), which has three independent FLP-out genes, two of which, when activated, express reporters driven by constitutive promoters (*ubi-GFP* and *act-lacZ*). The third is a *FLP-out Gal4*; these clones express *UAS-ykiCA*. While *ykiCA*-expressing clones are obviously overgrown, we also observed occasional large neutral clones that appeared to be composed of cells that were close to the perimeter of the *ykiCA*-expressing clones, including anterior clones that have elevated full-length Ci (Figure 5.1 C' and Figure 5.4, D and E). These clones were not as evident when a *UAS-dppRNAi* transgene was coexpressed with *ykiCA*. Neutral clones adjacent to *ykiCA*-expressing clones were significantly larger than those adjacent to *ykiCA*, *dppRNAi*-expressing clones (Figure 5.4, F to H, and Figure 5.7 O). This suggests that Dpp secreted by *ykiCA*

clones may be able to promote the growth of adjacent cells, especially in lateral regions of the disc (Figure 5.4 I).

## Discussion

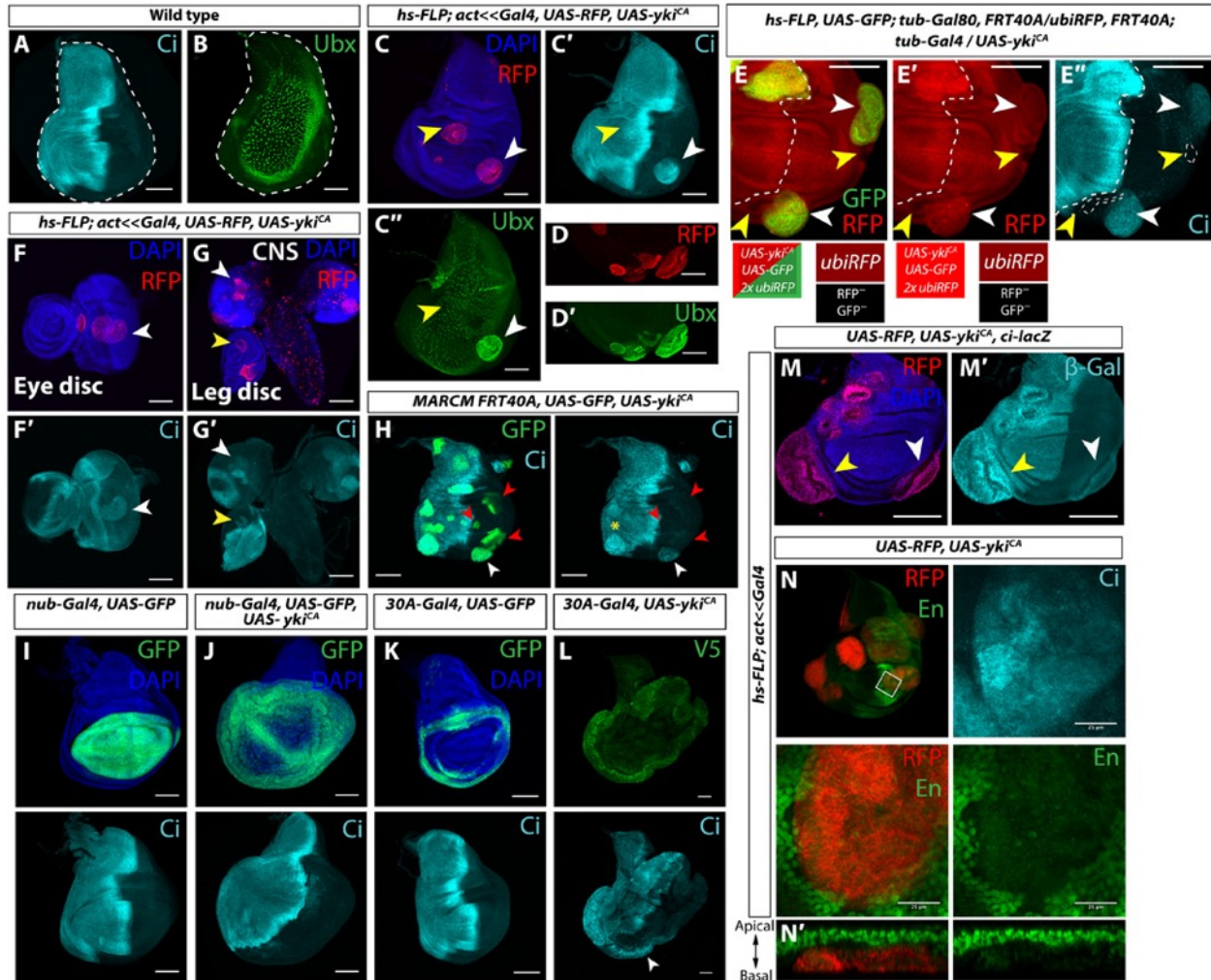
Human cancers are characterized by multiple genetic lesions, a subset of which are driver mutations that are thought to be responsible for their tumorous characteristics. It is estimated that most cancers have two to eight driver mutations (Vogelstein et al., 2013). This makes it difficult to evaluate the contribution of each mutation to any particular characteristic of the tumor. We have taken advantage of the ability of single-gene manipulations to cause overgrowth in *Drosophila* imaginal discs to assess the ability of three different oncogenes to destabilize established patterns of selector gene expression and find that *yki*, the *Drosophila* ortholog of Yap and Taz, is especially potent in doing so. The patterns of expression of *En*, *Ci*, and *Ubx* are established relatively early in embryogenesis and maintained stably in imaginal discs during the larval stages of development. These patterns of expression can be disrupted in clones expressing an activated form of Yki. Expression of a wild-type form of Yki is capable of disrupting these expression patterns in combination with other genetic manipulations such as overexpression of *ban* or *tara*. This latter scenario is more likely to apply to human cancers; increased Yap or Taz activity has been described in multiple human cancers (Zanconato, Cordenonsi, & Piccolo, 2016), which often also have other genetic lesions.

Our studies show that *sd*, *ban*, and *tara* make important contributions to the pathway by which YkiCA destabilizes gene expression; reducing the expression of any of these in clones expressing YkiCA greatly reduces ectopic *Ci* expression, and increasing expression of both genes can cause ectopic *Ci* expression. It is likely that other mechanisms function in parallel to destabilize selector gene expression since combined overexpression of *ban* and *tara* increased ectopic *Ci* expression but did not reduce *En* expression.

We also demonstrate that changing selector gene expression within an overgrowing clone can create interactions at the clone margin that are reminiscent of compartment boundaries and result in the production of morphogens. A recent study showed that forced expression of *En* in *Igl* clones can elicit similar phenomena in anterior clones (Bajpai & Sinha, 2020). In addition, *ykiCA* clones are often extruded, consistent with previous observations that heterotypic interactions caused by overexpressing patterning genes also promotes extrusion (Bielmeier et al., 2016; Gibson & Perrimon, 2005; Shen & Dahmann, 2005). Previous work found that *ci* RNA levels were increased in *wts* mutant tissue (Oh et al., 2013), yet we did not see ectopic *Ci* protein expression in *wts* mutant clones or wild-type Yki-overexpressing clones. Our work shows therefore that sustained expression of very high Yki levels is necessary to destabilize expression of selector genes. However, even under these conditions, the effect on ectopic *Ci* expression is Sd dependent. Moreover, we have shown that even wild-type Yki can, in combination with increased expression of *ban* or *tara*, induce ectopic *Ci* expression. While these changes in gene expression are most obvious with above-physiological

levels of Yki, they nevertheless reflect a previously unknown ability of this pathway to alter patterning gene expression and furthermore to change the growth characteristics of neighboring wild-type cells. Differences in selector gene expression between human cancers or precancerous lesions and their wild-type neighbors have received relatively little attention, and our results call attention to tumor margins as sites where heterotypic interactions could create signaling centers that affect the behavior of tumor cells.

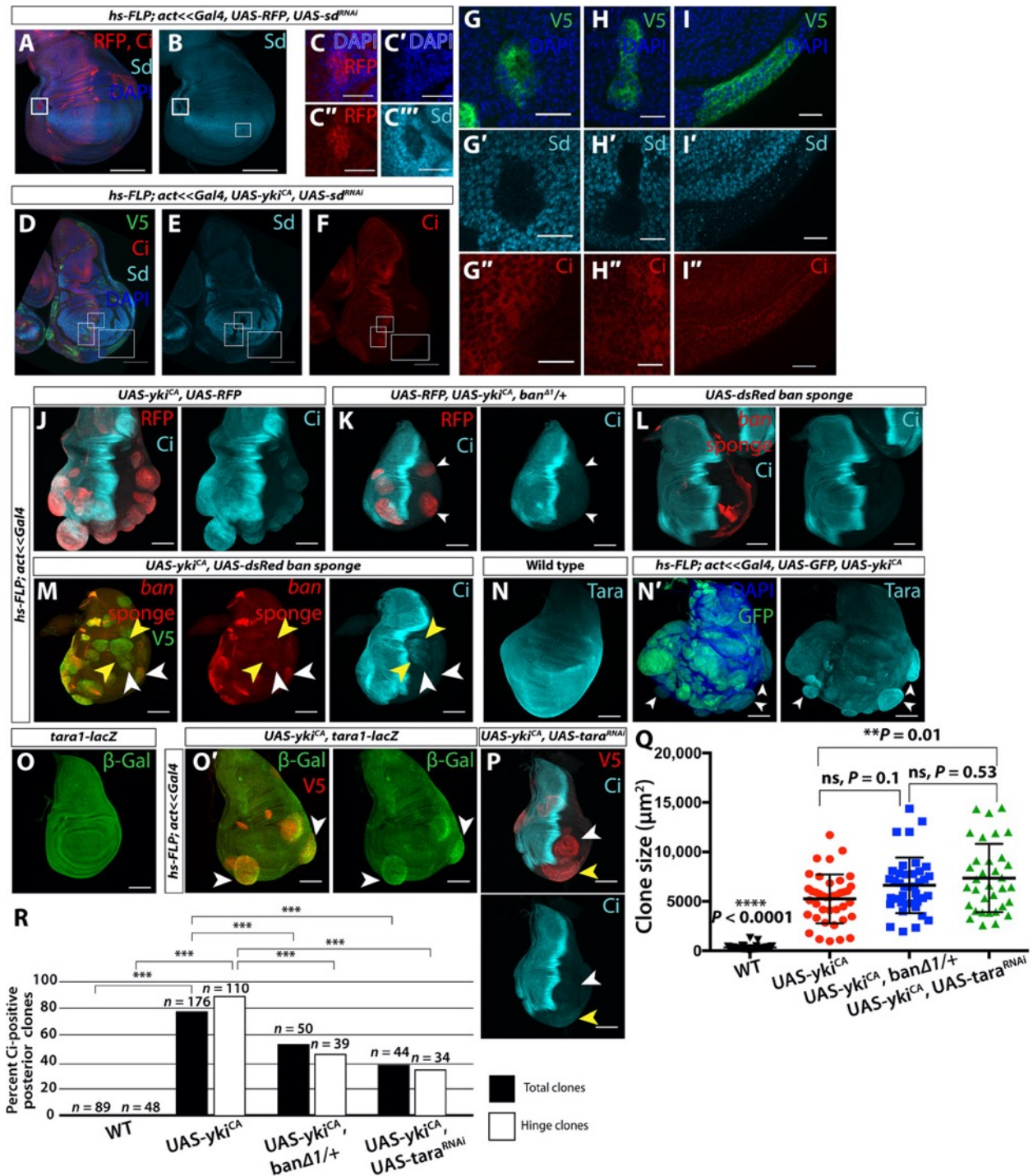
## Figures



**Figure 5.1: Constitutively active Yorkie ( $Yki^{CA}$ ) disrupts stable selector gene expression.**

(A and B) Wild-type (WT) wing imaginal discs; Ci is expressed in anterior compartment, and Ubx is expressed in squamous peripodial cells. (C to C'') Clones expressing activated Yki ( $UAS-yki^{CA}$ ). Anterior clone (yellow arrowhead) expresses more Ci; posterior clone (white arrowhead) expresses ectopic Ci and Ubx (C''). Discs with Ci-positive clones:  $n = 74$  of 76. Discs with Ubx-positive clones:  $n = 23$  of 28. (D and D') Ubx-expressing  $yki^{CA}$  clones in the disc proper. (E to E'') Mitotic recombination:  $yki^{CA}$ -expressing clones express red fluorescent protein (RFP) and green fluorescent protein (GFP) (white arrowheads), and neighboring twin spots (yellow arrowheads) express neither. (F and G)  $yki^{CA}$  clones in the eye disc (F and F'), leg disc [(G) and (G'), yellow arrow], and larval brain [(G) and (G'), white arrow]. CNS, central nervous system. (H) Posterior  $yki^{CA}$  marked with GFP expresses Ci in the hinge (white arrowhead) but inconsistently in the pouch (red arrowheads). Anterior clones express more Ci (yellow asterisk). (I to L) *nubbin-Gal4*,  $UAS-yki^{CA}$  does not cause ectopic Ci [(J), marked by GFP, control disc in (I)], but *30A-Gal4*  $UAS-yki^{CA}$  does [(L), V5 tag on  $Yki^{CA}$ , control disc

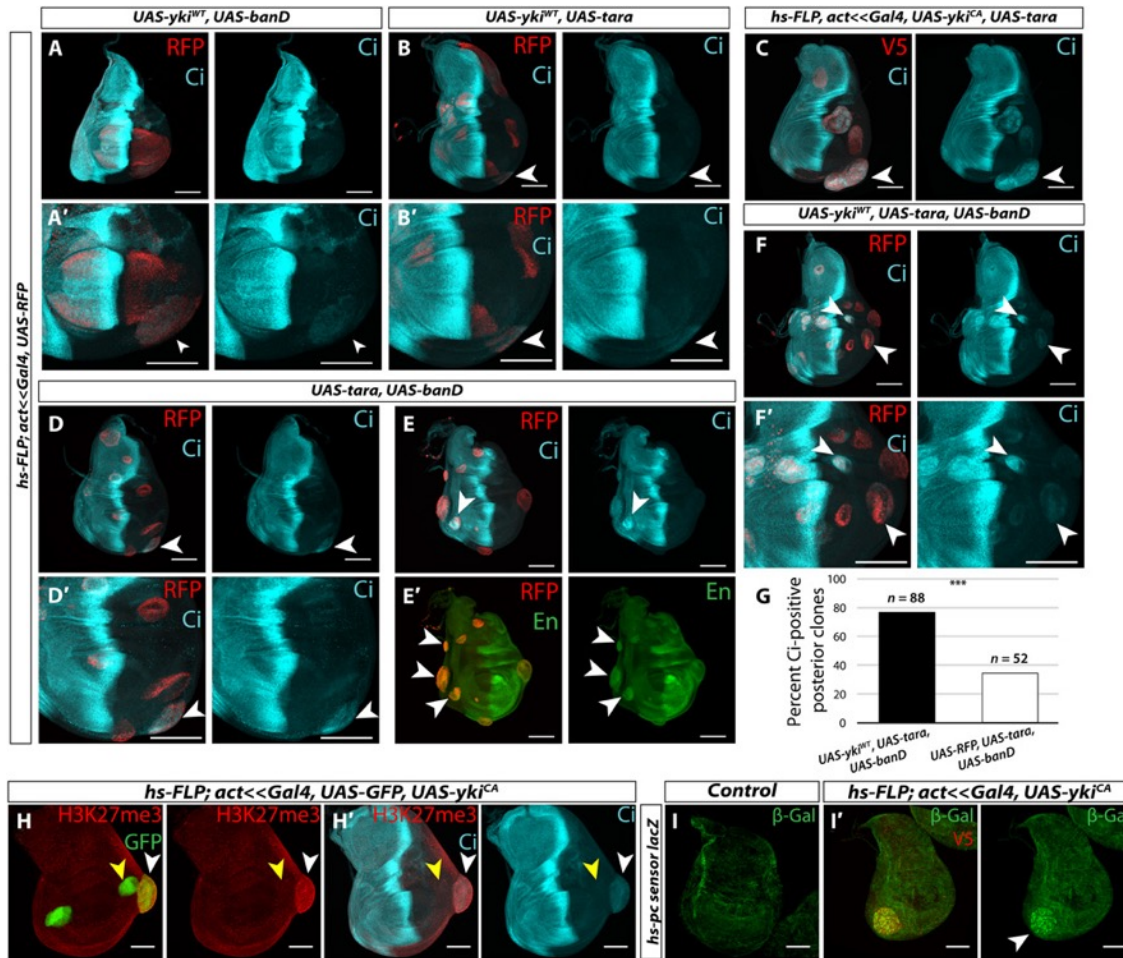
in (K)], especially in the ventral hinge (arrowhead). (**M** and **M'**) *ci-lacZ* is expressed in posterior clones (white arrowheads), and expression is increased in anterior clones (yellow arrowheads). (**N**) A posterior *yki<sup>CA</sup>* clone with down-regulated En and ectopic Ci expression. (**N'**) XZ section of a posterior *yki<sup>CA</sup>* that has been extruded basally. Anterior is left in all images. Scale bars, 100  $\mu$ m. DAPI, 4',6-diamidino-2-phenylindole;  $\beta$ -Gal,  $\beta$ -galactosidase.

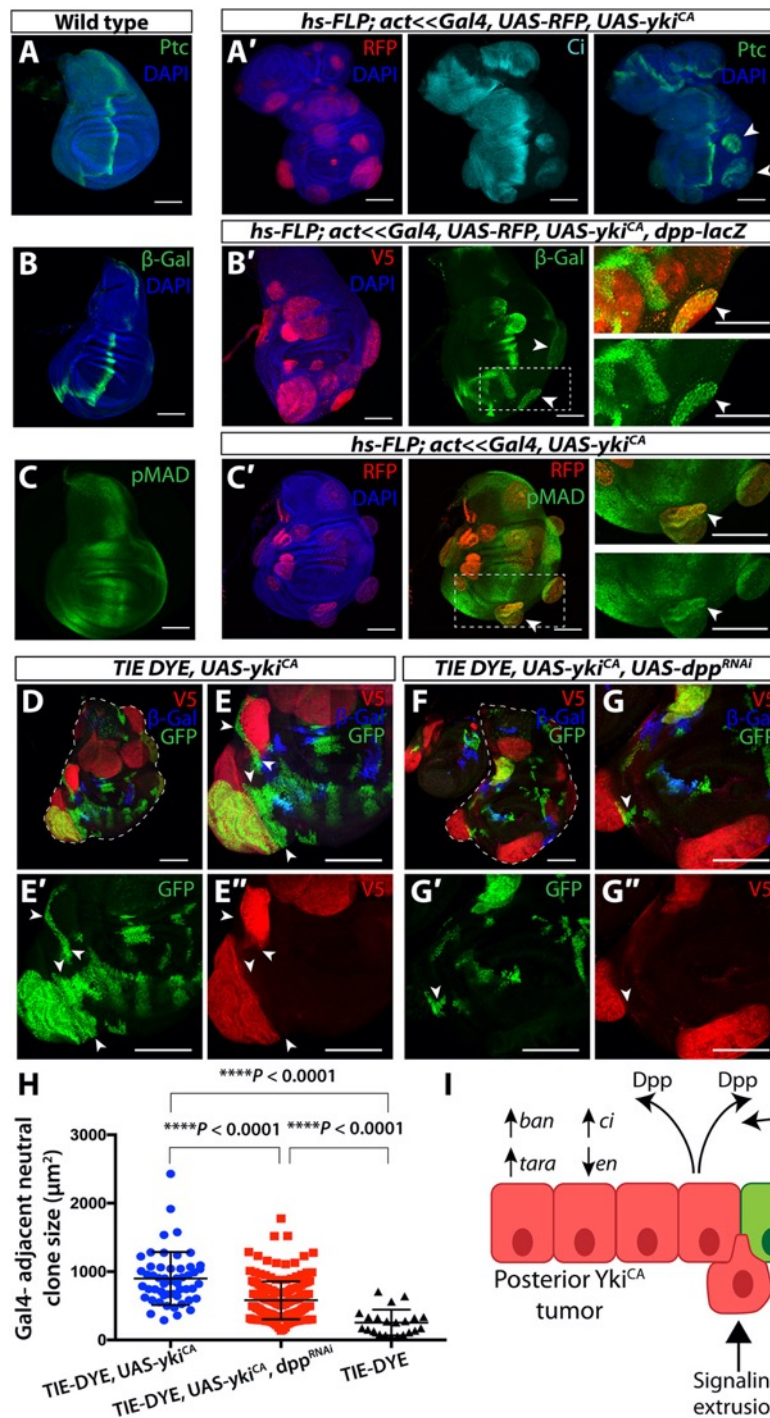


**Figure 5.2: *yki<sup>CA</sup>* clones require *sd*, *ban*, and *tara* to disrupt patterning gene expression.**

(A to I) RNA interference (RNAi) of *sd* [validated in (A) to (C'')] using anti-Sd] in anterior *yki<sup>CA</sup>* clones prevents increased Ci expression (D to F, G to G'', and H to H'') and Ci expression in posterior clones (D to F and I to I''). (J and K) *yki<sup>CA</sup>* clones in *ban<sup>Δ1/+</sup>* discs (K) are overgrown but express less ectopic Ci [compared to (J)]. (L and M) *ban* sponge reduces *ban* microRNA levels. dsRed levels inversely correlate with *ban* levels. Clones expressing *ban* sponge express uniformly high dsRed and no

ectopic Ci (L). Posterior clones expressing  $Yki^{CA}$  and *ban* sponge show variation in both dsRed and Ci expression (M). High dsRed-expressing posterior clones are smaller and do not express Ci (white arrowheads); low- or no-dsRed clones are overgrown and express Ci (yellow arrowheads). (**N** and **O**)  $Yki^{CA}$  clones have increased expression of Tara protein (N and N') and *tara1-lacZ* (O and O'), especially in the hinge (arrowheads). (**P**) *tara* RNAi allows overgrowth but reduces Ci expression. (**Q**) Size of posterior hinge clones of indicated genotypes.  $yki^{CA}$  clones in *ban $\Delta$ 1/+* discs are not significantly smaller than those in WT discs;  $yki^{CA} + tara^{RNAi}$  clones are significantly larger than  $yki^{CA}$  clones. (**R**) Ectopic Ci is observed less often in  $yki^{CA}$  clones when *ban* or *tara* levels are reduced. White boxes, hinge clones; black boxes, hinge and pouch clones. Statistics: See Materials and Methods. ns, not significant.

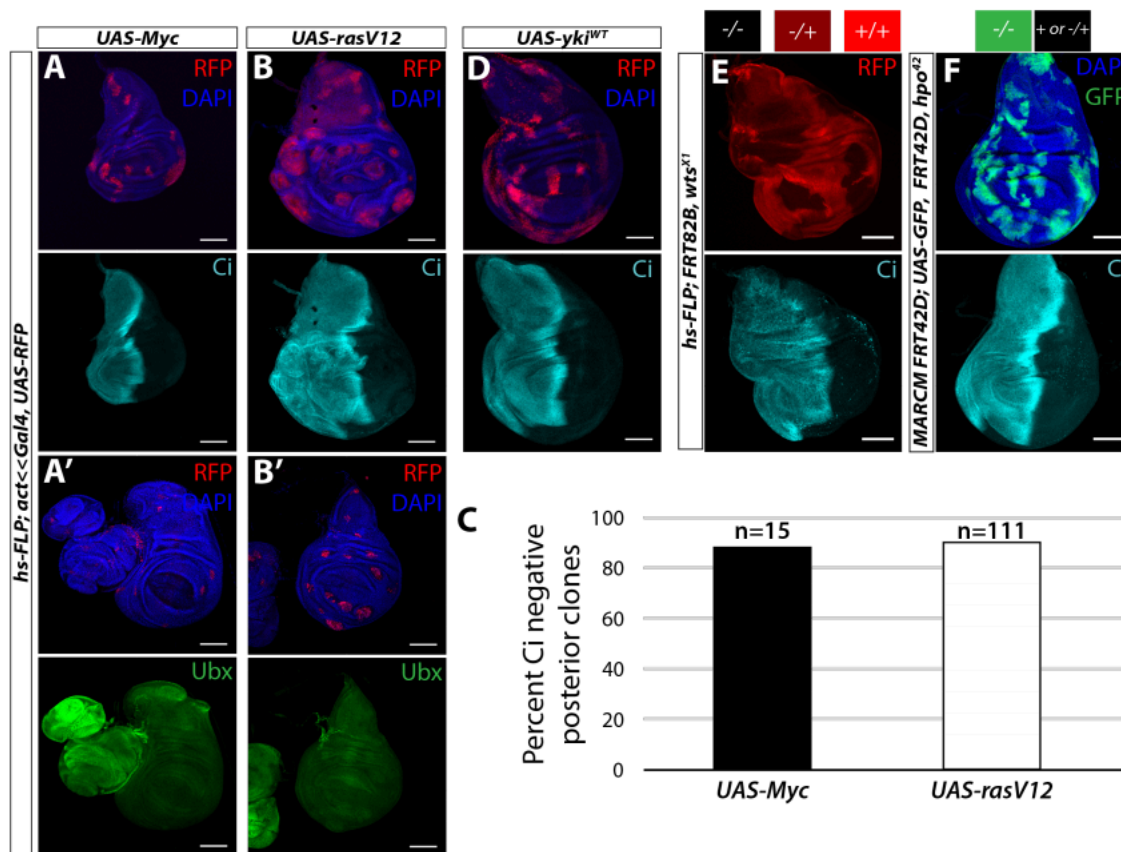




**Figure 5.4: *yki*<sup>CA</sup> clones activate a developmental signaling cascade.**

(A) *yki*<sup>CA</sup> clones that express Ci also express Ptc (A') and *dpp-lacZ* (B') at clone margin and have increased pMAD near clones (C'). Control discs without *yki*<sup>CA</sup> clones are shown in (A) to (C). (D and E) *yki*<sup>CA</sup> clones cause nonautonomous overgrowth in neighboring WT tissue. The TIE-DYE system has three independent FLP-out transgenes that express Gal4, GFP, and *lacZ*. Clones might express none of these or any combination of these depending on the number of FLP-out events in founder cells.

Gal4-expressing clones express *UAS-yki<sup>CA</sup>* and are visualized with anti-V5. Neutral GFP-expressing clones are shown in green, and lacZ-expressing clones are shown in blue. Arrowheads indicate two unusually large GFP-positive WT clones that are immediately adjacent to overgrown *Yki<sup>CA</sup>*-expressing clones (red). **(F and G)** Knockdown of *dpp* in *yki<sup>CA</sup>* clones. In these discs, neutral clones adjacent to *yki<sup>CA</sup>* clones are not as overgrown (arrowheads). **(H)** Quantification of size of neutral clones directly adjacent to Gal4-expressing clones [expressing *UAS-yki<sup>CA</sup>* (neutral clone,  $n = 52$ ), *UAS-yki<sup>CA</sup>* and *UAS-dpp<sup>RNAi</sup>* (neutral clone,  $n = 184$ ), or *UAS-RFP* (neutral clone,  $n = 22$ )]. **(I)** Model: *Yki<sup>CA</sup>* causes changes in selector gene expression in the posterior compartment via up-regulation of *ban* and *tara*. As a result of heterotypic interactions at clone boundaries, ectopic organizing centers are created resulting in the production of morphogens (e.g., Dpp), as well as extrusion of *yki<sup>CA</sup>* tissue. Statistics: See Materials and Methods.



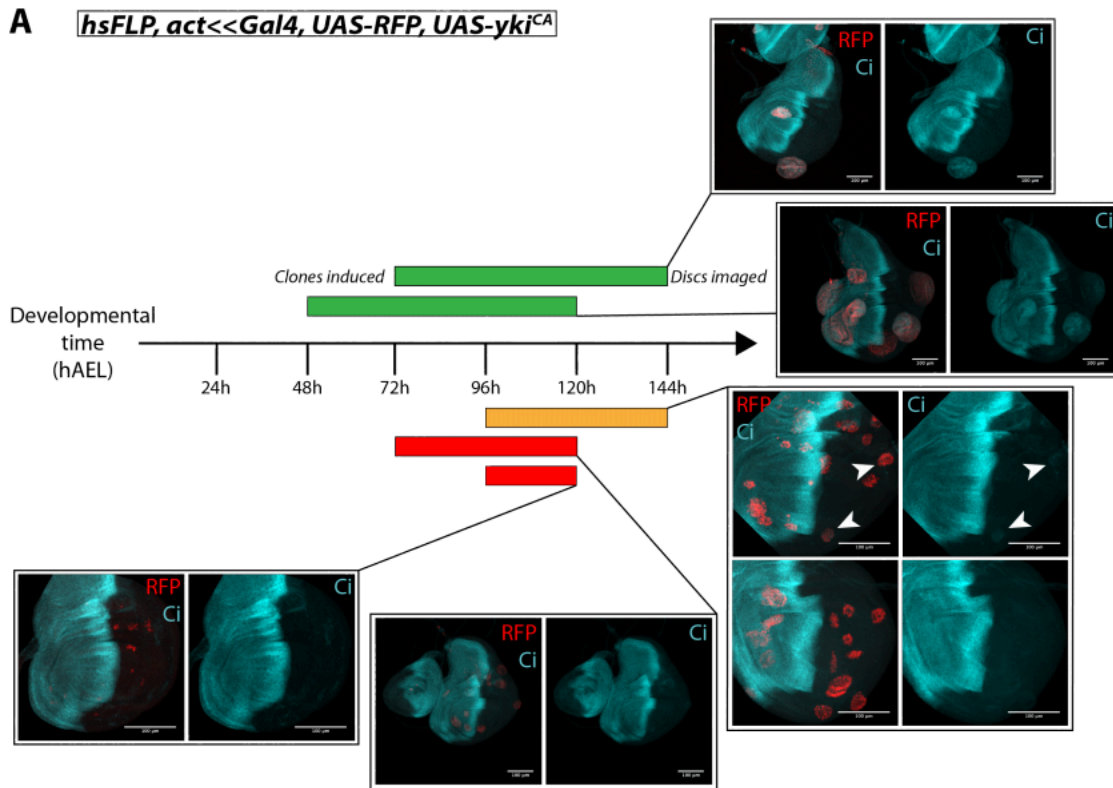


**Figure 5.6:  $yki^{CA}$  clones disrupt patterning gene expression late in clone development.**

(A) *FLP-out* clones expressing  $yki^{CA}$  were induced at different developmental time points and allowed to grow for different durations before dissection. Start point of colored boxes indicates when clones were induced, and end point of colored boxes indicates when discs were dissected and imaged. Length of box corresponds to the amount of time between clone induction and disc imaging, or the duration of clone growth. Red-filled boxes indicate that no ectopic Ci was seen under that clone induction/imaging condition, green-filled boxes indicate ectopic Ci was seen consistently, and yellow filled boxes indicate ectopic Ci was sometimes seen. All larvae were raised at 25° C and heat shocked at 37° C.

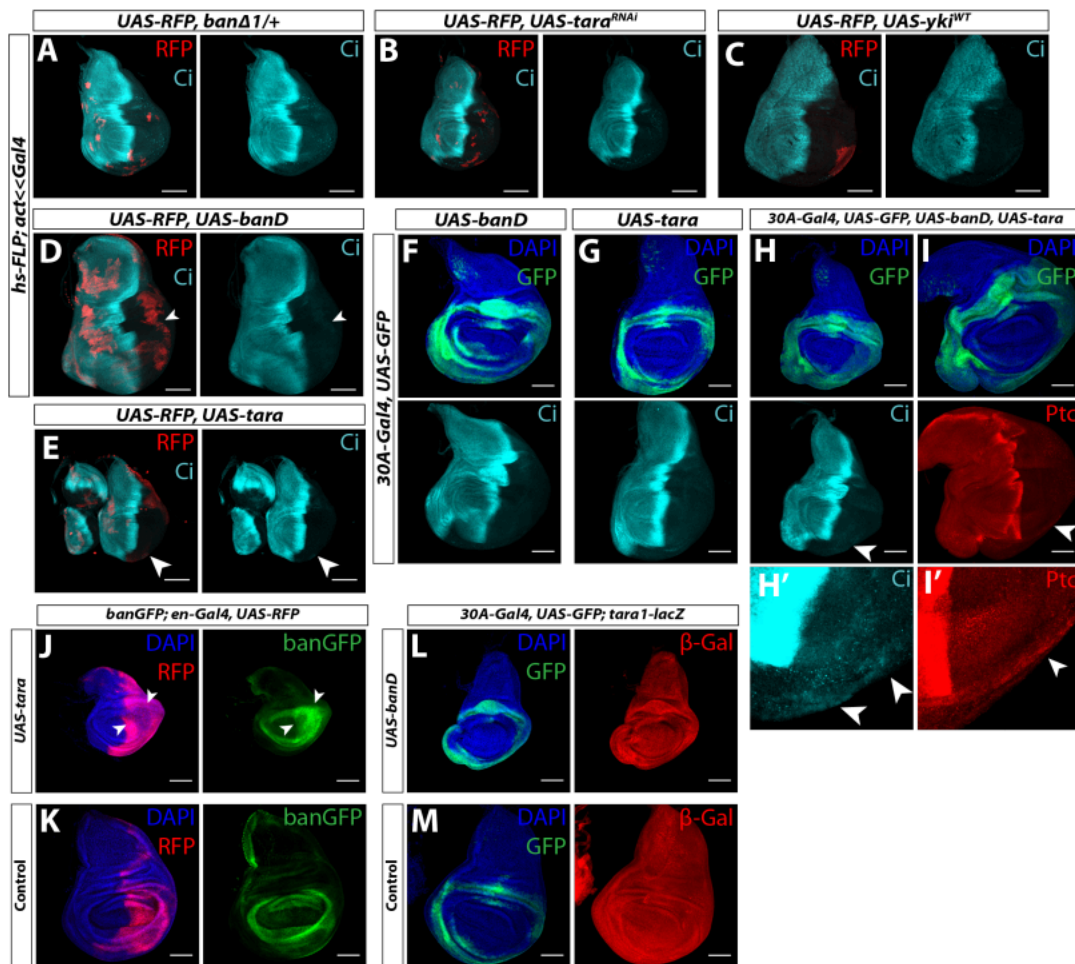


**Figure 5.7: Manipulating *ban* or *tara* alone in wild-type cells does not alter Ci levels.** (A) RFP-marked neutral clones induced in a *banD1* /+ disc are small and do not express ectopic Ci. (B) Clones expressing *taraRNAi* alone do not express ectopic Ci. (C) *Yki*<sup>WT</sup> expression alone also did not induce ectopic Ci, or did so at a very low level. (D) Clones expressing *banD*, did not express ectopic Ci, or did so at a very low level. (E) Overexpression of *tara* alone causes a low level of ectopic Ci expression on its own. This is especially evident in the hinge (white arrows). (F) *ban* overexpression in the hinge using *30A-Gal4* caused overgrowth, but not upregulation of Ci in the posterior. (G) Overexpression of Tara in the hinge using *30A-Gal4* did not cause overgrowth or ectopic Ci in the posterior. (H-I) Overexpression of both *ban* and *tara* together in the hinge using *30A-Gal4* caused a marked increase in overgrowth, as well as subtle but consistent upregulation of Ci (H') and Ptc in the posterior hinge (I'). (J-K) Overexpression of *tara* with *en-Gal4* causes upregulation of *ban-GFP* in the posterior compartment (white arrows). (L-M) Overexpression of *banD* in the hinge with *30A-Gal4* does not cause obvious upregulation of *tara-lacZ*.

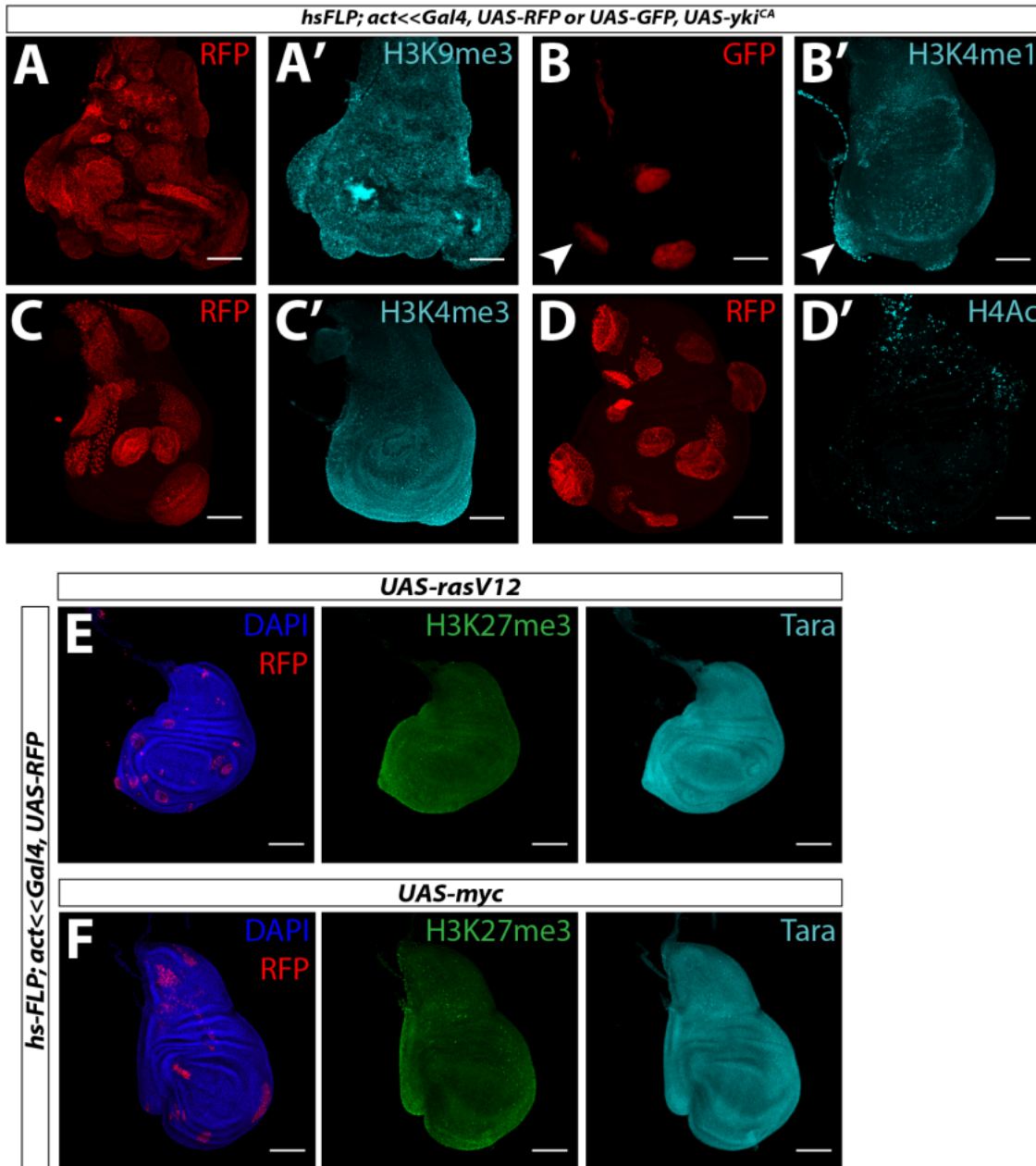


**Figure 5.8: *yki<sup>CA</sup>* clones do not show alterations in all chromatin markers.** (A-A') A typical marker of heterochromatin, H3K9 trimethylation, is not altered in *yki<sup>CA</sup>* clones. (B-B') *yki<sup>CA</sup>* clones (visualized with GFP) show increased H4K3 monomethylation, a mark of active enhancers, in the hinge, though not less than H3K27me3. (C-D) Two markers of active genes, H3K4 trimethylation and H4 acetylation, are not altered in *yki<sup>CA</sup>* clones. H3K4 trimethylation in *yki<sup>CA</sup>* clones is the same as surrounding wild type tissue (C-C'), and H4 acetylation is largely absent throughout the disc (D-D'). (E-F) Overexpression of either *rasV12* or *myc* does not change expression of H3K27me3 or Tara.

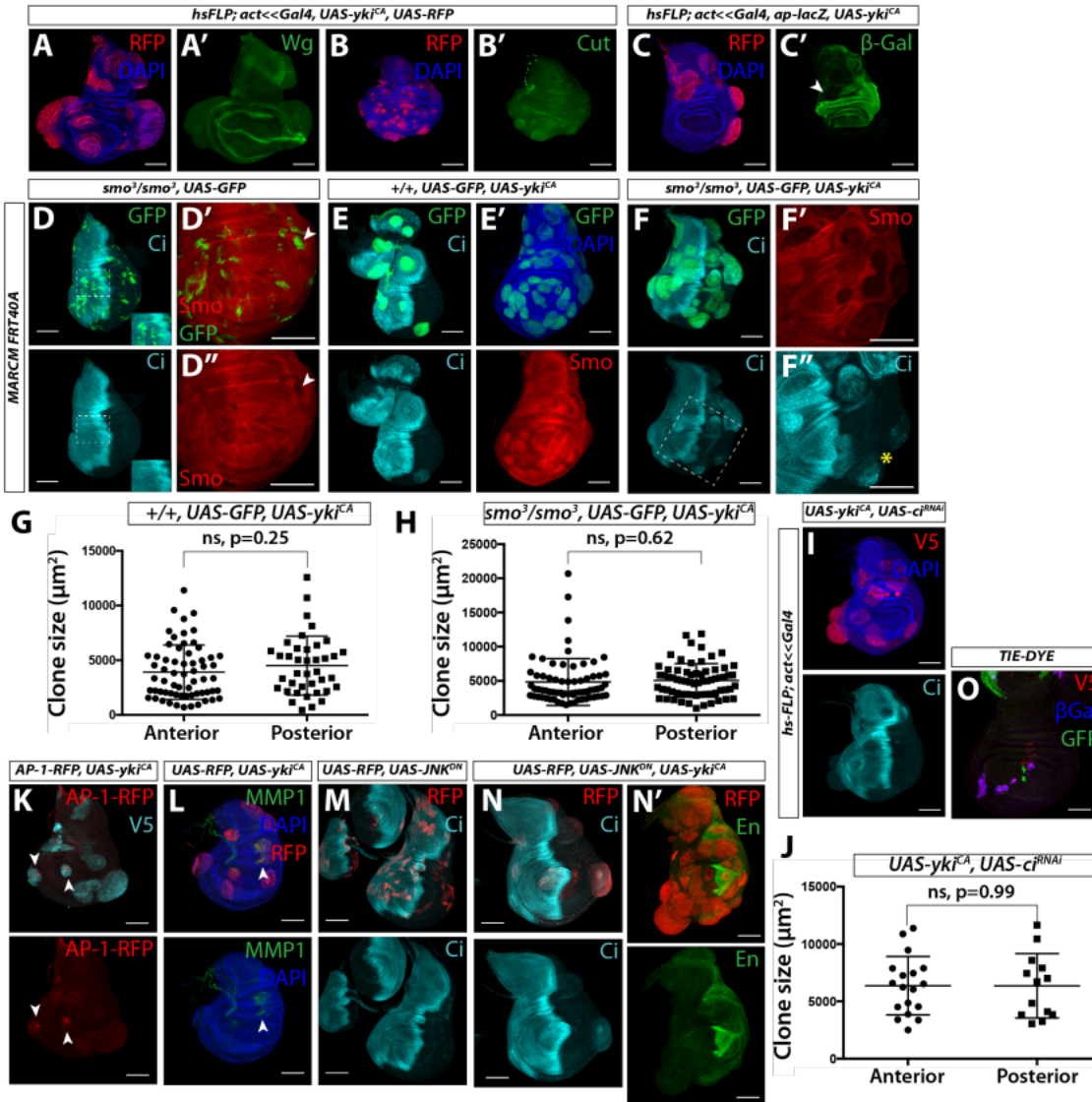


**Figure 5.9: Overgrowth and ectopic Ci expression in *yki<sup>CA</sup>* clones is not dependent on Hh signaling or the JNK pathway.**

(A-C) Clones expressing *UAS-yki<sup>CA</sup>* do not ectopically express the dorsoventral boundary marker Wg (A-A'), but do infrequently express the dorsoventral boundary marker Cut in the ventral compartment (B-B'). Clones do not ectopically express the dorsal compartment marker Ap (C-C'). 43% (13/30) of dorsal *yki<sup>CA</sup>* clones had reduced or absent ap-lacZ (white arrow in B'). (D-F) Clones made by mitotic recombination using the MARCM system such that clones lacking Gal80 express *UAS-GFP* and/or *UAS-yki<sup>CA</sup>*. (D) MARCM *smo3/smo3* clones expressing GFP are small and irregular. (E) MARCM *+/+* clones expressing *UAS-yki<sup>CA</sup>* and *UAS-GFP* are overgrown with smooth boundaries. Ectopic Ci is observed in posterior ventral hinge clones. (F) MARCM *smo3/smo3* clones expressing *UAS-yki<sup>CA</sup>* and *UAS-GFP* are also overgrown and have smooth edges. Although Smo protein is absent in clones (F'), ectopic Ci protein is still observed (F''). Thus, Ci expression per se is not dependent on Hh signaling. Hh

signaling could potentially affect the relative amounts of the activator and repressor form of Ci. (G, H) Anterior and posterior clones are not significantly different in size for MARCM +/- clones expressing *UAS-yki<sup>CA</sup>* (G) or MARCM *smo3/smo3* clones expressing *UAS-yki<sup>CA</sup>* (H). (I) Ci expression is not required for Yki<sup>CA</sup>-induced overgrowth. Clones expressing *UAS-yki<sup>CA</sup>* and *UAS-ciRNAi* lack Ci expression in clones (including ectopic Ci in posterior clones) but still overgrow. (J) Anterior and posterior clones expressing *UAS-yki<sup>CA</sup>* and *UAS-ciRNAi* are not significantly different in size. (K) Some Yki<sup>CA</sup>-expressing clones (marked with V5) express the AP-1 reporter, *AP-1-RFP* (arrows), but most clones express a low level or no RFP. (L) A minority of *yki<sup>CA</sup>* clones (marked with RFP) express MMP1 (arrows), a target of JNK signaling, but most clones do not express MMP1. (M, N) Clones expressing Yki<sup>CA</sup> and Jnk<sup>DN</sup> overgrow and express ectopic Ci, similar to Yki<sup>CA</sup> alone. (M) Expression of JNK<sup>DN</sup> in wild-type clones does not alter Ci expression. (N) Clones expressing Yki<sup>CA</sup> and Jnk<sup>DN</sup> express ectopic Ci and also downregulate En (N'). (O) TIEDYE control disc.

## References

- Abdul Kadir, L., Stacey, M., & Barrett-Jolley, R. (2018). Emerging Roles of the Membrane Potential: Action Beyond the Action Potential. *Front Physiol*, *9*, 1661. doi:10.3389/fphys.2018.01661
- Adachi-Yamada, T., & O'Connor, M. B. (2002). Morphogenetic apoptosis: a mechanism for correcting discontinuities in morphogen gradients. *Dev Biol*, *251*(1), 74-90. doi:10.1006/dbio.2002.0821
- Adachi-Yamada, T., & O'Connor, M. B. (2004). Mechanisms for removal of developmentally abnormal cells: cell competition and morphogenetic apoptosis. *J Biochem*, *136*(1), 13-17. doi:10.1093/jb/mvh099
- Adams, C. M., Anderson, M. G., Motto, D. G., Price, M. P., Johnson, W. A., & Welsh, M. J. (1998). Ripped pocket and pickpocket, novel Drosophila DEG/ENaC subunits expressed in early development and in mechanosensory neurons. *J Cell Biol*, *140*(1), 143-152. doi:10.1083/jcb.140.1.143
- Adams, D. S., & Levin, M. (2012). Measuring resting membrane potential using the fluorescent voltage reporters DiBAC4(3) and CC2-DMPE. *Cold Spring Harb Protoc*, *2012*(4), 459-464. doi:10.1101/pdb.prot067702
- Adams, M. D., & Sekelsky, J. J. (2002). From sequence to phenotype: reverse genetics in Drosophila melanogaster. *Nat Rev Genet*, *3*(3), 189-198. doi:10.1038/nrg752
- Alexandre, C., Jacinto, A., & Ingham, P. W. (1996). Transcriptional activation of hedgehog target genes in Drosophila is mediated directly by the cubitus interruptus protein, a member of the GLI family of zinc finger DNA-binding proteins. *Genes Dev*, *10*(16), 2003-2013. doi:10.1101/gad.10.16.2003
- Allis, C. D., & Jenuwein, T. (2016). The molecular hallmarks of epigenetic control. *Nat Rev Genet*, *17*(8), 487-500. doi:10.1038/nrg.2016.59
- Atsuta, Y., Tomizawa, R. R., Levin, M., & Tabin, C. J. (2019). L-type voltage-gated Ca(2+) channel Ca(V)1.2 regulates chondrogenesis during limb development. *Proc Natl Acad Sci U S A*, *116*(43), 21592-21601. doi:10.1073/pnas.1908981116
- Axelsen, J. B., Lotem, J., Sachs, L., & Domany, E. (2007). Genes overexpressed in different human solid cancers exhibit different tissue-specific expression profiles. *Proc Natl Acad Sci U S A*, *104*(32), 13122-13127. doi:10.1073/pnas.0705824104
- Ayers, K. L., Gallet, A., Staccini-Lavenant, L., & Therond, P. P. (2010). The long-range activity of Hedgehog is regulated in the apical extracellular space by the glypican Dally and the hydrolase Notum. *Dev Cell*, *18*(4), 605-620. doi:10.1016/j.devcel.2010.02.015
- Aza-Blanc, P., Ramírez-Weber, F. A., Laget, M. P., Schwartz, C., & Kornberg, T. B. (1997). Proteolysis that is inhibited by hedgehog targets Cubitus interruptus protein to the nucleus and converts it to a repressor. *Cell*, *89*(7), 1043-1053. doi:10.1016/s0092-8674(00)80292-5
- Baines, R. A., Uhler, J. P., Thompson, A., Sweeney, S. T., & Bate, M. (2001). Altered electrical properties in Drosophila neurons developing without synaptic transmission. *J Neurosci*, *21*(5), 1523-1531. doi:10.1523/jneurosci.21-05-01523.2001
- Bajpai, A., & Sinha, P. (2020). Hh signaling from de novo organizers drive Igl neoplasia in Drosophila epithelium. *Dev Biol*, *457*(1), 1-8. doi:10.1016/j.ydbio.2019.09.011

- Baker, N. E. (1987). Molecular cloning of sequences from wingless, a segment polarity gene in *Drosophila*: the spatial distribution of a transcript in embryos. *Embo j*, 6(6), 1765-1773. Retrieved from <https://www.ncbi.nlm.nih.gov/pubmed/16453776>
- Baker, N. E. (2017). Mechanisms of cell competition emerging from *Drosophila* studies. *Curr Opin Cell Biol*, 48, 40-46. doi:10.1016/j.ceb.2017.05.002
- Barbado, M., Fablet, K., Ronjat, M., & De Waard, M. (2009). Gene regulation by voltage-dependent calcium channels. *Biochim Biophys Acta*, 1793(6), 1096-1104. doi:10.1016/j.bbamcr.2009.02.004
- Beira, J. V., & Paro, R. (2016). The legacy of *Drosophila* imaginal discs. *Chromosoma*, 125(4), 573-592. doi:10.1007/s00412-016-0595-4
- Belus, M. T., Rogers, M. A., Elzubeir, A., Josey, M., Rose, S., Andreeva, V., . . . Bates, E. A. (2018). Kir2.1 is important for efficient BMP signaling in mammalian face development. *Dev Biol*, 444 Suppl 1(Suppl 1), S297-s307. doi:10.1016/j.ydbio.2018.02.012
- Bielmeier, C., Alt, S., Weichselberger, V., La Fortezza, M., Harz, H., Julicher, F., . . . Classen, A. K. (2016). Interface Contractility between Differently Fated Cells Drives Cell Elimination and Cyst Formation. *Curr Biol*, 26(5), 563-574. doi:10.1016/j.cub.2015.12.063
- Blackiston, D. J., McLaughlin, K. A., & Levin, M. (2009). Bioelectric controls of cell proliferation: ion channels, membrane voltage and the cell cycle. *Cell Cycle*, 8(21), 3527-3536. doi:10.4161/cc.8.21.9888
- Blair, S. S., & Ralston, A. (1997). Smoothed-mediated Hedgehog signalling is required for the maintenance of the anterior-posterior lineage restriction in the developing wing of *Drosophila*. *Development*, 124(20), 4053-4063. Retrieved from <https://www.ncbi.nlm.nih.gov/pubmed/9374402>
- Bosveld, F., Bonnet, I., Guirao, B., Tlili, S., Wang, Z., Petitalot, A., . . . Bellaiche, Y. (2012). Mechanical control of morphogenesis by Fat/Dachsous/Four-jointed planar cell polarity pathway. *Science*, 336(6082), 724-727. doi:10.1126/science.1221071
- Brennecke, J., Hipfner, D. R., Stark, A., Russell, R. B., & Cohen, S. M. (2003). bantam encodes a developmentally regulated microRNA that controls cell proliferation and regulates the proapoptotic gene hid in *Drosophila*. *Cell*, 113(1), 25-36. doi:10.1016/s0092-8674(03)00231-9
- Britten, R. J., & Davidson, E. H. (1969). Gene regulation for higher cells: a theory. *Science*, 165(3891), 349-357. doi:10.1126/science.165.3891.349
- Britton, J. S., Lockwood, W. K., Li, L., Cohen, S. M., & Edgar, B. A. (2002). *Drosophila*'s insulin/PI3-kinase pathway coordinates cellular metabolism with nutritional conditions. *Dev Cell*, 2(2), 239-249. doi:10.1016/s1534-5807(02)00117-x
- Brown, N. H., Gregory, S. L., Rickoll, W. L., Fessler, L. I., Prout, M., White, R. A., & Fristrom, J. W. (2002). Talin is essential for integrin function in *Drosophila*. *Dev Cell*, 3(4), 569-579. doi:10.1016/s1534-5807(02)00290-3
- Brumby, A. M., & Richardson, H. E. (2003). scribble mutants cooperate with oncogenic Ras or Notch to cause neoplastic overgrowth in *Drosophila*. *Embo j*, 22(21), 5769-5779. doi:10.1093/emboj/cdg548
- Bunch, T. A., Salatino, R., Engelsjerd, M. C., Mukai, L., West, R. F., & Brower, D. L. (1992). Characterization of mutant alleles of myospheroid, the gene encoding the

- beta subunit of the Drosophila PS integrins. *Genetics*, 132(2), 519-528. Retrieved from <https://www.ncbi.nlm.nih.gov/pubmed/1427041>
- Burke, R., Nellen, D., Bellotto, M., Hafen, E., Senti, K. A., Dickson, B. J., & Basler, K. (1999). Dispatched, a novel sterol-sensing domain protein dedicated to the release of cholesterol-modified hedgehog from signaling cells. *Cell*, 99(7), 803-815. doi:10.1016/s0092-8674(00)81677-3
- Calgaro, S., Boube, M., Cribbs, D. L., & Bourbon, H. M. (2002). The Drosophila gene taranis encodes a novel trithorax group member potentially linked to the cell cycle regulatory apparatus. *Genetics*, 160(2), 547-560. Retrieved from <https://www.ncbi.nlm.nih.gov/pubmed/11861561>
- Callejo, A., Biloni, A., Mollica, E., Gorfinkiel, N., Andres, G., Ibanez, C., . . . Guerrero, I. (2011). Dispatched mediates Hedgehog basolateral release to form the long-range morphogenetic gradient in the Drosophila wing disk epithelium. *Proc Natl Acad Sci U S A*, 108(31), 12591-12598. doi:10.1073/pnas.1106881108
- Chanas, G., Lavrov, S., Iral, F., Cavalli, G., & Maschat, F. (2004). Engrailed and polyhomeotic maintain posterior cell identity through cubitus-interruptus regulation. *Dev Biol*, 272(2), 522-535. doi:10.1016/j.ydbio.2004.05.020
- Chatterjee, N., & Bohmann, D. (2012). A versatile PhiC31 based reporter system for measuring AP-1 and Nrf2 signaling in Drosophila and in tissue culture. *PLoS ONE*, 7(4), e34063. doi:10.1371/journal.pone.0034063
- Chen, C., Jack, J., & Garofalo, R. S. (1996). The Drosophila insulin receptor is required for normal growth. *Endocrinology*, 137(3), 846-856. doi:10.1210/endo.137.3.8603594
- Chen, M. H., Li, Y. J., Kawakami, T., Xu, S. M., & Chuang, P. T. (2004). Palmitoylation is required for the production of a soluble multimeric Hedgehog protein complex and long-range signaling in vertebrates. *Genes Dev*, 18(6), 641-659. doi:10.1101/gad.1185804
- Chen, W., Huang, H., Hatori, R., & Kornberg, T. B. (2017). Essential basal cytonemes take up Hedgehog in the Drosophila wing imaginal disc. *Development*, 144(17), 3134-3144. doi:10.1242/dev.149856
- Cheng, Y., Brunner, A. L., Kremer, S., DeVido, S. K., Stefaniuk, C. M., & Kassis, J. A. (2014). Co-regulation of invected and engrailed by a complex array of regulatory sequences in Drosophila. *Dev Biol*, 395(1), 131-143. doi:10.1016/j.ydbio.2014.08.021
- Chifflet, S., Hernandez, J. A., Grasso, S., & Cirillo, A. (2003). Nonspecific depolarization of the plasma membrane potential induces cytoskeletal modifications of bovine corneal endothelial cells in culture. *Exp Cell Res*, 282(1), 1-13. doi:10.1006/excr.2002.5664
- Christiansen, A. E., Ding, T., & Bergmann, A. (2012). Ligand-independent activation of the Hedgehog pathway displays non-cell autonomous proliferation during eye development in Drosophila. *Mech Dev*, 129(5-8), 98-108. doi:10.1016/j.mod.2012.05.009
- Codelia, V. A., Sun, G., & Irvine, K. D. (2014). Regulation of YAP by mechanical strain through Jnk and Hippo signaling. *Curr Biol*, 24(17), 2012-2017. doi:10.1016/j.cub.2014.07.034

- Cone, C. D., Jr. (1969). Electroosmotic interactions accompanying mitosis initiation in sarcoma cells in vitro. *Trans N Y Acad Sci*, 31(4), 404-427. doi:10.1111/j.2164-0947.1969.tb02926.x
- Coste, B., Mathur, J., Schmidt, M., Earley, T. J., Ranade, S., Petrus, M. J., . . . Patapoutian, A. (2010). Piezo1 and Piezo2 are essential components of distinct mechanically activated cation channels. *Science*, 330(6000), 55-60. doi:10.1126/science.1193270
- Coste, B., Xiao, B., Santos, J. S., Syeda, R., Grandl, J., Spencer, K. S., . . . Patapoutian, A. (2012). Piezo proteins are pore-forming subunits of mechanically activated channels. *Nature*, 483(7388), 176-181. doi:10.1038/nature10812
- Dahal, G. R., Pradhan, S. J., & Bates, E. A. (2017). Inwardly rectifying potassium channels influence Drosophila wing morphogenesis by regulating Dpp release. *Development*, 144(15), 2771-2783. doi:10.1242/dev.146647
- Dahal, G. R., Rawson, J., Gassaway, B., Kwok, B., Tong, Y., Ptacek, L. J., & Bates, E. (2012). An inwardly rectifying K<sup>+</sup> channel is required for patterning. *Development*, 139(19), 3653-3664. doi:10.1242/dev.078592
- Daley, W. P., & Yamada, K. M. (2013). ECM-modulated cellular dynamics as a driving force for tissue morphogenesis. *Curr Opin Genet Dev*, 23(4), 408-414. doi:10.1016/j.gde.2013.05.005
- Deivasikamani, V., Dhayalan, S., Abudushalamu, Y., Mughal, R., Visnagri, A., Cuthbertson, K., . . . Sukumar, P. (2019). Piezo1 channel activation mimics high glucose as a stimulator of insulin release. *Sci Rep*, 9(1), 16876. doi:10.1038/s41598-019-51518-w
- Delling, M., DeCaen, P. G., Doerner, J. F., Febvay, S., & Clapham, D. E. (2013). Primary cilia are specialized calcium signalling organelles. *Nature*, 504(7479), 311-314. doi:10.1038/nature12833
- Dellino, G. I., Schwartz, Y. B., Farkas, G., McCabe, D., Elgin, S. C., & Pirrotta, V. (2004). Polycomb silencing blocks transcription initiation. *Mol Cell*, 13(6), 887-893. doi:10.1016/s1097-2765(04)00128-5
- Desprat, N., Supatto, W., Pouille, P. A., Beaurepaire, E., & Farge, E. (2008). Tissue deformation modulates twist expression to determine anterior midgut differentiation in Drosophila embryos. *Dev Cell*, 15(3), 470-477. doi:10.1016/j.devcel.2008.07.009
- Discher, D. E., Janmey, P., & Wang, Y. L. (2005). Tissue cells feel and respond to the stiffness of their substrate. *Science*, 310(5751), 1139-1143. doi:10.1126/science.1116995
- Dixon, R. E., Cheng, E. P., Mercado, J. L., & Santana, L. F. (2012). L-type Ca<sup>2+</sup> channel function during Timothy syndrome. *Trends Cardiovasc Med*, 22(3), 72-76. doi:10.1016/j.tcm.2012.06.015
- Donaldson, M. R., Yoon, G., Fu, Y. H., & Ptacek, L. J. (2004). Andersen-Tawil syndrome: a model of clinical variability, pleiotropy, and genetic heterogeneity. *Ann Med*, 36 Suppl 1, 92-97. doi:10.1080/17431380410032490
- Dong, J., Feldmann, G., Huang, J., Wu, S., Zhang, N., Comerford, S. A., . . . Pan, D. (2007). Elucidation of a universal size-control mechanism in Drosophila and mammals. *Cell*, 130(6), 1120-1133. doi:10.1016/j.cell.2007.07.019

- Duchemin, A. L., Vignes, H., & Vermot, J. (2019). Mechanically activated piezo channels modulate outflow tract valve development through the Yap1 and Klf2-Notch signaling axis. *eLife*, 8. doi:10.7554/eLife.44706
- Ducuing, A., Mollereau, B., Axelrod, J. D., & Vincent, S. (2013). Absolute requirement of cholesterol binding for Hedgehog gradient formation in *Drosophila*. *Biol Open*, 2(6), 596-604. doi:10.1242/bio.20134952
- Dutta, P., & Li, W. X. (2017). The SERTAD protein Taranis plays a role in Polycomb-mediated gene repression. *PLoS ONE*, 12(6), e0180026. doi:10.1371/journal.pone.0180026
- Eaton, S., & Kornberg, T. B. (1990). Repression of *ci-D* in posterior compartments of *Drosophila* by engrailed. *Genes Dev*, 4(6), 1068-1077. doi:10.1101/gad.4.6.1068
- Emmons-Bell, M., & Hariharan, I. K. (2021). Membrane potential regulates Hedgehog signalling in the *Drosophila* wing imaginal disc. *EMBO Rep*, e51861. doi:10.15252/embr.202051861
- Enomoto, M., & Igaki, T. (2013). Src controls tumorigenesis via JNK-dependent regulation of the Hippo pathway in *Drosophila*. *EMBO Rep*, 14(1), 65-72. doi:10.1038/embor.2012.185
- Enomoto, M., Kizawa, D., Ohsawa, S., & Igaki, T. (2015). JNK signaling is converted from anti- to pro-tumor pathway by Ras-mediated switch of Warts activity. *Dev Biol*, 403(2), 162-171. doi:10.1016/j.ydbio.2015.05.001
- Fang, X. Z., Zhou, T., Xu, J. Q., Wang, Y. X., Sun, M. M., He, Y. J., . . . Shang, Y. (2021). Structure, kinetic properties and biological function of mechanosensitive Piezo channels. *Cell Biosci*, 11(1), 13. doi:10.1186/s13578-020-00522-z
- Flavahan, W. A., Gaskell, E., & Bernstein, B. E. (2017). Epigenetic plasticity and the hallmarks of cancer. *Science*, 357(6348). doi:10.1126/science.aal2380
- Garcia-Bellido, A., & Merriam, J. R. (1971). Clonal parameters of tergite development in *Drosophila*. *Dev Biol*, 26(2), 264-276. doi:10.1016/0012-1606(71)90126-6
- Garcia-Bellido, A., Ripoll, P., & Morata, G. (1973). Developmental compartmentalisation of the wing disk of *Drosophila*. *Nat New Biol*, 245(147), 251-253. doi:10.1038/newbio245251a0
- Garty, H. (1994). Molecular properties of epithelial, amiloride-blockable Na<sup>+</sup> channels. *Faseb j*, 8(8), 522-528. doi:10.1096/fasebj.8.8.8181670
- Germani, F., Hain, D., Sternlicht, D., Moreno, E., & Basler, K. (2018). The Toll pathway inhibits tissue growth and regulates cell fitness in an infection-dependent manner. *eLife*, 7. doi:10.7554/eLife.39939
- Gibson, M. C., & Perrimon, N. (2005). Extrusion and death of DPP/BMP-compromised epithelial cells in the developing *Drosophila* wing. *Science*, 307(5716), 1785-1789. doi:10.1126/science.1104751
- Goetz, J. A., Singh, S., Suber, L. M., Kull, F. J., & Robbins, D. J. (2006). A highly conserved amino-terminal region of sonic hedgehog is required for the formation of its freely diffusible multimeric form. *J Biol Chem*, 281(7), 4087-4093. doi:10.1074/jbc.M511427200
- Golic, K. G. (1991). Site-specific recombination between homologous chromosomes in *Drosophila*. *Science*, 252(5008), 958-961. doi:10.1126/science.2035025

- Gong, X., Qian, H., Cao, P., Zhao, X., Zhou, Q., Lei, J., & Yan, N. (2018). Structural basis for the recognition of Sonic Hedgehog by human Patched1. *Science*, 361(6402). doi:10.1126/science.aas8935
- González-Méndez, L., Seijo-Barandiarán, I., & Guerrero, I. (2017). Cytoskeleton-mediated cell-cell contacts for Hedgehog reception. *eLife*, 6. doi:10.7554/eLife.24045
- Goulev, Y., Fauny, J. D., Gonzalez-Marti, B., Flagiello, D., Silber, J., & Zider, A. (2008). SCALLOPED interacts with YORKIE, the nuclear effector of the hippo tumor-suppressor pathway in Drosophila. *Curr Biol*, 18(6), 435-441. doi:10.1016/j.cub.2008.02.034
- Griffin, R., Binari, R., & Perrimon, N. (2014). Genetic odyssey to generate marked clones in Drosophila mosaics. *Proc Natl Acad Sci U S A*, 111(13), 4756-4763. doi:10.1073/pnas.1403218111
- Hamaratoglu, F., Affolter, M., & Pyrowolakis, G. (2014). Dpp/BMP signaling in flies: from molecules to biology. *Semin Cell Dev Biol*, 32, 128-136. doi:10.1016/j.semcdb.2014.04.036
- Han, Y., Liu, C., Zhang, D., Men, H., Huo, L., Geng, Q., . . . Jia, Z. (2019). Mechanosensitive ion channel Piezo1 promotes prostate cancer development through the activation of the Akt/mTOR pathway and acceleration of cell cycle. *Int J Oncol*, 55(3), 629-644. doi:10.3892/ijo.2019.4839
- Hariharan, I. K. (2015). Organ Size Control: Lessons from Drosophila. *Dev Cell*, 34(3), 255-265. doi:10.1016/j.devcel.2015.07.012
- He, L., Si, G., Huang, J., Samuel, A. D. T., & Perrimon, N. (2018). Mechanical regulation of stem-cell differentiation by the stretch-activated Piezo channel. *Nature*, 555(7694), 103-106. doi:10.1038/nature25744
- Herranz, H., Hong, X., & Cohen, S. M. (2012). Mutual repression by bantam miRNA and Capicua links the EGFR/MAPK and Hippo pathways in growth control. *Curr Biol*, 22(8), 651-657. doi:10.1016/j.cub.2012.02.050
- Hipfner, D. R., Weigmann, K., & Cohen, S. M. (2002). The bantam gene regulates Drosophila growth. *Genetics*, 161(4), 1527-1537. Retrieved from <https://www.ncbi.nlm.nih.gov/pubmed/12196398>
- Hiramatsu, R., Matsuoka, T., Kimura-Yoshida, C., Han, S. W., Mochida, K., Adachi, T., . . . Matsuo, I. (2013). External mechanical cues trigger the establishment of the anterior-posterior axis in early mouse embryos. *Dev Cell*, 27(2), 131-144. doi:10.1016/j.devcel.2013.09.026
- Hodge, J. J. (2009). Ion channels to inactivate neurons in Drosophila. *Front Mol Neurosci*, 2, 13. doi:10.3389/neuro.02.013.2009
- Hooper, J. E., & Scott, M. P. (1989). The Drosophila patched gene encodes a putative membrane protein required for segmental patterning. *Cell*, 59(4), 751-765. doi:10.1016/0092-8674(89)90021-4
- Hsia, E. Y. C., Zhang, Y., Tran, H. S., Lim, A., Chou, Y. H., Lan, G., . . . Zheng, X. (2017). Hedgehog mediated degradation of Ihog adhesion proteins modulates cell segregation in Drosophila wing imaginal discs. *Nat Commun*, 8(1), 1275. doi:10.1038/s41467-017-01364-z
- Huang, J., Wu, S., Barrera, J., Matthews, K., & Pan, D. (2005). The Hippo signaling pathway coordinately regulates cell proliferation and apoptosis by inactivating

- Yorkie, the Drosophila Homolog of YAP. *Cell*, 122(3), 421-434.  
doi:10.1016/j.cell.2005.06.007
- Hunter, G. L., Crawford, J. M., Genkins, J. Z., & Kiehart, D. P. (2014). Ion channels contribute to the regulation of cell sheet forces during Drosophila dorsal closure. *Development*, 141(2), 325-334. doi:10.1242/dev.097097
- Igaki, T., Pastor-Pareja, J. C., Aonuma, H., Miura, M., & Xu, T. (2009). Intrinsic tumor suppression and epithelial maintenance by endocytic activation of Eiger/TNF signaling in Drosophila. *Dev Cell*, 16(3), 458-465.  
doi:10.1016/j.devcel.2009.01.002
- Inagaki, H. K., Jung, Y., Hoopfer, E. D., Wong, A. M., Mishra, N., Lin, J. Y., . . . Anderson, D. J. (2014). Optogenetic control of Drosophila using a red-shifted channelrhodopsin reveals experience-dependent influences on courtship. *Nat Methods*, 11(3), 325-332. doi:10.1038/nmeth.2765
- Ingham, P. W. (2018). From Drosophila segmentation to human cancer therapy. *Development*, 145(21). doi:10.1242/dev.168898
- Ingham, P. W., Nystedt, S., Nakano, Y., Brown, W., Stark, D., van den Heuvel, M., & Taylor, A. M. (2000). Patched represses the Hedgehog signalling pathway by promoting modification of the Smoothed protein. *Curr Biol*, 10(20), 1315-1318. doi:10.1016/s0960-9822(00)00755-7
- Irvine, K. D., & Harvey, K. F. (2015). Control of organ growth by patterning and hippo signaling in Drosophila. *Cold Spring Harb Perspect Biol*, 7(6).  
doi:10.1101/cshperspect.a019224
- Jam, F. A., Morimune, T., Tsukamura, A., Tano, A., Tanaka, Y., Mori, Y., . . . Mori, M. (2020). Neuroepithelial cell competition triggers loss of cellular juvenescence. *Sci Rep*, 10(1), 18044. doi:10.1038/s41598-020-74874-4
- Jiang, J., & Hui, C. C. (2008). Hedgehog signaling in development and cancer. *Dev Cell*, 15(6), 801-812. doi:10.1016/j.devcel.2008.11.010
- Johnston, L. A. (2009). Competitive interactions between cells: death, growth, and geography. *Science*, 324(5935), 1679-1682. doi:10.1126/science.1163862
- Johnston, L. A., & Edgar, B. A. (1998). Wingless and Notch regulate cell-cycle arrest in the developing Drosophila wing. *Nature*, 394(6688), 82-84. doi:10.1038/27925
- Johnston, L. A., Prober, D. A., Edgar, B. A., Eisenman, R. N., & Gallant, P. (1999). Drosophila myc regulates cellular growth during development. *Cell*, 98(6), 779-790. doi:10.1016/s0092-8674(00)81512-3
- Karim, F. D., & Rubin, G. M. (1998). Ectopic expression of activated Ras1 induces hyperplastic growth and increased cell death in Drosophila imaginal tissues. *Development*, 125(1), 1-9. Retrieved from <https://www.ncbi.nlm.nih.gov/pubmed/9389658>
- Kassis, J. A., Kennison, J. A., & Tamkun, J. W. (2017). Polycomb and Trithorax Group Genes in Drosophila. *Genetics*, 206(4), 1699-1725.  
doi:10.1534/genetics.115.185116
- Katsukawa, M., Ohsawa, S., Zhang, L., Yan, Y., & Igaki, T. (2018). Serpin Facilitates Tumor-Suppressive Cell Competition by Blocking Toll-Mediated Yki Activation in Drosophila. *Curr Biol*, 28(11), 1756-1767 e1756. doi:10.1016/j.cub.2018.04.022

- Klatt Shaw, D., Gunther, D., Juryneec, M. J., Chagovetz, A. A., Ritchie, E., & Grunwald, D. J. (2018). Intracellular Calcium Mobilization Is Required for Sonic Hedgehog Signaling. *Dev Cell*, *45*(4), 512-525.e515. doi:10.1016/j.devcel.2018.04.013
- Kornberg, T., Siden, I., O'Farrell, P., & Simon, M. (1985). The engrailed locus of *Drosophila*: in situ localization of transcripts reveals compartment-specific expression. *Cell*, *40*(1), 45-53. doi:10.1016/0092-8674(85)90307-1
- Krüger, J., & Bohrmann, J. (2015). Bioelectric patterning during oogenesis: stage-specific distribution of membrane potentials, intracellular pH and ion-transport mechanisms in *Drosophila* ovarian follicles. *BMC Dev Biol*, *15*, 1. doi:10.1186/s12861-015-0051-3
- Landsberg, K. P., Farhadifar, R., Ranft, J., Umetsu, D., Widmann, T. J., Bittig, T., . . . Dahmann, C. (2009). Increased cell bond tension governs cell sorting at the *Drosophila* anteroposterior compartment boundary. *Curr Biol*, *19*(22), 1950-1955. doi:10.1016/j.cub.2009.10.021
- Lawrence, P. A., Green, S. M., & Johnston, P. (1978). Compartmentalization and growth of the *Drosophila* abdomen. *J Embryol Exp Morphol*, *43*, 233-245. Retrieved from <https://www.ncbi.nlm.nih.gov/pubmed/632739>
- Lebovitz, R. M., Takeyasu, K., & Fambrough, D. M. (1989). Molecular characterization and expression of the (Na<sup>+</sup> + K<sup>+</sup>)-ATPase alpha-subunit in *Drosophila melanogaster*. *Embo j*, *8*(1), 193-202.
- Lecuit, T., Brook, W. J., Ng, M., Calleja, M., Sun, H., & Cohen, S. M. (1996). Two distinct mechanisms for long-range patterning by Decapentaplegic in the *Drosophila* wing. *Nature*, *381*(6581), 387-393. doi:10.1038/381387a0
- Lee, R. T., Zhao, Z., & Ingham, P. W. (2016). Hedgehog signalling. *Development*, *143*(3), 367-372. doi:10.1242/dev.120154
- Legoff, L., Rouault, H., & Lecuit, T. (2013). A global pattern of mechanical stress polarizes cell divisions and cell shape in the growing *Drosophila* wing disc. *Development*, *140*(19), 4051-4059. doi:10.1242/dev.090878
- Li, S., Chen, Y., Shi, Q., Yue, T., Wang, B., & Jiang, J. (2012). Hedgehog-regulated ubiquitination controls smoothed trafficking and cell surface expression in *Drosophila*. *PLoS Biol*, *10*(1), e1001239. doi:10.1371/journal.pbio.1001239
- Lin, J. Y., Knutsen, P. M., Muller, A., Kleinfeld, D., & Tsien, R. Y. (2013). ReaChR: a red-shifted variant of channelrhodopsin enables deep transcranial optogenetic excitation. *Nat Neurosci*, *16*(10), 1499-1508. doi:10.1038/nn.3502
- Luan, H., Lemon, W. C., Peabody, N. C., Pohl, J. B., Zelensky, P. K., Wang, D., . . . White, B. H. (2006). Functional dissection of a neuronal network required for cuticle tanning and wing expansion in *Drosophila*. *J Neurosci*, *26*(2), 573-584. doi:10.1523/jneurosci.3916-05.2006
- Luchetti, G., Sircar, R., Kong, J. H., Nachtergaele, S., Sagner, A., Byrne, E. F., . . . Rohatgi, R. (2016). Cholesterol activates the G-protein coupled receptor Smoothed to promote Hedgehog signaling. *eLife*, *5*. doi:10.7554/eLife.20304
- Lumsden, A., & Keynes, R. (1989). Segmental patterns of neuronal development in the chick hindbrain. *Nature*, *337*(6206), 424-428. doi:10.1038/337424a0
- Ma, C., Zhou, Y., Beachy, P. A., & Moses, K. (1993). The segment polarity gene hedgehog is required for progression of the morphogenetic furrow in the

- developing *Drosophila* eye. *Cell*, 75(5), 927-938. doi:10.1016/0092-8674(93)90536-y
- Ma, X., Wang, H., Ji, J., Xu, W., Sun, Y., Li, W., . . . Xue, L. (2017). Hippo signaling promotes JNK-dependent cell migration. *Proc Natl Acad Sci U S A*, 114(8), 1934-1939. doi:10.1073/pnas.1621359114
- Mandaravally Madhavan, M., & Schneiderman, H. A. (1977). Histological analysis of the dynamics of growth of imaginal discs and histoblast nests during the larval development of *Drosophila melanogaster*. *Wilehm Roux Arch Dev Biol*, 183(4), 269-305. doi:10.1007/BF00848459
- Mann, R. S. (1994). Engrailed-mediated repression of Ultrabithorax is necessary for the parasegment 6 identity in *Drosophila*. *Development*, 120(11), 3205-3212. Retrieved from <https://www.ncbi.nlm.nih.gov/pubmed/7720563>
- Martin, F. A., Herrera, S. C., & Morata, G. (2009). Cell competition, growth and size control in the *Drosophila* wing imaginal disc. *Development*, 136(22), 3747-3756. doi:10.1242/dev.038406
- Milan, M., Campuzano, S., & Garcia-Bellido, A. (1996). Cell cycling and patterned cell proliferation in the *Drosophila* wing during metamorphosis. *Proc Natl Acad Sci U S A*, 93(21), 11687-11692. doi:10.1073/pnas.93.21.11687
- Miura, G. I., & Treisman, J. E. (2006). Lipid modification of secreted signaling proteins. *Cell Cycle*, 5(11), 1184-1188. doi:10.4161/cc.5.11.2804
- Miyazaki, A., Sugimoto, A., Yoshizaki, K., Kawarabayashi, K., Iwata, K., Kurogoushi, R., . . . Iwamoto, T. (2019). Coordination of WNT signaling and ciliogenesis during odontogenesis by piezo type mechanosensitive ion channel component 1. *Sci Rep*, 9(1), 14762. doi:10.1038/s41598-019-51381-9
- Morata, G. (2021). Cell competition: A historical perspective. *Dev Biol*. doi:10.1016/j.ydbio.2021.02.012
- Morata, G., & Ripoll, P. (1975). Minutes: mutants of *drosophila* autonomously affecting cell division rate. *Dev Biol*, 42(2), 211-221. doi:10.1016/0012-1606(75)90330-9
- Morth, J. P., Pedersen, B. P., Toustrup-Jensen, M. S., Sørensen, T. L., Petersen, J., Andersen, J. P., . . . Nissen, P. (2007). Crystal structure of the sodium-potassium pump. *Nature*, 450(7172), 1043-1049. doi:10.1038/nature06419
- Muller, J., Hart, C. M., Francis, N. J., Vargas, M. L., Sengupta, A., Wild, B., . . . Simon, J. A. (2002). Histone methyltransferase activity of a *Drosophila* Polycomb group repressor complex. *Cell*, 111(2), 197-208. doi:10.1016/s0092-8674(02)00976-5
- Myers, B. R., Neahring, L., Zhang, Y., Roberts, K. J., & Beachy, P. A. (2017). Rapid, direct activity assays for Smoothed reveal Hedgehog pathway regulation by membrane cholesterol and extracellular sodium. *Proc Natl Acad Sci U S A*, 114(52), E11141-e11150. doi:10.1073/pnas.1717891115
- Nagel, G., Szellas, T., Huhn, W., Kateriya, S., Adeishvili, N., Berthold, P., . . . Bamberg, E. (2003). Channelrhodopsin-2, a directly light-gated cation-selective membrane channel. *Proc Natl Acad Sci U S A*, 100(24), 13940-13945. doi:10.1073/pnas.1936192100
- Nakano, Y., Guerrero, I., Hidalgo, A., Taylor, A., Whittle, J. R., & Ingham, P. W. (1989). A protein with several possible membrane-spanning domains encoded by the *Drosophila* segment polarity gene patched. *Nature*, 341(6242), 508-513. doi:10.1038/341508a0

- Nellen, D., Burke, R., Struhl, G., & Basler, K. (1996). Direct and long-range action of a DPP morphogen gradient. *Cell*, *85*(3), 357-368. doi:10.1016/s0092-8674(00)81114-9
- Nin, V., Hernandez, J. A., & Chifflet, S. (2009). Hyperpolarization of the plasma membrane potential provokes reorganization of the actin cytoskeleton and increases the stability of adherens junctions in bovine corneal endothelial cells in culture. *Cell Motil Cytoskeleton*, *66*(12), 1087-1099. doi:10.1002/cm.20416
- Nishimura, G., Lausch, E., Savarirayan, R., Shiba, M., Spranger, J., Zabel, B., . . . Unger, S. (2012). TRPV4-associated skeletal dysplasias. *Am J Med Genet C Semin Med Genet*, *160C*(3), 190-204. doi:10.1002/ajmg.c.31335
- Nitabach, M. N., Wu, Y., Sheeba, V., Lemon, W. C., Strumbos, J., Zelensky, P. K., . . . Holmes, T. C. (2006). Electrical hyperexcitation of lateral ventral pacemaker neurons desynchronizes downstream circadian oscillators in the fly circadian circuit and induces multiple behavioral periods. *J Neurosci*, *26*(2), 479-489. doi:10.1523/jneurosci.3915-05.2006
- Nolo, R., Morrison, C. M., Tao, C., Zhang, X., & Halder, G. (2006). The bantam microRNA is a target of the hippo tumor-suppressor pathway. *Curr Biol*, *16*(19), 1895-1904. doi:10.1016/j.cub.2006.08.057
- Norman, M., Wisniewska, K. A., Lawrenson, K., Garcia-Miranda, P., Tada, M., Kajita, M., . . . Fujita, Y. (2012). Loss of Scribble causes cell competition in mammalian cells. *J Cell Sci*, *125*(Pt 1), 59-66. doi:10.1242/jcs.085803
- Nusslein-Volhard, C., & Wieschaus, E. (1980). Mutations affecting segment number and polarity in *Drosophila*. *Nature*, *287*(5785), 795-801. doi:10.1038/287795a0
- O'Brochta, D. A., & Bryant, P. J. (1985). A zone of non-proliferating cells at a lineage restriction boundary in *Drosophila*. *Nature*, *313*(5998), 138-141. doi:10.1038/313138a0
- Oh, H., & Irvine, K. D. (2008). In vivo regulation of Yorkie phosphorylation and localization. *Development*, *135*(6), 1081-1088. doi:10.1242/dev.015255
- Oh, H., & Irvine, K. D. (2011). Cooperative regulation of growth by Yorkie and Mad through bantam. *Dev Cell*, *20*(1), 109-122. doi:10.1016/j.devcel.2010.12.002
- Oh, H., Slattery, M., Ma, L., Crofts, A., White, K. P., Mann, R. S., & Irvine, K. D. (2013). Genome-wide association of Yorkie with chromatin and chromatin-remodeling complexes. *Cell Rep*, *3*(2), 309-318. doi:10.1016/j.celrep.2013.01.008
- Pai, V. P., Lemire, J. M., Paré, J. F., Lin, G., Chen, Y., & Levin, M. (2015). Endogenous gradients of resting potential instructively pattern embryonic neural tissue via Notch signaling and regulation of proliferation. *J Neurosci*, *35*(10), 4366-4385. doi:10.1523/jneurosci.1877-14.2015
- Palm, W., Swierczynska, M. M., Kumari, V., Ehrhart-Bornstein, M., Bornstein, S. R., & Eaton, S. (2013). Secretion and signaling activities of lipoprotein-associated hedgehog and non-sterol-modified hedgehog in flies and mammals. *PLoS Biol*, *11*(3), e1001505. doi:10.1371/journal.pbio.1001505
- Patel, N. H., Martin-Blanco, E., Coleman, K. G., Poole, S. J., Ellis, M. C., Kornberg, T. B., & Goodman, C. S. (1989). Expression of engrailed proteins in arthropods, annelids, and chordates. *Cell*, *58*(5), 955-968. doi:10.1016/0092-8674(89)90947-1

- Pelham, C. J., Nagane, M., & Madan, E. (2020). Cell competition in tumor evolution and heterogeneity: Merging past and present. *Semin Cancer Biol*, *63*, 11-18. doi:10.1016/j.semcancer.2019.07.008
- Petrov, K., Wierbowski, B. M., & Salic, A. (2017). Sending and Receiving Hedgehog Signals. *Annu Rev Cell Dev Biol*, *33*, 145-168. doi:10.1146/annurev-cellbio-100616-060847
- Pfleger, C. M. (2017). The Hippo Pathway: A Master Regulatory Network Important in Development and Dysregulated in Disease. *Curr Top Dev Biol*, *123*, 181-228. doi:10.1016/bs.ctdb.2016.12.001
- Plaster, N. M., Tawil, R., Tristani-Firouzi, M., Canún, S., Bendahhou, S., Tsunoda, A., . . . Ptáček, L. J. (2001). Mutations in Kir2.1 cause the developmental and episodic electrical phenotypes of Andersen's syndrome. *Cell*, *105*(4), 511-519. doi:10.1016/s0092-8674(01)00342-7
- Price, M. A., & Kalderon, D. (1999). Proteolysis of cubitus interruptus in *Drosophila* requires phosphorylation by protein kinase A. *Development*, *126*(19), 4331-4339.
- Prober, D. A., & Edgar, B. A. (2000). Ras1 promotes cellular growth in the *Drosophila* wing. *Cell*, *100*(4), 435-446. doi:10.1016/s0092-8674(00)80679-0
- Raleigh, D. R., & Reiter, J. F. (2019). Misactivation of Hedgehog signaling causes inherited and sporadic cancers. *J Clin Invest*, *129*(2), 465-475. doi:10.1172/jci120850
- Ramírez-Weber, F.-A., & Kornberg, T. B. (1999). Cytonemes. *Cell*, *97*(5), 599-607. doi:10.1016/s0092-8674(00)80771-0
- Ramírez-Weber, F. A., Casso, D. J., Aza-Blanc, P., Tabata, T., & Kornberg, T. B. (2000). Hedgehog signal transduction in the posterior compartment of the *Drosophila* wing imaginal disc. *Mol Cell*, *6*(2), 479-485. doi:10.1016/s1097-2765(00)00046-0
- Ren, D., Navarro, B., Xu, H., Yue, L., Shi, Q., & Clapham, D. E. (2001). A prokaryotic voltage-gated sodium channel. *Science*, *294*(5550), 2372-2375. doi:10.1126/science.1065635
- Rhiner, C., Lopez-Gay, J. M., Soldini, D., Casas-Tinto, S., Martin, F. A., Lombardia, L., & Moreno, E. (2010). Flower forms an extracellular code that reveals the fitness of a cell to its neighbors in *Drosophila*. *Dev Cell*, *18*(6), 985-998. doi:10.1016/j.devcel.2010.05.010
- Rodriguez, I., & Basler, K. (1997). Control of compartmental affinity boundaries by hedgehog. *Nature*, *389*(6651), 614-618. doi:10.1038/39343
- Roy, M., Sivan-Loukianova, E., & Eberl, D. F. (2013). Cell-type-specific roles of Na<sup>+</sup>/K<sup>+</sup> ATPase subunits in *Drosophila* auditory mechanosensation. *Proc Natl Acad Sci U S A*, *110*(1), 181-186. doi:10.1073/pnas.1208866110
- Schroll, C., Riemensperger, T., Bucher, D., Ehmer, J., Völler, T., Erbguth, K., . . . Fiala, A. (2006). Light-induced activation of distinct modulatory neurons triggers appetitive or aversive learning in *Drosophila* larvae. *Curr Biol*, *16*(17), 1741-1747. doi:10.1016/j.cub.2006.07.023
- Schuster, K. J., & Smith-Bolton, R. K. (2015). Taranis Protects Regenerating Tissue from Fate Changes Induced by the Wound Response in *Drosophila*. *Dev Cell*, *34*(1), 119-128. doi:10.1016/j.devcel.2015.04.017

- Schwank, G., & Basler, K. (2010). Regulation of organ growth by morphogen gradients. *Cold Spring Harb Perspect Biol*, 2(1), a001669. doi:10.1101/cshperspect.a001669
- Schwartz, C., Locke, J., Nishida, C., & Kornberg, T. B. (1995). Analysis of cubitus interruptus regulation in *Drosophila* embryos and imaginal disks. *Development*, 121(6), 1625-1635. Retrieved from <https://www.ncbi.nlm.nih.gov/pubmed/7600980>
- Shen, J., & Dahmann, C. (2005). Extrusion of cells with inappropriate Dpp signaling from *Drosophila* wing disc epithelia. *Science*, 307(5716), 1789-1790. doi:10.1126/science.1104784
- Shingleton, A. W., Das, J., Vinicius, L., & Stern, D. L. (2005). The temporal requirements for insulin signaling during development in *Drosophila*. *PLoS Biol*, 3(9), e289. doi:10.1371/journal.pbio.0030289
- Spannl, S., Buhl, T., Nellas, I., Zeidan, S. A., Iyer, K. V., Khaliullina, H., . . . Eaton, S. (2020). Glycolysis regulates Hedgehog signalling via the plasma membrane potential. *Embo j*, 39(21), e101767. doi:10.15252/emboj.2019101767
- Spemann, H., & Mangold, H. (2001). Induction of embryonic primordia by implantation of organizers from a different species. 1923. *Int J Dev Biol*, 45(1), 13-38. Retrieved from <https://www.ncbi.nlm.nih.gov/pubmed/11291841>
- Srivastava, N., Traynor, D., Piel, M., Kabla, A. J., & Kay, R. R. (2020). Pressure sensing through Piezo channels controls whether cells migrate with blebs or pseudopods. *Proc Natl Acad Sci U S A*, 117(5), 2506-2512. doi:10.1073/pnas.1905730117
- Strigini, M., & Cohen, S. M. (1997). A Hedgehog activity gradient contributes to AP axial patterning of the *Drosophila* wing. *Development*, 124(22), 4697-4705.
- Sundelacruz, S., Levin, M., & Kaplan, D. L. (2009). Role of membrane potential in the regulation of cell proliferation and differentiation. *Stem Cell Rev Rep*, 5(3), 231-246. doi:10.1007/s12015-009-9080-2
- Tabata, T., Eaton, S., & Kornberg, T. B. (1992). The *Drosophila* hedgehog gene is expressed specifically in posterior compartment cells and is a target of engrailed regulation. *Genes Dev*, 6(12B), 2635-2645. doi:10.1101/gad.6.12b.2635
- Tabata, T., & Kornberg, T. B. (1994). Hedgehog is a signaling protein with a key role in patterning *Drosophila* imaginal discs. *Cell*, 76(1), 89-102. doi:10.1016/0092-8674(94)90175-9
- Taipale, J., Cooper, M. K., Maiti, T., & Beachy, P. A. (2002). Patched acts catalytically to suppress the activity of Smoothed. *Nature*, 418(6900), 892-897. doi:10.1038/nature00989
- Tamori, Y., Suzuki, E., & Deng, W. M. (2016). Epithelial Tumors Originate in Tumor Hotspots, a Tissue-Intrinsic Microenvironment. *PLoS Biol*, 14(9), e1002537. doi:10.1371/journal.pbio.1002537
- Tanaka, Y., Okada, Y., & Hirokawa, N. (2005). FGF-induced vesicular release of Sonic hedgehog and retinoic acid in leftward nodal flow is critical for left-right determination. *Nature*, 435(7039), 172-177. doi:10.1038/nature03494
- Tanimoto, H., Itoh, S., ten Dijke, P., & Tabata, T. (2000). Hedgehog creates a gradient of DPP activity in *Drosophila* wing imaginal discs. *Mol Cell*, 5(1), 59-71. doi:10.1016/s1097-2765(00)80403-7

- Thistle, R., Cameron, P., Ghorayshi, A., Dennison, L., & Scott, K. (2012). Contact chemoreceptors mediate male-male repulsion and male-female attraction during *Drosophila* courtship. *Cell*, *149*(5), 1140-1151. doi:10.1016/j.cell.2012.03.045
- Thompson, B. J., & Cohen, S. M. (2006). The Hippo pathway regulates the bantam microRNA to control cell proliferation and apoptosis in *Drosophila*. *Cell*, *126*(4), 767-774. doi:10.1016/j.cell.2006.07.013
- Ulrich, T. A., de Juan Pardo, E. M., & Kumar, S. (2009). The mechanical rigidity of the extracellular matrix regulates the structure, motility, and proliferation of glioma cells. *Cancer Res*, *69*(10), 4167-4174. doi:10.1158/0008-5472.CAN-08-4859
- Umetsu, D., Dunst, S., & Dahmann, C. (2014). An RNA interference screen for genes required to shape the anteroposterior compartment boundary in *Drosophila* identifies the Eph receptor. *PLoS ONE*, *9*(12), e114340. doi:10.1371/journal.pone.0114340
- Vandenberg, L. N., Morrie, R. D., & Adams, D. S. (2011). V-ATPase-dependent ectodermal voltage and pH regionalization are required for craniofacial morphogenesis. *Dev Dyn*, *240*(8), 1889-1904. doi:10.1002/dvdy.22685
- Verghese, S., & Su, T. T. (2016). *Drosophila* Wnt and STAT Define Apoptosis-Resistant Epithelial Cells for Tissue Regeneration after Irradiation. *PLoS Biol*, *14*(9), e1002536. doi:10.1371/journal.pbio.1002536
- Vire, E., Brenner, C., Deplus, R., Blanchon, L., Fraga, M., Didelot, C., . . . Fuks, F. (2006). The Polycomb group protein EZH2 directly controls DNA methylation. *Nature*, *439*(7078), 871-874. doi:10.1038/nature04431
- Vogelstein, B., Papadopoulos, N., Velculescu, V. E., Zhou, S., Diaz, L. A., Jr., & Kinzler, K. W. (2013). Cancer genome landscapes. *Science*, *339*(6127), 1546-1558. doi:10.1126/science.1235122
- Von Ohlen, T., Lessing, D., Nusse, R., & Hooper, J. E. (1997). Hedgehog signaling regulates transcription through cubitus interruptus, a sequence-specific DNA binding protein. *Proc Natl Acad Sci U S A*, *94*(6), 2404-2409. doi:10.1073/pnas.94.6.2404
- Weir, M. P., & Lo, C. W. (1984). Gap-junctional communication compartments in the *Drosophila* wing imaginal disk. *Dev Biol*, *102*(1), 130-146. doi:10.1016/0012-1606(84)90181-7
- Weiss, I., & Bohrmann, J. (2019a). Electrochemical gradients are involved in regulating cytoskeletal patterns during epithelial morphogenesis in the *Drosophila* ovary. *BMC Dev Biol*, *19*(1), 22. doi:10.1186/s12861-019-0203-y
- Weiss, I., & Bohrmann, J. (2019b). Electrochemical patterns during *Drosophila* oogenesis: ion-transport mechanisms generate stage-specific gradients of pH and membrane potential in the follicle-cell epithelium. *BMC Dev Biol*, *19*(1), 12. doi:10.1186/s12861-019-0192-x
- Wietek, J., Rodriguez-Rozada, S., Tutas, J., Tenedini, F., Grimm, C., Oertner, T. G., . . . Wiegert, J. S. (2017). Anion-conducting channelrhodopsins with tuned spectra and modified kinetics engineered for optogenetic manipulation of behavior. *Sci Rep*, *7*(1), 14957. doi:10.1038/s41598-017-14330-y
- Wietek, J., Wiegert, J. S., Adeishvili, N., Schneider, F., Watanabe, H., Tsunoda, S. P., . . . Hegemann, P. (2014). Conversion of channelrhodopsin into a light-gated chloride channel. *Science*, *344*(6182), 409-412. doi:10.1126/science.1249375

- Willsey, H. R., Zheng, X., Carlos Pastor-Pareja, J., Willsey, A. J., Beachy, P. A., & Xu, T. (2016). Localized JNK signaling regulates organ size during development. *eLife*, 5. doi:10.7554/eLife.11491
- Wolpert, L. (1969). Positional information and the spatial pattern of cellular differentiation. *J Theor Biol*, 25(1), 1-47. doi:10.1016/s0022-5193(69)80016-0
- Worley, M. I., Setiawan, L., & Hariharan, I. K. (2013). TIE-DYE: a combinatorial marking system to visualize and genetically manipulate clones during development in *Drosophila melanogaster*. *Development*, 140(15), 3275-3284. doi:10.1242/dev.096057
- Wozniak, M. A., & Chen, C. S. (2009). Mechanotransduction in development: a growing role for contractility. *Nat Rev Mol Cell Biol*, 10(1), 34-43. doi:10.1038/nrm2592
- Wu, F., Zhang, Y., Sun, B., McMahon, A. P., & Wang, Y. (2017). Hedgehog Signaling: From Basic Biology to Cancer Therapy. *Cell Chem Biol*, 24(3), 252-280. doi:10.1016/j.chembiol.2017.02.010
- Xavier, G. M., Seppala, M., Barrell, W., Birjandi, A. A., Geoghegan, F., & Cobourne, M. T. (2016). Hedgehog receptor function during craniofacial development. *Dev Biol*, 415(2), 198-215. doi:10.1016/j.ydbio.2016.02.009
- Xue, Z., Wu, M., Wen, K., Ren, M., Long, L., Zhang, X., & Gao, G. (2014). CRISPR/Cas9 mediates efficient conditional mutagenesis in *Drosophila*. *G3 (Bethesda)*, 4(11), 2167-2173. doi:10.1534/g3.114.014159
- Yao, C. K., Lin, Y. Q., Ly, C. V., Ohyama, T., Haueter, C. M., Moiseenkova-Bell, V. Y., . . . Bellen, H. J. (2009). A synaptic vesicle-associated Ca<sup>2+</sup> channel promotes endocytosis and couples exocytosis to endocytosis. *Cell*, 138(5), 947-960. doi:10.1016/j.cell.2009.06.033
- Yu, J., & Pan, D. (2018). Validating upstream regulators of Yorkie activity in Hippo signaling through scalloped-based genetic epistasis. *Development*, 145(4). doi:10.1242/dev.157545
- Zanconato, F., Cordenonsi, M., & Piccolo, S. (2016). YAP/TAZ at the Roots of Cancer. *Cancer Cell*, 29(6), 783-803. doi:10.1016/j.ccell.2016.05.005
- Zhang, C., Williams, E. H., Guo, Y., Lum, L., & Beachy, P. A. (2004). Extensive phosphorylation of Smoothed in Hedgehog pathway activation. *Proc Natl Acad Sci U S A*, 101(52), 17900-17907. doi:10.1073/pnas.0408093101
- Zhao, Q., Zhou, H., Chi, S., Wang, Y., Wang, J., Geng, J., . . . Xiao, B. (2018). Structure and mechanogating mechanism of the Piezo1 channel. *Nature*, 554(7693), 487-492. doi:10.1038/nature25743
- Zhou, Y., Wong, C. O., Cho, K. J., van der Hoeven, D., Liang, H., Thakur, D. P., . . . Hancock, J. F. (2015). SIGNAL TRANSDUCTION. Membrane potential modulates plasma membrane phospholipid dynamics and K-Ras signaling. *Science*, 349(6250), 873-876. doi:10.1126/science.aaa5619
- Zhu, A. J., Zheng, L., Suyama, K., & Scott, M. P. (2003). Altered localization of *Drosophila* Smoothed protein activates Hedgehog signal transduction. *Genes Dev*, 17(10), 1240-1252. doi:10.1101/gad.1080803